Feedback of 2025 IDRC Review Report

中国科学院高能物理研究所
Institute of High Energy Physics
Chinese Academy of Sciences

Outline

Machine Detector Interface

Findings

- F-A-3-1: A layout of the interaction region—including the anti-solenoid, final focus quadrupoles, IP beam pipe, and Luminosity Monitor—has been presented. Although not yet final, it is sufficiently advanced to proceed with detailed component design.
- The Be beam pipe has an inner diameter of 10 mm and a length of 220 mm. It consists of an inner Be layer 0.2 mm thick and an outer Be layer 0.15 mm thick, separated by a 0.2 mm gap, which seems quite aggressive. The default coolant is water, with paraffin as a backup. The cooling technology is well-established, and the cost estimates are considered reliable. The coolant flow remains in the stable laminar regime. Mechanical analyses for cantilever support during installation have been performed, and no issues have been found. With an inlet water temperature of 15° C, the Be pipe temperature remains below 20° C, which is within acceptable limits.
- F-A-3-2: Beam background sources—including synchrotron radiation (SR) photons, pairs, and off-energy particles—have been studied in detail, along with other minor contributions. For SR photons, important interactions such as the photoelectric effect and Rayleigh scattering have been simulated. It was found critically important to employ high-Z SR masks to protect the IP beam pipe region. Pair backgrounds are mitigated by designing the IP beam pipe to stay outside the high- density region. The hit rate on the first layer of the vertex detector (VTX) is estimated to be around 1 hit per cm^2 per bunch crossing. Backgrounds from off-energy particles are suppressed by placing collimators at strategic points around the ring and heavy metal masks near the IP to absorb secondary showers.
- F-A-3-3: Experience from BESIII was presented, showing that real background levels were about 1/5 of those predicted by simulation.
- F-A-3-4: An updated design of the LumiCal, using a silicon detector and LYSO crystals for pile-up event veto, is included in the Reference TDR. Mechanical design and optimization are complete, and construction of a large prototype is planned for the EDR phase. The selected technology appears feasible, although achieving the required luminosity precision will demand electron impact position measurements at the level of better than ten microns.

Comments

- C-A-3-1: From the presentations and draft Ref-TDR, it is unclear whether a gold (Au) coating is applied to the inside of the Be beam pipe, and if so, what thickness is used. Further study on this issue may be necessary.
- Answer: The 10um Au coating is implemented, as indicated in Ref-TDR MDI Chapter: “The gold coating on the inner surface of the central beryllium pipe has a thickness of 10 μm .”
- C-A-3-2: The current SR mask configurations require further study. In particular, changes in beam or bit— such as during commissioning—must be considered to ensure continued protection of the Be beam pipe region.
- Answer: Sure. Currently, only the ideal beam with some tail has been studied. The changes in beam orbit will be studied in future together with accelerator colleagues to figure out the working scenarios and the parameters.
- C-A-3-3: While heavy metal masks can effectively reduce backgrounds from off-energy particles, they may also generate secondary backgrounds. This study suggests the effect is moderate, but further investigation is needed, especially concerning the tungsten (W) masks near the IP.
- Answer: The secondaries has been studied. We also realize that the SR masks in the -1.9m may also increase the other sources of beam induced backgrounds. We are optimizing our design of the SR masks, by introducing some dedicated SR collimators relatively far away from the IP, the decrease the height of the SR mask to mitigate the secondaries introduced by it. These work is still on going.

Comments

- C-A-3-4: The discrepancy between real background measurements and simulations observed at BESIII is a significant concern. Although the energy scales differ between BESIII and CEPC, understanding this discrepancy is critical for evaluating the reliability of CEPC background predictions.
- Answer: The previous study already decreased the discrepancy as shown in the text, and we will perform more dedicated study in future when we have machine times.
- C-A-3-5: Although background rates (after shielding) are presented, detailed histograms and numerical data characterizing these backgrounds (e.g., energy spectra, multiplicity, polar and azimuthal angle distributions) are often missing. Such information is essential to assess the impact on the entire apparatus, particularly on the first layers of the vertex detector and LumiCal.
- Answer: We have those information, and all these information have been given to the subdetector designers as indicated in MDI Chapter. Further optimization for LumiCal is also needed, and the study taking the beam induced background at LumiCal is still on going.

Recommendations

- R-A-3-1: Conduct studies to finalize the decision on the Au coating inside the Be beam pipe, including its thickness and the possibility of omitting it.
- Answer: The 10um Au coating is implemented, as indicated in Ref-TDR MDI Chapter: “The gold coating on the inner surface of the central beryllium pipe has a thickness of 10 μm.”
- R-A-3-2: Continue detailed studies of SR mask configurations and materials, considering the effects of beam orbit steering in collaboration with the accelerator group.
- Answer: Currently, only the ideal beam has been studied. The changes in beam orbit will be studied in future together with our accelerator colleagues when they have the results of the orbit corrections and the parameters and designs used for the commissioning phase.
- R-A-3-3: Further investigate the role of heavy metal masks in absorbing particle backgrounds, including the possibility of operating without them.
- Answer: The secondaries has been studied. We also realize that the SR masks in the -1.9m may also increase the other sources of beam induced backgrounds. We are optimizing our design of the SR masks, by introducing some dedicated SR collimators relatively far away from the IP, the decrease the height of the SR mask to mitigate the secondaries introduced by it. These work is still on going.

Recommendations

- R-A-3-4: Pursue deeper studies of BESIII backgrounds to understand the discrepancy between simulation and data.
- Answer: The previous study already decreased the discrepancy as indicated in MDI Chapter: ”Such discrepancy was mainly due to the incomplete particle tracking and insufficiently modeled interactions involving complex components in IR in the simulation and was already decreased from more than 10^4 to current level by the improving of the geometry and adding the study on tip-scattering on the collimators”, and we will perform more dedicated study in future. We are working on the analysis of the data currently taking from BEPCIIU, and plan to perform this years dedicated beam induced backgrounds study and experiments at BEPCII when possible.
- R-A-3-5: Continue dedicated studies on LumiCal readout electronics at high rates, followed by beam tests with detector prototypes at later stages.
- R-A-3-6: Study the effects of beam backgrounds on LumiCal reconstruction for realistic configurations.
- Answer: The shielding optimization and further mitigation of the beam induced background at LumiCal is still ongoing. Current beam induced background level is high at LumiCal, therefore the dedicated optimization must be performed to control the level and let the LumiCal works better. Also the bhabha and Radiative bhabha scattering needs to consider the beam-beam deflection, which is not considered yet. The data rate due to the beam induced backgrounds are already considered when design the electronics of the LumiCal. Such studies are ongoing at the same time to give us an idea how the situation would be. We are currently invistigating the generator guinea-pig++, and plan to implemented it with APES.

Vertex Detector

Findings

- F-A-4-1: The design and technology choice for the vertex detector is highly ambitious and at the forefront of technological innovation. The baseline option—thin, bendable silicon CMOS sensors that can be stitched together to create a large, lightweight vertex detector—is certainly a very challenging yet promising approach. The backup solution, which also employs thin CMOS sensors mounted on ladders, remains technologically advanced. The project has made significant progress since the last review.
- F-A-4-2: The vertex detector is expected to operate for 10 years during Higgs and low-luminosity Z running, after which it will need to be replaced for high-luminosity Z, WW, and $t\bar{t}$ operations. The ability to run at high-luminosity Z mode imposes additional demands on an already extremely challenging design (e.g., larger data rate capabilities, shorter charge collection times, lower noise, and tighter power consumption constraints).
- F-A-4-3: There are several major challenges for the vertex detector. Achieving the desired position resolution has been demonstrated with the TaichuPix-3 chip in TJ180 nm technology. However, this process has limitations, particularly its high-power consumption (>100 mW/cm²), which is too high for air cooling. Transitioning to the TPSCo65 process is a way forward, reducing power consumption to approximately 40 mW/cm². The required position resolution and uniform hit efficiency have already been demonstrated in this new process.
- F-A-4-4: The real challenge now lies in the development of large-area stitched sensors of ~40 μm thickness that can be bent to radii as small as 11 mm, achieving a material budget of just 0.06% X_0. Successful bending of dummy 40 μm wafers has been demonstrated, but bending fully processed wafers (including metal layers for data and power lines) remains to be achieved. Securing access to TPSCo65 technology, including a modified process optimized for particle detection, is crucial. An alternative approach under early exploration is the HLMC 55 nm technology, although it has yet to be demonstrated.
- F-A-4-5: The mechanical design is quite advanced for this stage, with many demonstrators and mock-up parts already tested, including a full ladder demonstrator. The simulations shown for mechanical and thermal performance, efficiency coverage, and background hit rates are detailed and of high quality. The impact of background hit rates on physics performance has been found to be negligible. The planned laser alignment system is a very positive development, but its effective operation must still be demonstrated.
- F-A-4-6: The fifth double layer of the vertex detector employs a more conventional ladder design, achieving approximately 0.25% X_0. At the larger radius of the fifth layer, this becomes necessary but also requires parallel development. Importantly, this ladder design offers a reliable fallback option in case insurmountable problems arise with the stitched sensor technology for the inner layers.
- However, adopting this backup would come at the cost of a slightly higher material budget, and thus a somewhat degraded p_t resolution at lower energies.

Comments

- C-A-4-1: **The chapter in the TDR is very long and detailed. In sections covering previously published R&D, the level of detail could be reduced.** However, we found it very positive that past efforts from various groups were acknowledged, and that valuable experience and knowledge have been incorporated into the current vertex detector design.
  - This section has been reduced from ~60 pages to 40 pages
- C-A-4-2: Although pursuing the HLMC 55 nm process could dilute focus and resources, it remains a worthwhile avenue, especially if difficulties arise in securing access to TPSCo65.
- C-A-4-3: While the mechanical design, simulations, and testing are advanced for this stage, maintaining mechanical stability and achieving efficient cooling remain significant challenges.
- C-A-4-4: The foreseen cost of sensors (~4.0 MCHF) appears reasonable. The relatively higher cost per unit area compared to other silicon detectors likely reflects the fact that the baseline sensor producer is not domestic.
- C-A-4-5: The estimated costs for mechanics, electronics, and the alignment system are of the correct order of magnitude but constitute only a fraction of the sensor cost

Recommendations

•R-A-4-1: Re-evaluate the required performance specifications, focusing on operation during ZH and low-luminosity Z runs over the first 10 years.

•Answer: the new result of hit rate with latest simulation is updated in Sec 4.1.3.

•R-A-4-2: We reiterate our previous recommendation to expand the current manpower dedicated to design and R&D efforts. A close collaboration with ALICE-ITS3 on stitched sensor development is strongly encouraged.

•Answer: synergy with sensor development in future ALICE3 upgrade is expected.

•R-A-4-3: Explore constructing a mock-up with dummy heaters for thermal performance tests, to be used also for simulation validation.

•Answer: has added this suggestion into future plan section in vertex chapter sec. 4.8. 'The plan begins with exploring the construction of a mock-up featuring dummy heaters for thermal performance testing. Results will also validate thermal simulation models.'

•R-A-4-4: While pixel functionalities are similar for the ladder and stitched sensor options, significant differences in chip-to-chip (RSU-to-RSU) connectivity could impact performance. Address potential challenges (e.g., power and data distribution across large, stitched sensors) as early as possible through simulation studies

•Answer: will perform simulation on stitching design when we are about to tape out the next version of sensor by the end of 2025. Most of this potential challenges can be simulated with design kits when the stitching design is in shape.

Comments on Draft v0.4.1

C-B-4-1:

Daniela's comment:

I read the tracker section and found that the structure of the reference TDR has improved.

Nonetheless, the Barcelona version still needs substantial editing. In addition, some figure captions — for example, Figure 4.8: "For we could not completely handle high-lumi Z mode now, as well as the major difference between high-lumi Z with Z mode is luminosity which means their hit rate distribution is similar, the hit rate distribution of high-lumi Z would not be shown here." — indicate that there is still an unresolved issue with the high-lumi Z mode.

This should be addressed carefully.

Answer:

We added this statement in Section 4.2 "The readout architecture can accommodate the data rates in both the Higgs factory mode and the low-luminosity Z boson factory mode during the first ten years of operation. A replacement of the VTX with upgraded technology is foreseen thereafter, with the readout architecture for the high-luminosity Z boson factory mode discussed in Chapter 11.2."

"The process involves: buffering detector signals and background data on the front-end chip; the trigger system generating fast trigger arbitration information quickly and sending it to the front-end chip via a dedicated channel; the front-end chip comparing buffered data with the fast trigger information and transmitting preliminarily arbitrated data to the BEE."

Comments on Draft v0.4.1

Gregor:

- **General observation:**

- C-B-4-2: The Chapter has improved significantly from the April draft in terms of length, restriction to important information and clarity. The length is appropriate and some unnecessary details from the first draft are left out.
- C-B-4-3: Alignment and laser alignment monitoring system are adequately addressed.
- C-B-4-4: Rich and at that stage advanced R&D is in a separate section which is positive. It is difficult in part to disentangle different objectives of JadePix and TaichuPix
- ANSWER -->we rephase the first part of Section 4.5 (R & D section): The JadePix project focuses on optimizing the charge collection diode design and the analog front-end circuitry, with particular emphasis on achieving low power consumption in the analog domain. In contrast, the TaichuPix project is dedicated to developing a fully functional digital architecture, incorporating in-pixel logic and a data-driven, column-drain readout scheme. This design is specifically tailored to meet the stringent timing and data throughput requirements of the high-luminosity CEPC environment, particularly during the low-luminosity Z-pole operation with high event rates.
- C-B-4-5: The cost estimate from April was already reasonable and wasn't touched in the review.

Comments on Draft v0.4.1

- C-B-4-6: Is the Layer 5,6 the exactly the same design/concept as L1,2 and L3,4 of the backup design? The stitching concept is very attractive, but also very innovative and **unproven** which poses a significant risk. Given the development of the backup (baseline for L5,6) will have to go hand in hand with stitched-chip design it may be worth presenting the impact of using conventional design on performance (not only d0,z as in 4.6 but maybe a subset of physics channels) . Also a possible lack of technology access or resources may force you to abandon stitched-MAPS part baseline option. If you are confident in stitched-chip technology wouldn't it be worth finding the way to use it also in L5,6?

→ Yes, Layer 5,6 in baseline layout the exactly the same design/concept as L1,2 and L3,4 of the backup layout.

Due to wafer size limitation and the yield issue, we still don't have a good solution for stitched-chip technology in Layer 5/6 yet.

- C-B-4-7: VTX design for for high lumi Zmode which only comes after 10 y is super challenging. Relaxing design parameters for longer BX may lead to more robust design. VTX is not very large and a better design for high lumi Zpole running may emerge with time.

→ We optimized the VTX for the first 10 year operation including Higgs and low-lumi Z, the design parameters already related. More dedicated design for high-lumi Z pole runs is expected to be performed for the VTX replacement before high-lumi Z runs.

Comments on Draft v0.4.1

- C-B-4-8: Background studies from ee and synchrotron radiation are crucial for understanding the background. Mixing the tables and plots with/without different background contributions is difficult to follow and evaluate.

→ The dominated component of background contribution is pair production. That is the reason why we did not talk further about the contribution from different component. Detailed information about different background is mentioned in section 3.

- C-B-4-9: Laser alignment is an important tool and if implemented will reveal many unknowns about the mechanical stability of such objects not demonstrated in real experiment before. However, illuminations at shallow angles on almost entirely metalized surfaces are much more complicated that for e.g. strip detectors. Understanding all reflections and ways to induce signals will be a challenge.

→ more study with illuminations at shallow angles on prototype sensors will be performance in a short time scale.

We will investigate laser alignment with infrared laser shotting at backside (without metal) of the MAPS. In this way, the reflection can be reduced.

In longer time scale, the laser alignment method will be checked with vertex detector prototype with stitched sensors

Comments on Draft v0.4.1

C-B-4-10: Remarks/questions and editorial comments:

- C-B-4-10-1: L2444 - dead zone -> inefficient region (all over the text) ->Done
- C-B-4-10-2: L2479 - 65 nm or 55 nm (SMIC) - maybe it would be better not to limit yourself ->Added more info about alternative technology on 65/55nm
- C-B-4-10-3: Table 4.1 - time stamp precision should be without +/- ->Removed
- C-B-4-10-4: L2505 - using the word chip can be confusing as people use it for reticle size objects -> stitched-chip would make it clearer all over the text
- C-B-4-10-5: L2506 - to satisfy the coverage from 8.1-90 deg ->Corrected as |cos (theta)|<0.991
- C-B-4-10-6: Figure 4.2 : CMOS, MAPS used here imply as CMOS and MAPS are different detector technologies. Maybe planar CMOS sensors -> “single reticle MAPS” and “stitched MAPS” is a better terminology. → we now unify the wording stitched layer and planar layer
- C-B-4-10-7: Figure 4.6 - please put “not to scale” in the caption. ->Done
- C-B-4-10-8: Figure 4.7 - Please mention that the cell in this case is a single chip, for easier reading. The legend (Layer 1 and Layer 2 labels should be larger. The colour coding of the plots is not the most convenient. I would advise you to use the same scale on both plots! ->Corrected
- C-B-4-10-9: L2626 - remove Tower from the TPSCo ->removed.
- C-B-4-10-10: Table 4.7 and also in the text put the fill factor (sensitive area) of the RSU
  - → Table 4.7 (area for each functional block in MAPS) has been removed, since the design has not been finished yet. We will try to keep a highest possible fill factor during the design process.

Comments on Draft v0.4.1

- C-B-4-10-11: Figure 4.9 it is unclear to what the data interface part if the middle x~10 mm is stitched to (or "stitched" can be omitted)? For 1D stitching of RSU as I understand reticles are stitched along the z axis.
  - → stitching direction is along the z axis, we now indicated the stitching direction in Figure 4.3 and also in the text.

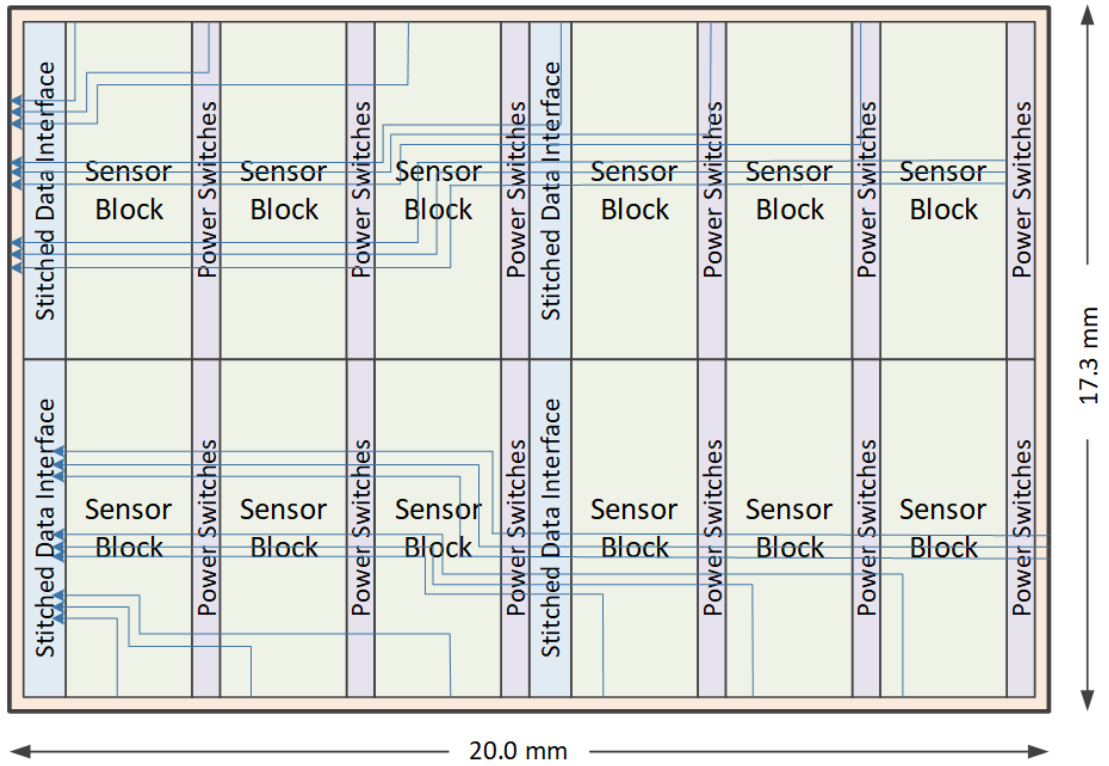

Comments on Draft v0.4.1

- C-B-4-10-12: L2699 - What about the n-spray implant (modified process) to find optimum between collection efficiency and position resolution. → we now added some tex to mention n-spray implant
- C-B-4-10-13: L2679 - “the leakage current should be controlled in 5 times of TaichuPix” - this doesn‘t read well. ->Removed
- C-B-4-10-14: L2840 – although some studies show that that bending of silicon to 11 mm is doable, this is far from certain and surprises may appear. → Thanks, we will keep that in mind.
- C-B-4-10-15: L2847-2849 – this needs a rewrite for easier reading. ->Rewrote
- C-B-4-10-16: L2876 – with our previous prototyped vertex design -> with an earlier prototype design. -> done
- C-B-4-10-17: L2906 – 300 mW/cm2 cooling with airflow needs a reference and also at what conditions. This may lead a reader to a false believe that around an order of magnitude less is trivial to cool. A fee more sentences are needed here: what flow was simulated (laminar/turbulent), if all obstacles were correctly accounted for. Have the thermal gradients along the flow been taken into consideration? → the simulation results indicated it is a turbulent flow. The thermal gradients along the flow has been considered, Not all the obstacles accounted for. We now added more information about the cooling simulation in the text. “To evaluate the performance of the cooling system, simulations were performed under various airflow speeds, as shown in Figure 4.18. The results indicate a turbulent pattern under the current geometry and flow conditions. “

Comments on Draft v0.4.1

- 4.4.1 looks a generic wish list. It is clear that presently the level of details known or needed is not large, but a bit more refined information would be welcome. →added more detailed “During the assembly phase of the CVTX layers, the thickness and curvature of the stitched sensors will be inspected. In later stages, the layer-to-layer coaxiality and ϕ-stagger across layers will also be checked and recorded. “
- 4.4.2./3 The alignment is critical and level of distortions at 3.5 m/s airflow which may change/oscillate with time is a big challenge for the first 4 layers. → In longer time scale, we will check the laser alignment in vertex prototype with stitched sensor.
- Figure 4.19: Please use (a), (b) and (c) so that the figure captions are coherent across the text. → done
- L3131 - Better wording would be lateral and more uniform depletion ->Rewrote as suggested
- 4.5.2.3 Prototype of a stitching CMOS detector - It is not clear what is the state of that prototype or the results from it. It is a very important piece of information of e.g. of LDOs performance … A few sentences summarizing the state of functional tests would be welcome. → added one paragraph in 4.5.2.3 of the function tests results.
- 4.6.1 - Genantino studies are well described, but it is not clear on how much the physics performance would degrade if e.g. fraction of hits=4 increases to say 1% and hits=5,6,7 are reduced. → More detailed will be done. According to Section 4.7.3, the performance degradation is limited when we turned off some fraction of the sensors.
- L3283 - I would replace "domestic" with "Chinese" or omit it, unless you want the TDR to be biased. → we omitted it.

Inner Tracker (ITK)

Findings

- F-A-5-1: The Inner Tracker (ITK) of the CEPC silicon tracking system adopts a baseline technology based on HV-CMOS monolithic active pixel sensors (SMIC 55), offering excellent spatial resolution (pixel size: 34 μm × 150 μm), moderate time resolution (3–5 ns), and low material per layer (<1% X_0). As an alternative for the endcap, a HV-CMOS strip sensor technology is also under development.
- F-A-5-2: Since the last review in October 2024, the project has made notable progress in ASIC development. The COFFEE3 chip (SMIC 55 nm)—the second-generation HV-CMOS prototype— was successfully submitted for fabrication in January 2025 and is expected to be delivered for testing in May 2025. COFFEE3 integrates two readout architectures, supports in-pixel time stamping, and includes significant improvements in power optimization and data-driven readout. In parallel, the CSC1 chip, which integrates a passive CMOS strip sensor and an analog front- end placed in the periphery (CMSC 180 nm process), is scheduled for tape-out in April 2025. Together, these developments demonstrate strong and steady progress in the ITK technology program.
- F-A-5-3: Significant system-level advancements have also been achieved, particularly in mechanical design, cooling, and thermal management. The ITK now incorporates a well-defined multi-loop water-cooling system capable of maintaining stable operation at a power density of ~200 mW/cm², with thermal gradients controlled below 4° C. Updated mechanical simulations confirm the structural integrity of staves and validate the mechanical design for integration and prototyping.

Comments

- C-A-5-1: The alternative ITK endcap technology based on CMOS strips, while offering slightly better intrinsic spatial resolution (~4 μm), presents greater challenges compared to the HVCMOS pixel baseline. Achieving 3D tracking requires stereo configurations, increasing the material budget and mechanical complexity. Furthermore, the integration of a CMOS readout circuit in the strip sensor periphery, although innovative, may introduce additional design and integration risks.

- C-A-5-2: The COFFEE3 chip successfully consolidates the sensor, analog front-end, coarse-fine TDC for time-of-arrival and time-over-threshold measurements, and data-driven digital readout into a single device. Achieving these capabilities within a power density of ~200 mW/cm² is an impressive technical goal. A successful validation of COFFEE3 would represent a major milestone, demonstrating the technological feasibility of the CEPC ITK concept

Recommendations

- R-A-5-1: Given the limited resources available for R&D and the increased complexity associated with the CMOS strip-based solution for the ITK endcap, we recommend a careful evaluation of the merit and timing of continuing this development. The CMOS strip approach remains a promising technological direction; however, it may be appropriate to continue work at a lower priority to preserve long-term potential, while focusing current resources on advancing the baseline HV-CMOS pixel system.

In our previous Ref-TDR draft, the CMOS strip was presented as a backup or alternative approach with low R&D priority. Following the Referee's comment , we have removed all content related to CMOS strip from the current Ref-TDR to better focus on HV-CMOS baseline.

- R-A-5-2: We strongly encourage prioritizing the COFFEE3 validation campaign. As a comprehensive integration of position sensing and timing capabilities within a monolithic HV-CMOS technology, successful testing of COFFEE3 would constitute a critical milestone for the CEPC silicon tracking system, helping to de-risk the ITK concept and validate the soundness of the baseline detector design.

The latest COFFEE3 sensor was received at the end of May, and the sensor test campaign was lunched immediately upon receipt. The test setup is fully prepared, and testing is currently underway. We are committed to completing the critical validation promptly, as it represents one of the most important milestones for the ITK.

COFFEE3 incorporates two readout architectures, both featuring nearly a complete ASIC readout framework. This solution can be extended to final chip.

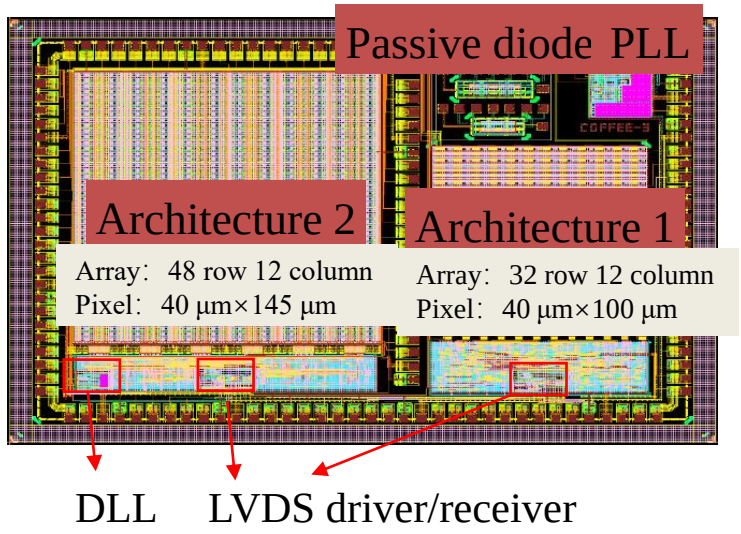

- **Architecture 1:** An optimized design framework based on the current process conditions (Triple-well process)；
- **Architecture 2:** An improved solution that requires process modification (Deep P-well required) to fully utilize the advantages of the 55 nm process node.

PLL (and IV) Test Board

- Mostly for PLL block only

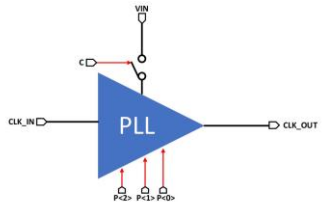

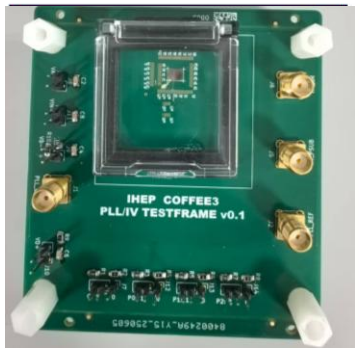

Caribou DAQ at IHEP

- both ZC706 and ZCU102 running fine with CaR boards

Left and Right Matrix Test Board

- Test Board (TB) designs for left and right matrix separately
- COFFEE3 left matrix is under test: laser, responce scan, SPI communication...

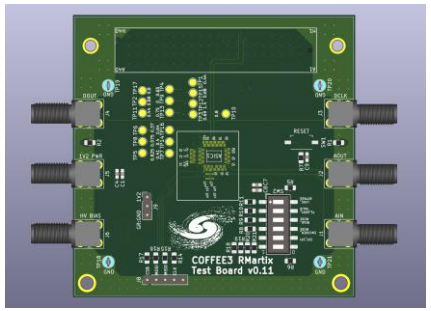

- SPI config between the FPGA and the CMOS matrix EOC
- power supply from Caribou DAQ
- reference voltage/current from Caribout to CMOS matrix
- 4 pixel CSA output from CMOS matrix => SMA cable => osc. scope
- ~10 Digitial signal output from EOC
- 6 DLL output
- LVDS Transceiver test between EOC and DAQ
  - Tx and Rx driver study
  - digital circuits for data serializer

Outer Tracker(OTK)

Findings

- F-A-5-4: The Outer Tracker (OTK) of the CEPC is a large area tracking system designed to provide precision timing and position measurements, complementing the inner tracking systems and the central Time Projection Chamber (TPC). It plays a critical role in improving momentum resolution for high-momentum tracks and mitigating performance degradation of the TPC in high-luminosity operations, where ion backflow-induced space charge can distort the drift field and impair tracking accuracy. The OTK is based on AC-coupled Low-Gain Avalanche Detectors (AC-LGADs) arranged as microstrip sensors, capable of delivering ~10 μm spatial and ~50 ps timing resolution, covering approximately 85 m^2 across the barrel and endcap sections.
- F-A-5-5: Since the October 2024 IDRC review, the CEPC OTK system has made significant progress in response to the committee's recommendations. The AC-LGAD sensor design was updated, reducing the baseline size from approximately 8 × 5 cm^2 to 4 × 5 cm^2 to improve timing performance and manage higher particle rates. A new prototype sensor layout was submitted for tape-out in February 2025, featuring a variety of strip lengths, pitches, and electrode widths to optimize capacitance, noise, and spatial resolution. In parallel, the LATRIC readout ASIC was finalized and submitted for tape-out in April 2025, integrating all main functionalities. Mechanical and thermal simulations were also updated, confirming stable operation under a heat flux of 300 mW/cm^2.

Comments

- C-A-5-3: The latest submission of the redesigned AC-LGAD sensor marks a key step toward determining the optimal strip geometry and layout for the OTK system. By systematically varying strip length, p-well doping, electrode width, pitch, and implementing isolation structures (e.g., trenches) to reduce capacitance, this prototype will provide crucial data to balance timing resolution, position resolution, power dissipation, and occupancy, ensuring the final design meets the stringent performance and rate requirements of the CEPC detector.
- C-A-5-4: The LATRIC ASIC is a critical demonstrator, consolidating all essential functionalities required in the OTK readout chain into a single chip. It includes a low-jitter analog frontend, clock generation via PLL, coarse-fine TDCs, internal calibration circuits, and a data readout architecture with serializer and control interfaces. Its successful validation will be essential to confirm the feasibility of a compact, low-power, fully integrated readout solution for the AC-LGAD-based OTK system

Recommendations

- R-A-5-3: To fully exploit the potential of this design iteration, it is strongly recommended to conduct exhaustive performance characterization of the newly submitted AC-LGAD sensors in test beams. These studies are critical to experimentally validate the effects of strip length, pitch, electrode width, n^+-well doping, and isolation structures on timing and position resolution, power dissipation, and occupancy. Given the importance of timely feedback 9 and the current unavailability of the LATRIC ASIC, it is advised to perform these measurements using fast discrete amplifiers until the LATRIC ASIC becomes available.

Following the submission of the new AC-LGAD prototype in March 2025, we are actively preparing the test setup for comprehensive sensor characterization. Once the sensors are received from tape-out, we will perform a series of measurements using radioactive sources and laser systems. To fully evaluate sensor performance, our dedicated team has a plan to carry out thorough assessments, including test beam studies.

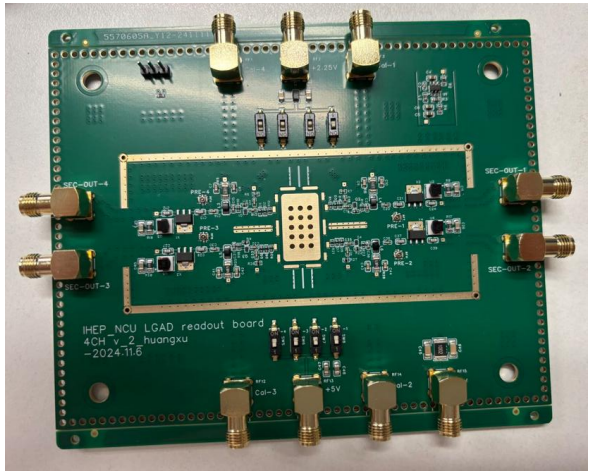

- 4-channels readout boards has been fabricated for AC-LGAD testing
- 2-stage amplifiers, Gain~70
- Signal shape has significantly improved, showing no oscillations.

Recommendations

OTK

- R-A-5-4: The collaboration should continue evaluating other LGAD sensor options and should closely follow novel developments, particularly the trench-isolated DC-LGADs currently under investigation by the team.

We are open to exploring various LGAD sensor options to achieve high performance through the optimization of spatial resolution, timing resolution, and power efficiency. Trench-isolated LGADs are particularly important, as the isolation structure reduces sensor capacitance and thus lowers power consumption. In addition to the LGAD prototype submitted in March, as previously reported, we are currently preparing another tape-out that includes trench-isolated designs with both DC- and AC-coupled variants. We will continue to closely follow ongoing developments and conduct detailed evaluations to identify the most suitable sensor technology for our application.

Recommendations

- R-A-5-5: It is recommended to ensure that the LATRIC ASIC is made available for sensor bonding as early as possible to enable realistic and fully representative characterization of the AC-LGAD sensor performance. Integrating the final readout ASIC with the sensor is crucial to obtaining accurate estimates of timing, position resolution, and power consumption. Given the critical role of the OTK in correcting space charge distortions in the TPC, it is essential that the OTK be robustly designed with service granularity in mind, exploring all known failure modes and developing strategies to mitigate them.

We are fully aware of the critical importance of the LATRIC ASIC, as it is essential to the success of the OTK. Our ASIC team, which includes several senior designers, has made substantial efforts to ensure the reliable and timely delivery of functional chips. The development process is carefully planned and regularly reviewed, with ongoing technical discussions to track progress and resolve challenges. All efforts are focused on accelerating the design and verification phases, so that the ASIC can be made available in a timely manner for sensor bonding and realistic performance characterization.

Comments from Ivan on Draft v0.4

- C-B-5-1: Concerning the chapter organization, this is significantly improved, facilitating the reading. The ITK and OTK dedicated sections now share the same subsection structure (design,electronics, mechanics, sensor technology and ASIC, and future plans); they also cover the important aspects of alignment, background estimations, and performance. As mentioned, the removal of the alternative sensor technologies for ITK and OTK has greatly improved the draft's readability.

Your suggestions have greatly improved the clarity and organization of our paper. We appreciate your positive feedback on the chapter structure and the revisions implemented.

Comments from Ivan on Draft v0.4

- C-B-5-2: The remaining content is very similar to the previous version; I noticed that the background hit rates are now lower than those presented in April's version, and the major missing part remains the definition of an approach to tackle the TPC performance degradation due to ion back-flow, but this will likely require considerably more time to address.

We are actively studying and improving the shielding design to reduce beam induced background. Since the last review, we have updated the MDI shielding design, which has enabled us to achieve a further reduction in background levels. In response to the referee's suggestion, we have added Section 6.3.2 (Ion back flow suppression), which outlines our proposed approach to mitigate ion back-flow effects in the TPC.

TPC

Findings

- The Time Projection Chamber (TPC) with pixelated micro-pattern gaseous detector readout has been chosen as the baseline for the central tracker. It offers continuous 3D tracking with minimal material budget over a large volume and provides particle identification (PID) capabilities. This is a solid and well-justified choice for the Reference TDR, building on extensive past TPC experience at lepton colliders and more recent developments from ALICE, the LCTPC, and DRD1 collaborations. Several technological advances have recently been achieved; notably, a novel ultra-light QM55 carbon fiber material is now used to construct the TPC cylinder.
- However, realizing the TPC as the tracker will require further significant efforts, particularly in mechanical design, structural integrity, and achieving uniform magnetic field conditions (see also the comments and recommendations in the Magnet chapter). Full simulation and digitization tools, based on the software framework and reconstruction algorithms, have been developed and must now be used to produce an updated set of performance plots (e.g., separation power plots).
- The possibility of using a drift chamber as an alternative tracking option is also presented in the TDR.

Finding on Draft v0.4.1

- The Barcelona version of the TPC chapter shows clear progress in terms of section organization and clarity compared to the previous drafts:
  - The overall structure is improved, with more logical sub-sections and better-defined description flow;
  - The mechanical design aspects (inner/outer cylinders and support structures) are more consistently described;
  - There is a better introductory explanation of the role of the TPC as the central tracking detector and its importance for the PID performance;
  - Prototype development efforts are more explicitly referenced, including pad readout, based on micro-pattern gas detector studies;
- These editorial and content enhancements are really appreciated and help to bring the chapter into more advanced stage. However, several technical issues raised in the previous review remain (partially) unresolved or are addressed only qualitatively.

Comments

- Since the IDRC 2024 review, significant progress has been made in the simulation of space charge distortions. For CEPC Higgs and low-luminosity Z runs, the maximum distortions after 3 meters of drift were found to be approximately 10 μm and 150 μm, respectively. Nevertheless, these figures require further verification, and careful evaluation of beam-related background effects must continue. In the longer term, dedicated simulation efforts are needed to develop and refine a "data driven" approach for extracting space-charge corrections, based on the alignment and correction models developed for the ALICE TPC

- Clarify target performance: For each open topic (e.g., ion backflow, pad size), provide the expected performance goals (e.g., maximum tolerable distortion, acceptable ion backflow level, target spatial resolution) that guide the ongoing design effort;

- The simulations and analysis of beam-induced background in the TPC have been continued with some collaboration (KEK, DESY). The low-energy photons (MeV) are the main source of positive ions in the TPC, both in the Higgs and low luminosity Z modes. The space charge density in the CEPC TPC is only about 1/60 of the ALICE TPC in the Higgs mode if the ion-backflow (IBF) can be suppressed to the primary ion level. Some optimization strategies are proposed to further reduce the backgrounds.
  - Reducing the beam lost rate.
  - Added shielding after the lumiCal.
  - Added a dedicated distortion correction in the section of Calibration and Alignment

Comments

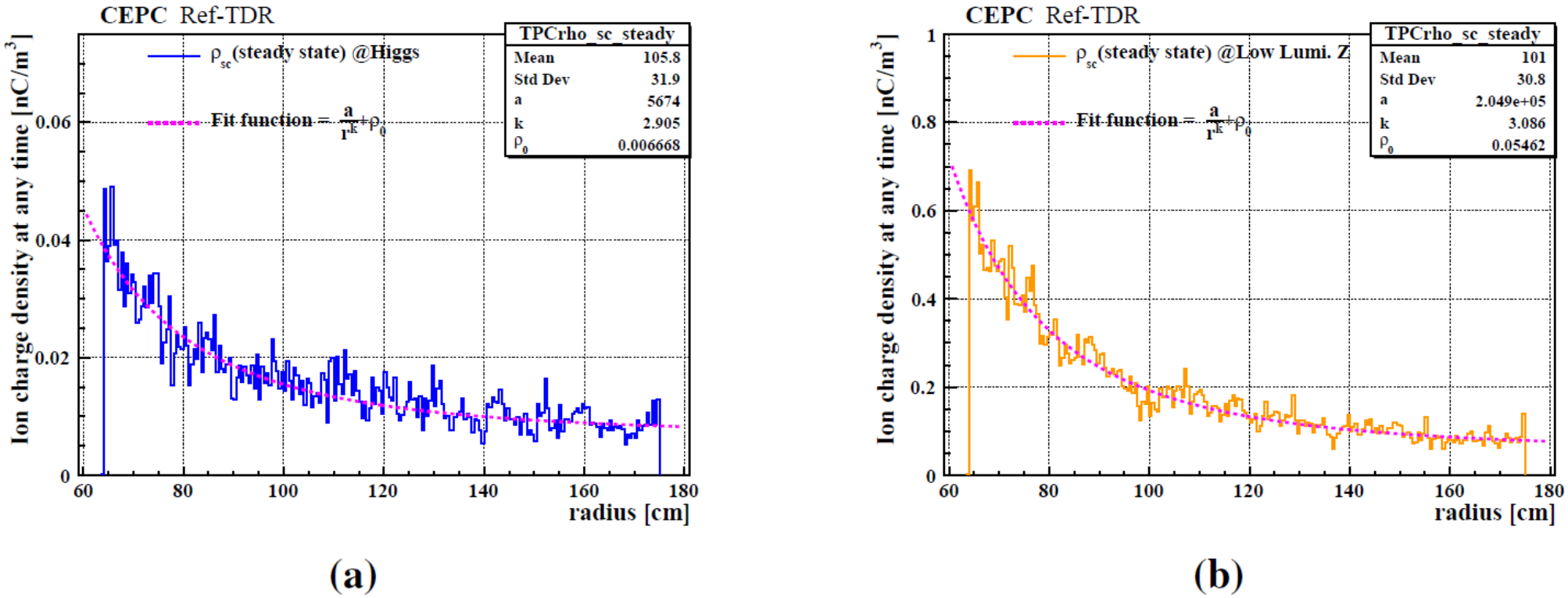

Figure 6.21: Charge density in the TPC as a function of radius (average in φ and z direction already) and fitted by an empirical Equation 6.2, (Magenta dashed line in the plots). (a): *H* mode (b): Low luminosity *Z* mode.

Comments

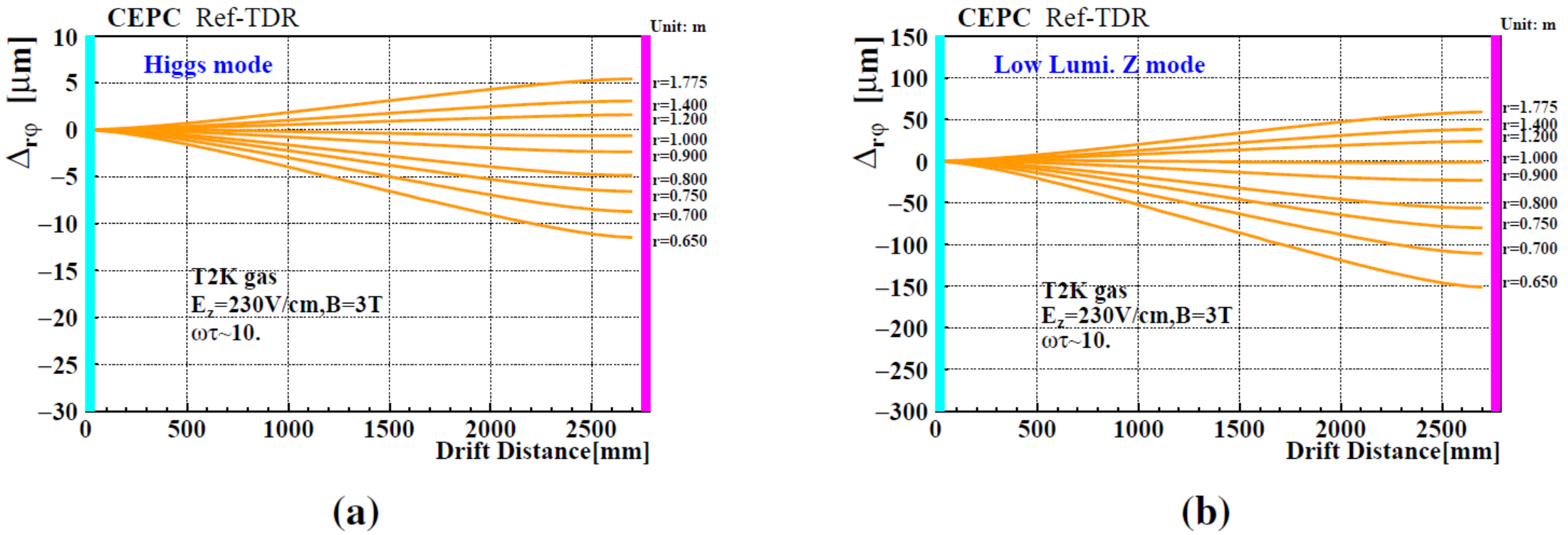

Figure 6.22: Azimuthal distortions as functions of drift distances at the CEPC *H* mode (a) and low luminosity *Z* mode (b) (without ≤ 10 MeV low energy photons). Each orange solid line represents distortions in azimuthal direction at different radii.

Comments on Draft v0.4.1

Space-Charge Distortion and Ion Backflow

- The chapter still lacks a quantitative description of space-charge distortion and its impact on tracking;
- The description of space-charge distortion and its impact on tracking have been added in the subsection of 6.3.2.4 (TPC space distortions estimation). The detailed R&D of its impact on tracking will do in next steps.

- There is no indication or explanation of how correction strategies (e.g., ALICE-like data-driven approaches) can be implemented, at least qualitatively;
- The brief description of the correction strategies have been added in the subsection (Calibration and alignment).

Comments

6.3.4 Calibration and alignment

During the data taking, many factors have negative impact on the TPC performance, including space-charge distortion, change in gas properties due to temperature and pres-

The track based calibration is essential for achieving high-precision calibration of drift velocity and correction of space-charge distortion. With the CEPC tracking system, charged tracks can be reconstructed with very high precision by combining both the inner and outer silicon trackers (ITK and OTK), which provides significant advantages for the TPC calibration. Bhabha events can be used for the TPC calibration. Based on the full track reconstruction, the charged track can be refit excluding the measured TPC cluster, to provide a reference for the spatial position correction of the TPC cluster, following the approach used in ALICE TPC calibration [35]. Through analysis of a large statistics of events, a three-dimensional function between the drift time and space point can be derived. The function will be saved in the calibration database and applied in the final data reconstruction. Monitoring of data quality will be performed throughout the data taking period to facilitate prompt calibration updates.

Space-point calibration of the ALICE TPC with track residuals

Marten Ole Schmidt[1,*] for the ALICE Collaboration
[1]Physikalisches Institut, University of Heidelberg, Germany

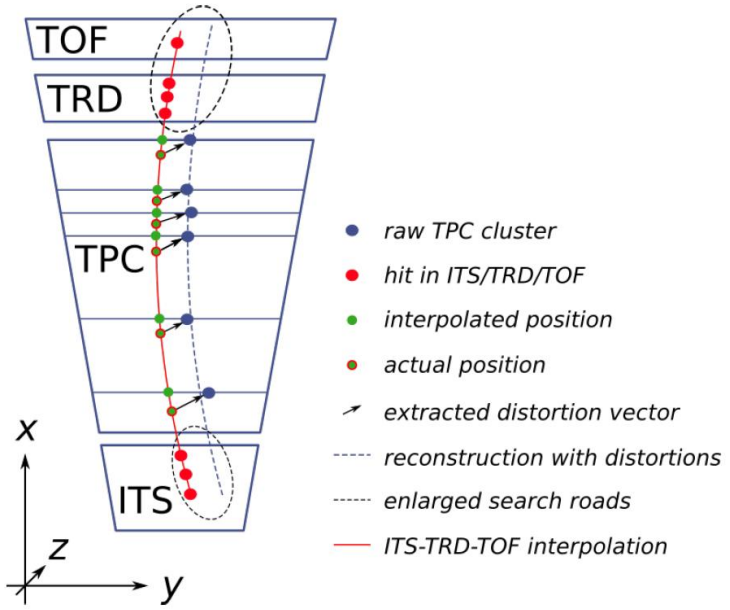

https://doi.org/10.1051/epjconf/202024501003

Comments

- The choice of the pixel readout chip (TEPIX) with a 500 × 500 μm² pixel size is currently driven by power consumption considerations. A TPC module prototype with 10 × 300 readout channels (using 24 TEPIX chips) has been developed and is planned for beam testing at DESY in 2025. Larger prototypes will need to be developed and tested during the EDR phase. Optimization of pad size and gas mixture must be finalized, clearly distinguishing between the digital pixel readout case and the pad readout case. These two approaches lead to distinctly different electronics requirements, particularly regarding the need for analog-todigital conversion in the pad case.

- Within the framework of the LCTPC and CERN DRD1 international collaboration, our research group has booked a beam test at the DESY Institute in Hamburg, Germany, scheduled for November 2025. We will use a 5 GeV electron beam to test the performance of a TPC prototype, providing solid experimental evidence for the existing pixelated readout, The functions of the analog-to digital conversion and digital readout mode have been started to do R&D in our collaboration group. The full size prototype will be considered also.

Comments

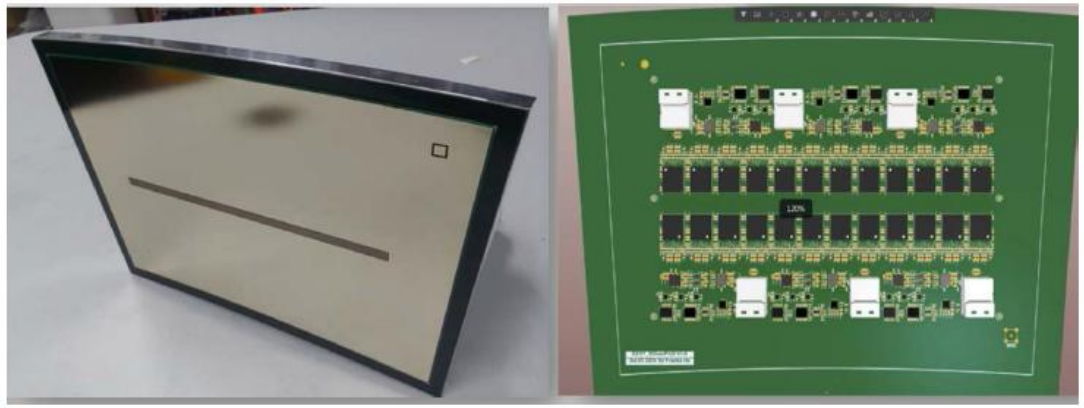

Figure 6.17: Prototype of the TPC readout detector module. The FEE for a single module has been described in the endplate design.

Using the prototype of TEPIX chip, a 32 × 32 pixel-array interposer prototype has been developed to integrate the readout TEPIX chips to the charge-collecting pixels (pixel size: 500 μm × 500 μm). Figure 6.17 illustrates the prototype of the readout detector module after integration of the Micromegas detector and the FEE. The prototypes developed by the other groups achieved smaller 55 μm × 55 μm granularity[21, 22]. The the total power consumption is excessive and would require a cooling beyond the capacity of a water cooling system.

Table 6.6: Test results of the TEPIX chip using 180 nm process.

Parameters	Test results
Number of channels	128
ENC	300 e^-
Dynamic range	25 fC
Integral Non-linearity (INL)	<1%
Time resolution	10 ns
ADC	10 bit
Time-To-Digital Converter (TDC)	14 bit
Total power consumption	0.3 mW/ch

Comments

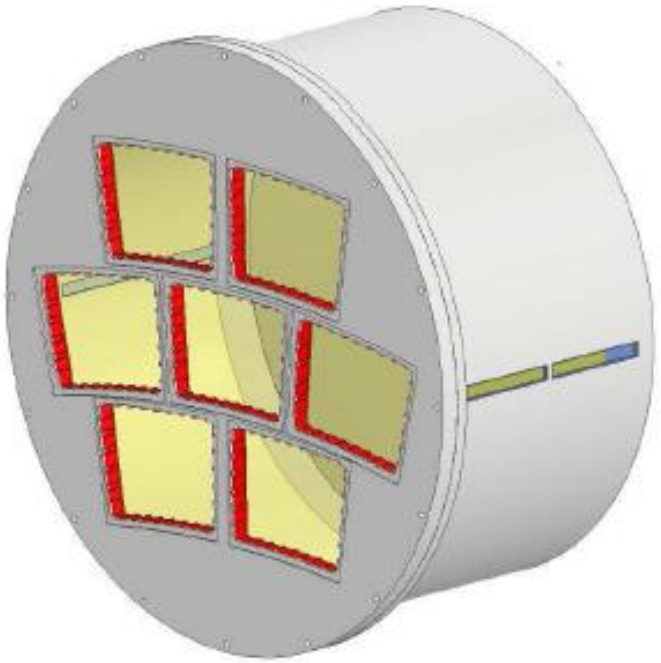

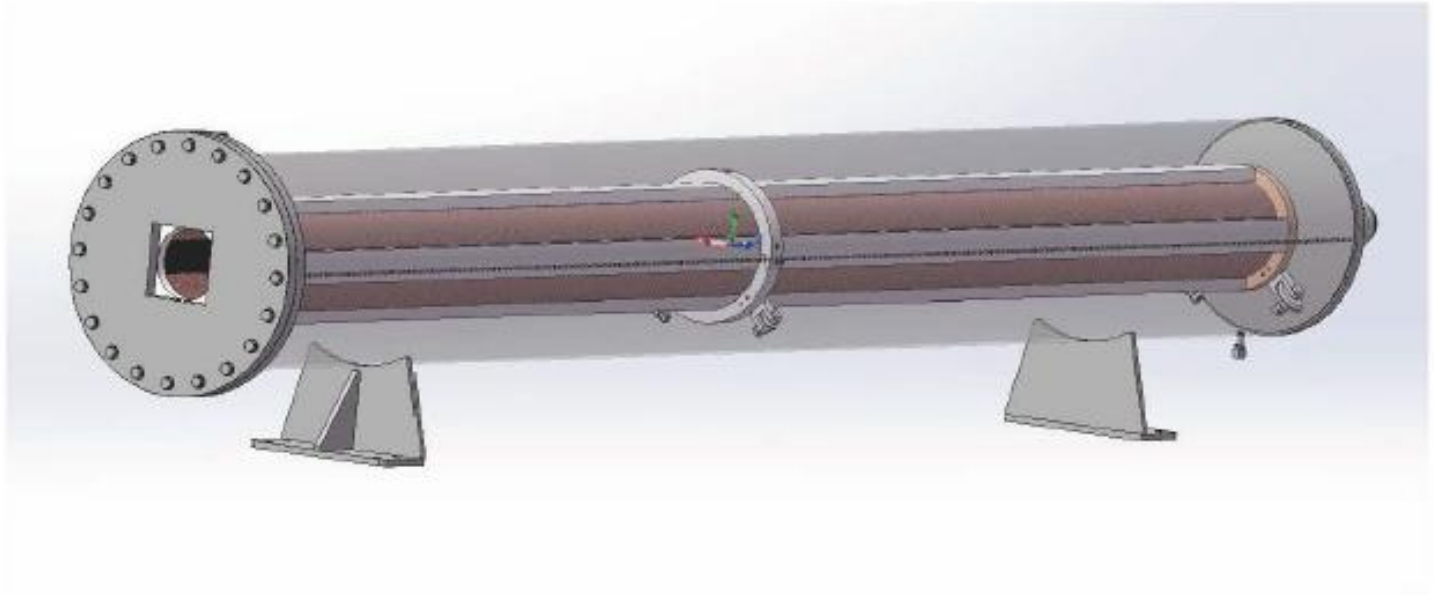

Study of the TPC prototype assembled with seven modules using UV laser and cosmic rays, the module size is same as the TPC module in TDR (Left). The prototype of the 2.9m full-length TPC is primarily designed to study the electric field and the electron drift (Right).

Comments

- If the alternative drift chamber option is pursued, it will be necessary to identify a hydrocarbon free gas mixture that maintains the required performance characteristics

- Thank you for the suggestion. Some updated simulations and optimizations of the gas mixture will be carried out beyond the TDR of CEPC , and the recycle gases system will be considered.

6.5 Alternative Solution: Drift Chamber

A drift chamber (Drift Chamber (DC)) has been designed as an alternative gaseous detector [39]. Its preliminary design specifies a 5800 mm total length and a radial span from 600 mm to 1800 mm. The inner wall is formed by a carbon-fiber cylinder, while the outer support comprises a carbon-fiber frame with eight longitudinal hollow beams and eight rings, all enclosed within a gas-tight envelope. To withstand the cumulative wire tension with minimal deformation, the aluminum end plates adopt a multi-stepped, tilted profile. In total, the chamber holds about 64 wire layers. To fulfill both PID and momentum-measurement requirements, full simulations dictated an 18 mm × 18 mm cell size. Each cell encloses a central 20 μm gold-plated tungsten sense wire, surrounded by eight 80 μm gold-plated aluminum field wires arranged in a square lattice. A 90% helium (He) plus 10% isobutane (iC_4H_{10}) gas mixture achieves the target primary-ionization density for dn/dx measurements.

Recommendations

- The structure of the TDR chapter needs better definition and further consolidation; some figures presented during the review must be updated in the document.

The structure and content of Chapter 06 have been updated within the CEPC community. The new version has been updated in the document.

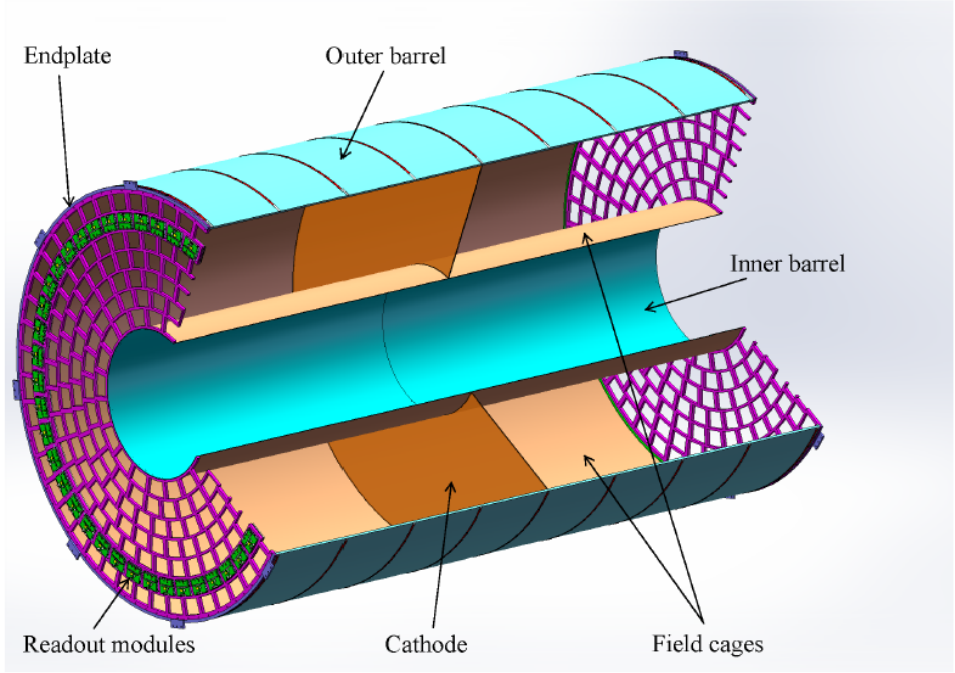

Figure 6.1: The TPC is as a cylindrical, gas-filled tracking device whose axis coincides with the nominal beam direction. The barrel encloses a field cage assembly that produces a uniform electric drift field along the Z-axis. Two readout endplates mechanically support the barrels, while the central cathode plane is positioned at the barrel's mid-plane.

Recommendations

- The updated results of FEA have been added in the document.

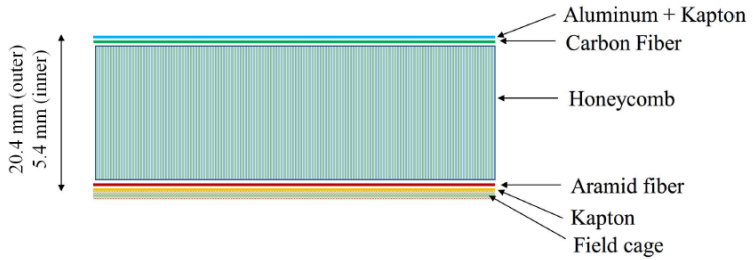

Figure 6.2: Structure of the TPC inner and outer cylinders, the Nomex honeycomb core is embedded between the carbon fiber layer and aramid paper layer, forming a light, rigid and gas-tight structure, with sufficient insulation between the the field cage and Faraday cage.

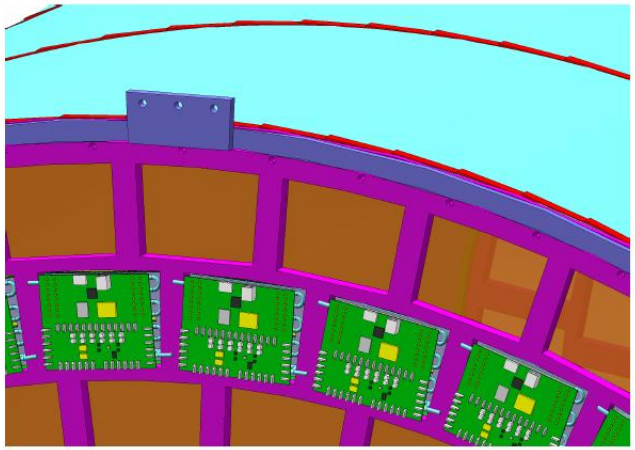

Figure 6.6: Examples of the readout modules installed on the endplate. Each endplate will be equipped with 248 individual detector modules.

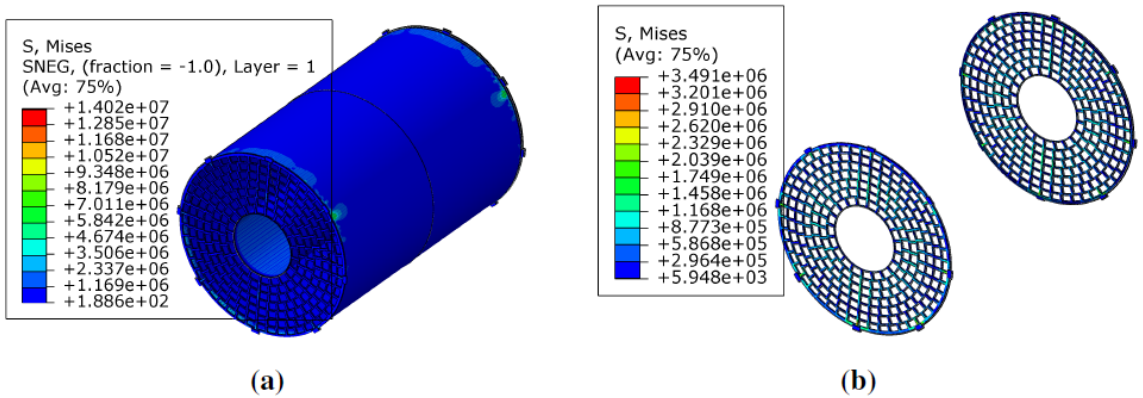

(a) (b)

Figure 6.8: The TPC von Mises stress contour plots based on FEA. Units are in Pa. (a) Stress in the barrel, (b) Stress in the Endplates. The maximum stress in the endplate is 3.5 Mpa, and the maximum stress in the barrel is shown as 14 Mpa at the connection between the barrel and the endplates, which is mainly caused by stress singularity, and the actual stress should be less than this value. Further detailed analysis will be conducted.

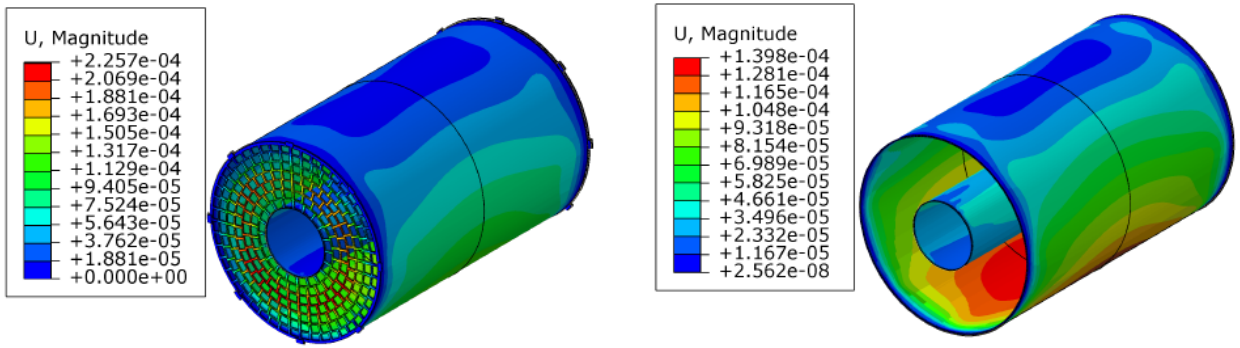

(a) (b)

Figure 6.9: The TPC deformation contour plots based on FEA. Units are in meter. (a) Deformation of the whole structure, (b) Deformation of the barrel. The maximum deformation of the whole structure is 226 μm, located at the endplates, and the maximum deformation of the barrel is 140 μm, located at the bottom of the outer cylinder.

Recommendations

- The updated figures of the field cage and detector module have been added in the document.

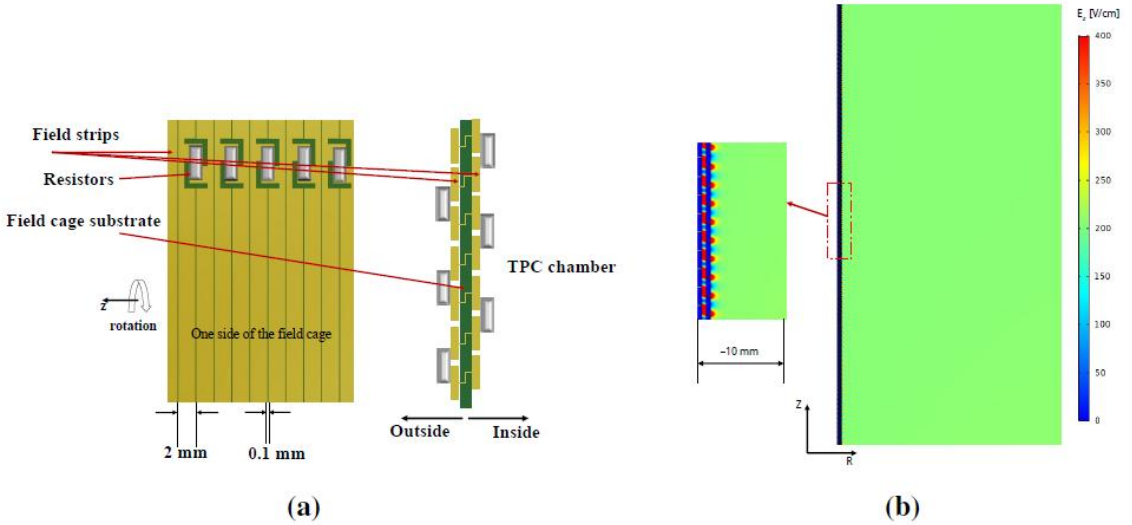

Figure 6.3: Design of the field cage. (a) Layout of double-layer copper strips with 2 mm width and 0.1 mm gap. (b) Finite element simulation result of drift electric field E_z of the double-layer field cage.

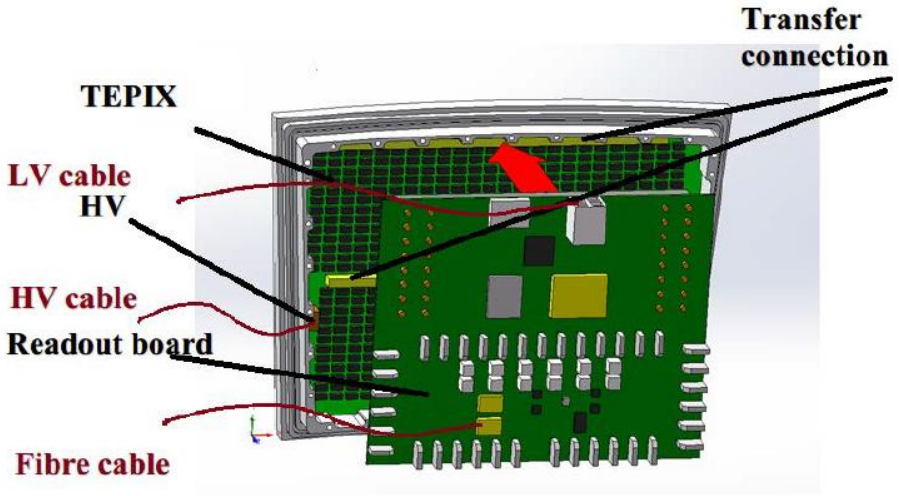

Figure 6.7: Design of the TPC endplate readout modules. Each module is mainly composed of a double-mesh Micromegas detector with a pixelated readout anode, a readout ASIC chip array mounted on the back of the anode board (FEE), and a readout board connected to the FEE board.

Recommendations

- The updated water cooling of the detector module and endplate have been added in the document.

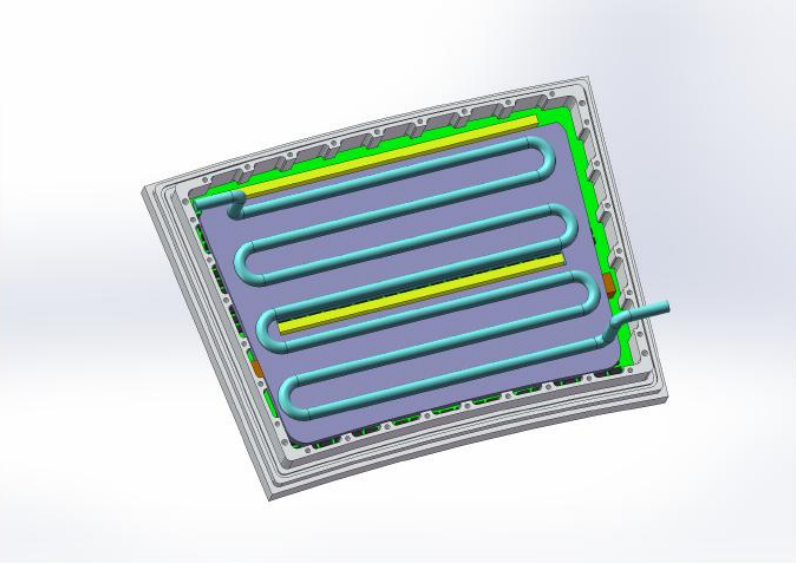

Figure 6.13: Schematic of the cooling scheme for a single readout module: a water-cooled plate with one inlet and one outlet tube is thermally coupled to the ASIC side. Two yellow interface pieces establish the mechanical and electrical connection to the readout board.

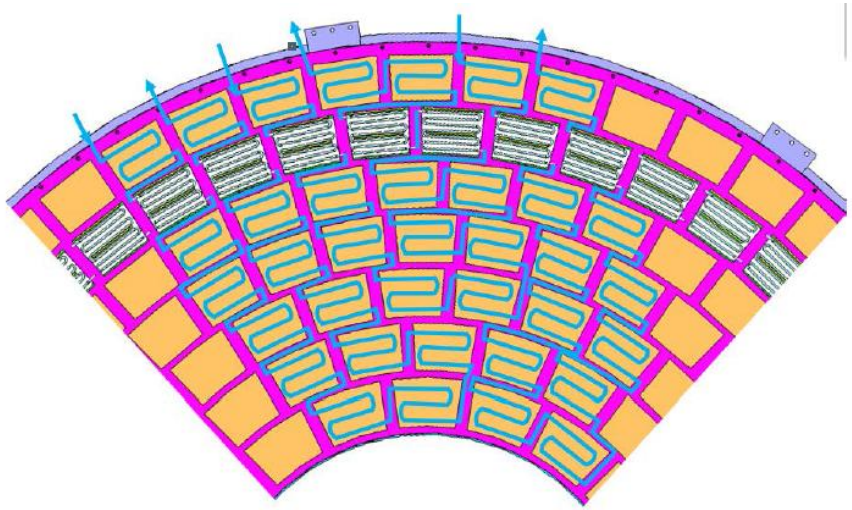

Figure 6.14: Schematic of cooling pipe routing scheme for one-sixth endplate sector. The sector contains three independent cooling circuits, and each circuit is connected in series to about 14 readout detector modules.

Recommendations

TPC

- Ion backflow during operation in low-luminosity Z-mode remains the primary concern. Further simulations of TPC space-charge distortions induced by beam-related backgrounds are necessary to optimize the Machine-Detector Interface (MDI). New module prototypes implementing advanced ion suppression techniques (e.g., double-grid structures or graphene layer coatings) should be studied. Mitigation strategies (e.g., double GEMs, gating grids, graphene coating) are mentioned, but not developed or prioritized for future studies;

- Acknowledge open issues: clearly define which aspects of the TPC design (e.g., ion backflow mitigation, space-charge correction, gas mixture optimization) are still under investigation, and describe the R&D or simulation path that will be followed to finalize these aspects at the next stage;

- The description of the IBF strategies has been added in the subsection 6.3.1.2 (Ion back flow suppression).
- In the design, the double mesh Micromegas has been designed as the baseline.

- After detailed discussions with Prof. Imad, we have explored the potential of graphene technology to control positive ion feedback. This exploration involved researching graphene membrane conversion technology and engaging with various institutions. Specifically, we have initiated collaborative research efforts with Shandong University, CEA-Saclay, Lyon University, the University of Bern, and CERN. These collaborations aim to leverage the unique properties of graphene to mitigate positive ion feedback, thereby enhancing the performance and reliability of our detectors.

Recommendations

- The updated double meshes Micromegas of the detector module have been added in the document.

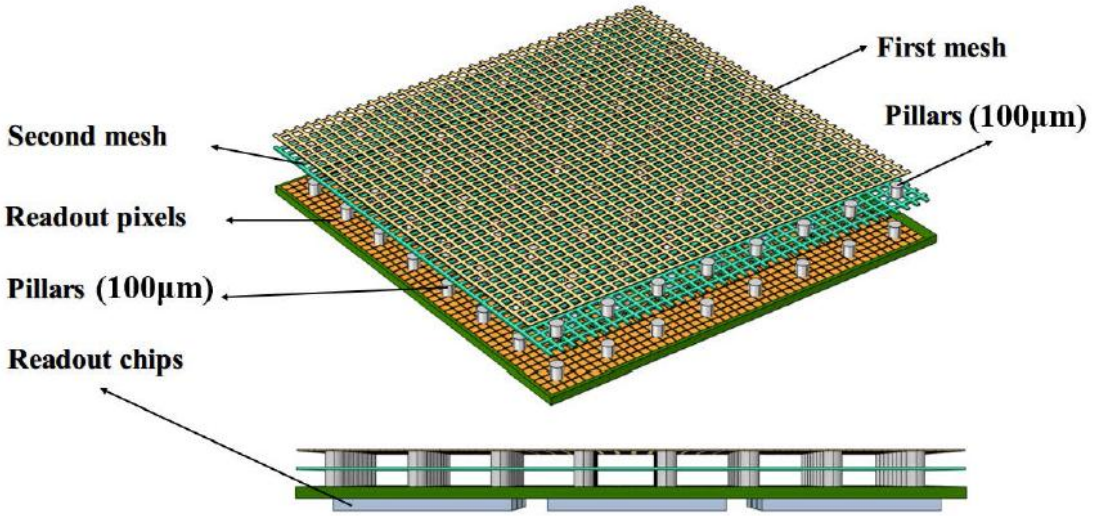

Figure 6.12: Conceptual drawing of the readout panel as viewed from the chamber side. The first mesh serves as the ion-back-flow barrier to suppress positive ions. The second mesh is positioned over the pilars on the multi-chip interposer (light blue) as the Micromegas detector. The interposer routes the charge collected on the pixels to the readout ASICs on the back of the interposer. One ASIC connects to 256 pixels.

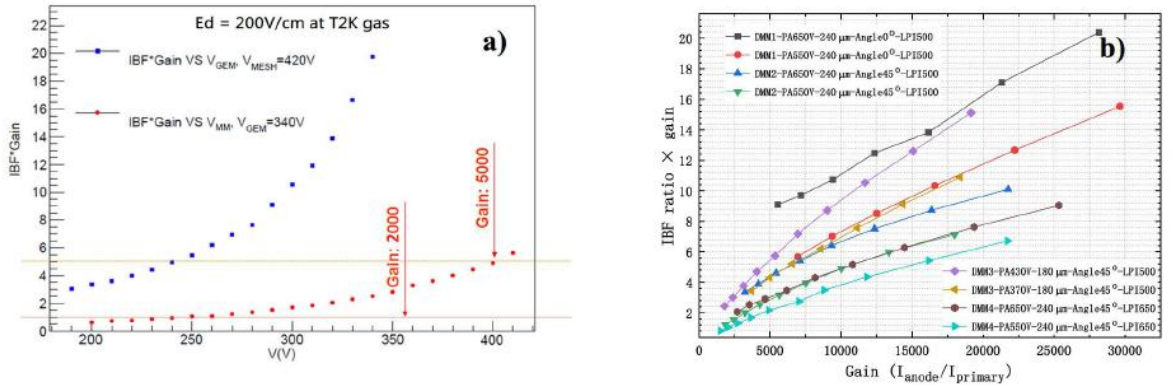

Figure 6.18: Results of the Ion back flow suppression. a) Using the hybrid structure detector (GEM as the pre-amplifier integrate with the Micromegas detector). The X-axis represents the operating high voltage of the Micromegas detector, and the IBF × Gain is approximately 1 at the gain of about 2000 [23]. b) Using the double meshes structure detector (the pre-amplification mesh integrate with the Micromegas detector). The X-axis represents the gain of the Micromegas detector, and less than 1 of the IBF × Gain is achieved at the gain of about 2500 [24].

Comments on Draft v0.4.1

Gas Mixture and Ion Backflow Suppression

- No clear indication about choice of gas mixture is presented. Therefore, the interplay between gas properties, backflow suppression, and long-term stability cannot be sufficiently discussed.
- The detector baseline operating gas is the T2K mixture, chosen for its high drift velocity and low diffusion.
- Next R&D stage, we will carry out gas-mixture optimization, circulation-system design, and long-term stability studies.

Table 6.1: Critical parameters of the TPC tracker

TPC detector	Key Parameters
Modules per endplate	248 readout modules
Potential at cathode	-62,000 V
Gas mixture	T2K: $Ar/CF_4/iC_4H_{10}$ = 95/3/2
Maximum drift time	34 μs
Cooling	Water cooling circulation system
Detector modules	Pixelated readout Micromegas

Recommendations

- The updated graphene R&D of the detector module have been added in the document.

6.6 Summary and Future Plan

In this chapter, a gaseous TPC tracking detector scheme with a pixelated readout is presented. The details of the TPC design, including the chamber geometry, field

In the forthcoming IBF study plan, a monolayer of graphene can also endure a pressure differential of one atmosphereand exhibits thermal stability, making it particularly suitable for use in TPC detectors to suppress ion back flow. The transmission rate of electrons with energies below 20 eVthrough graphene has been studied. The first priority is to integrate graphene with a mesh structure to reduce the IBF. These investigations will be carried out in collaboration with CEA-Saclay, Lyon University and NIKHEF.

Within the framework of the LCTPC and European Organization for Nuclear Research (CERN) Detector R&D (DRD)1[44] international collaboration, our research group has booked a beam test at the DESY Institute in Hamburg, Germany. We will use a 5 GeV electron beam to test the performance of a TPC prototype, providing solid experimental evidence for the existing pixelated readout. Among the sub-detectors, the feasibility study of TPC tracker detector was launched, with the goal of identifying viable technology

Comments on Draft v0.4.1

Tracking Performance and Simulation

- There is no significant update on spatial or momentum resolution, dE/dx performance, tracking efficiency, or fake rate studies;
- Simulation plans: Summarize how future simulations will validate TPC performance in full physics conditions (e.g., displaced vertices, Z-mode operation), if feasible;
- The update description on spatial or momentum resolution, dE/dx performance and tracking efficiency has been added in the subsection 6.4.3 (Spatial resolution and momentum resolution).
- Particle-identification research based on machine learning has already begun.

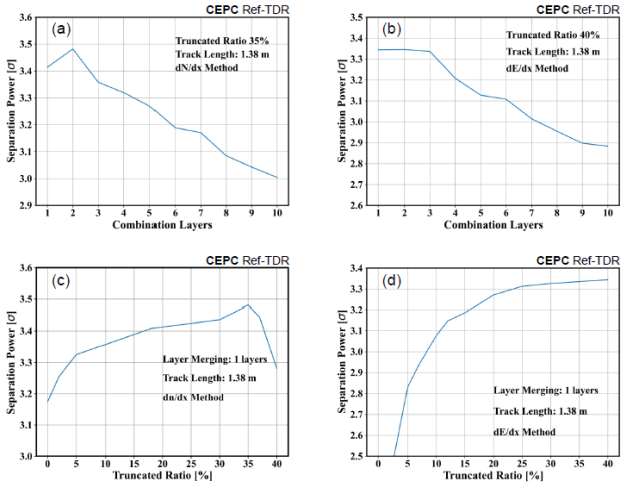

Figure 6.30: Optimized PID performance of dn/dx and dE/dx algorithms: (a) dn/dx with 35% truncation achieves optimal π/K discrimination at 2 layers; (b) dE/dx with 40% truncation performs best at 1 layer; (c) dn/dx shows optimal 35% truncation at fixed 1 layer; (d) dE/dx confirms best performance at 40% truncation (1 layer).

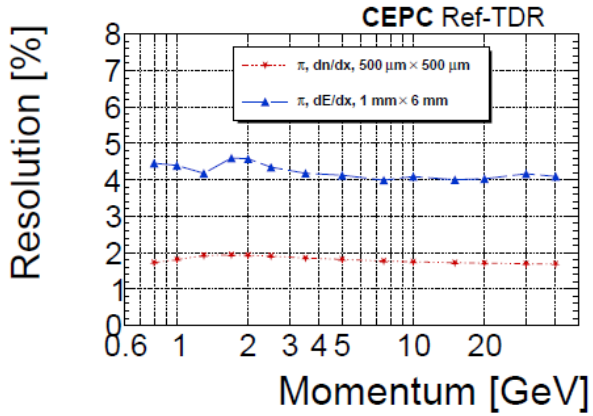

Figure 6.31: Resolution of dn/dx with 500 μm × 500 μm pixelated readout (red dotted line with stars) and dE/dx with 1 mm × 6 mm pad readout (blue dashed line with triangles) as a function of momentum for charged pions with an polar angle of 60°.

Comments on Draft v0.4.1

- Performance plots, especially in conjunction with the ITK/VTX system, are missing or remain in a preliminary stage;
- The update description of the performance plots in conjunction with the ITK/VTX system has been added in TDR document.

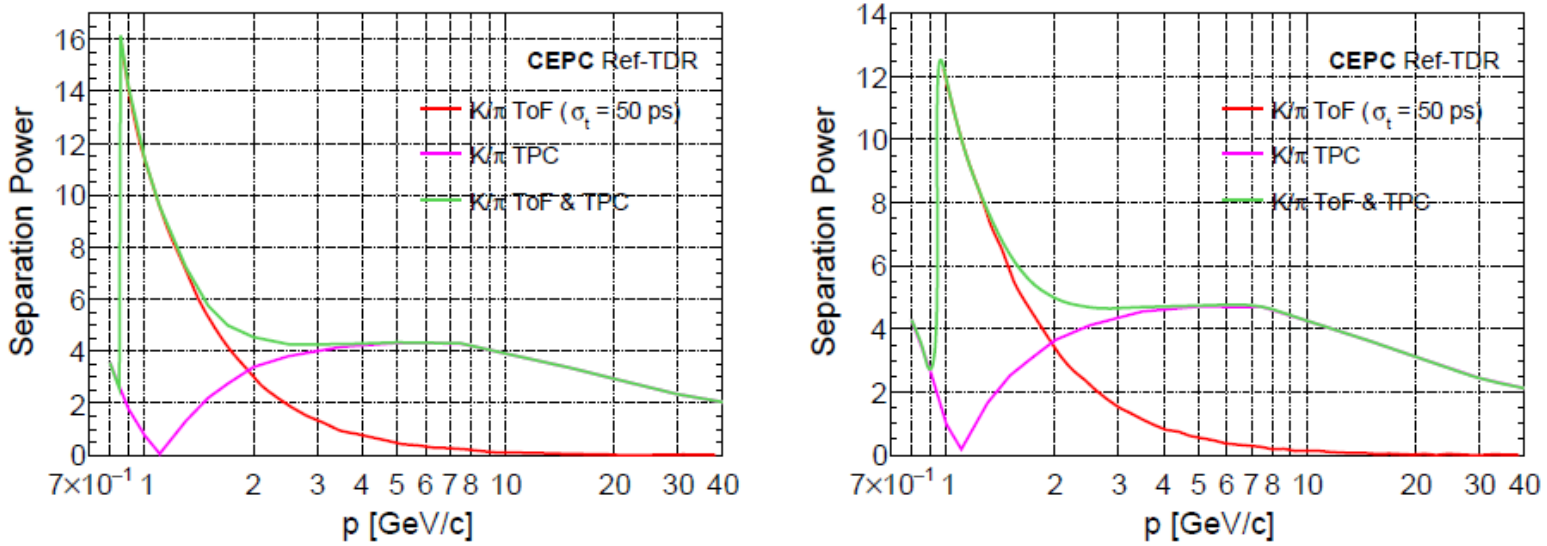

(a) $\theta = 85°$ (b) $\theta = 60°$

Figure 6.33: Separation power between K and π as a function of momentum, at the polar angles (a) $\theta = 85°$ and (b) $\theta = 60°$. The red lines, pink lines, and green lines indicate the separation power using only the ToF, only the TPC, and the combination of both, respectively.

Comments on Draft v0.4.1

Pad Size and Readout Architecture

- We understand that the choice between pad and digital pixel readout can not be finalized at this stage and remains uncertain. Still, some comments about the implications in terms of electronics complexity, data volume, and reconstruction performance would be beneficial; The absence of a baseline readout definition introduces uncertainty in downstream systems (DAQ, reconstruction).

- The TEPIX ASIC has undergone performance tests, and the resulting data are considered reliable for reference. Based on the current detector channel count and expected data volume, a complementary description has been added in the DAQ chapter.
- Detector-module R&D is now underway, the next step will use beam-test results to further refine the design and reduce readout-related uncertainties.

Comments on Draft v0.4.1

Pad Size and Readout Architecture

- Readout architecture: While a final decision may not be ready, describe the criteria that will drive the selection of the readout scheme and how each option will be validated. Summarize the impact of this choice on reconstruction, electronics design, and system integration. Clarify what is called a pixel TPC (digital readout) and a pad TPC with ADCs. Quantify power consumption in the two cases and document cluster counting for a digital readout;
- In the studies on TPC module and prototype, the pad readout TPC has been developed using 1mm*6mm pad size. Also a low-power readout ASIC with integrated ADC functionality has already been developed under the WASA chips. In TDR, the readout module is pixel readout detector module.

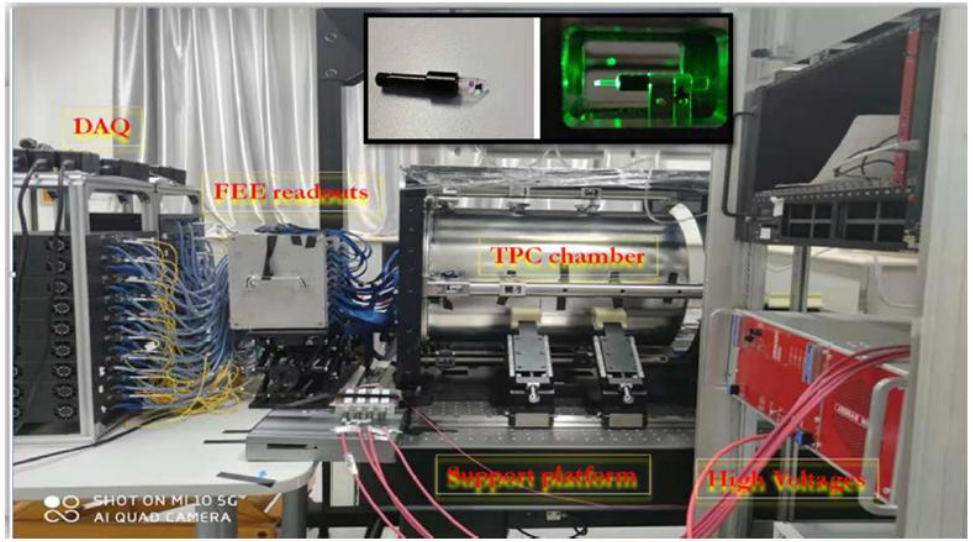

Figure 6.15: A TPC prototype integrated with six horizontal UV laser beams, with a drift length of 500 mm and an effective readout area of 200 mm × 200 mm.

Recommendations on Draft v0.4.1

Editorial additions

- Include a concise summary table linking current detector parameters and technologies to physics requirements. This will help contextualize the design and highlight where validation is still pending;
- Some revision have been updated in this new version chapter. The concise summary table has been updated in the overall detector chapter.

Table 2.1: Physics objects and key observables used as benchmarks for setting the requirements and the optimization of the CEPC detector.

Physics Objects	Measurands	Detector Subsystem	Performance Requirement
Tracking	Coverage Recon. Efficiency Resolution in Barrel Resolution in Endcap	Tracker	$\lvert\cos\theta\rvert \leq 0.99$ $\geq 99\%$ ($p_T > 1$ GeV) $\sigma_{p_T}/p_T < 0.3\%$ ($30^\circ < \theta \leq 90^\circ$) $\sigma_{p_T}/p_T < 3\%$ ($10^\circ < \theta \leq 30^\circ$)
Leptons (e, μ)	PID Efficiency Mis-ID Rate	Tracker, ECAL, HCAL, Muon	$\geq 99\%$ ($p > 5$ GeV, isolated) $\leq 2\%$ ($p > 5$ GeV, isolated)
Photons	PID Efficiency Mis-ID Rate Energy Resolution	ECAL, HCAL	$\geq 99\%$ ($E > 3$ GeV, isolated) $\leq 5\%$ ($E > 3$ GeV, isolated) $\sigma_E/E \leq 3\%/\sqrt{E(\text{GeV})} \oplus 1\%$
Vertex	Position Resolution	Vertex Detector	$\sigma_{r\phi} = 5 \oplus \frac{10}{p(\text{GeV})\times\sin^{3/2}\theta}(\mu\text{m})$
Hadronic Jets	Energy Resolution Mass Resolution	Tracker, ECAL, HCAL	$\sigma_E/E \sim 30\%/\sqrt{E(\text{GeV})} \oplus 4\%$ BMR $\leq 4\%$
Jet Flavor Tagging	b-tagging Efficiency c-tagging Efficiency	Full Detector	$\sim 80\%$, mis-ID of uds $< 0.3\%$ $\sim 50\%$, mis-ID of uds $< 1\%$
Charged Kaon	PID Efficiency, Purity	Tracker, TOF	$\geq 90\%$ (inclusive Z sample)

Recommendations on Draft v0.4.1

- Streamline English and revise references;
- The updated document has been polished.

References

[1] W. B. Atwood *et al.* "Performance of the ALEPH time projection chamber". *Nucl. Instrum. Meth. A* 306 (1991).

[2] C. Brand *et al.* "The DELPHI Time Projection Chamber". *Nucl. Instrum. Meth. A* 283 (1989).

[3] F. Shen *et al.* "MWPC prototyping and testing for STAR inner TPC upgrade". *JINST* 12.06 (2017). Ed. by Lev Shekhtman.

[4] David Rohr. "Tracking performance in high multiplicities environment at ALICE". *5th Large Hadron Collider Physics Conference*. Sept. 2017. arXiv: 1709.00618 [physics.ins-det].

[5] Alain Bellerive. "Studies of Micro Pattern Gas Detector modules of a Large Prototype TPC for the ILC". *PoS* ICHEP2016 (2016).

[6] Purba Bhattacharya *et al.* "Numerical Investigation on Electron and Ion Transmission of GEM-based Detectors". *EPJ Web Conf.* 174 (2018). Ed. by S. Dalla Torre *et al.*

[7] Jochen Kaminski. "TPC development by the LCTPC collaboration for the ILD detector at ILC". *J. Phys. Conf. Ser.* 2374.1 (2022). arXiv: 2203.03435 [physics.ins-det].

[8] Prakhar Garg *et al.* "Compact TPC with TimePix Readout: PID and tracking option for the ATHENA Detector at EIC". *APS Division of Nuclear Physics Meeting Abstracts*. Vol. 2021. 2021, EJ–007.

[9] Prakhar Garg. "GridPIX TPC as a compact PID and Tracking device". *Bulletin of the American Physical Society* (2024).

[10] Maxim P. Titov. "New Developments and Future Perspectives of Gaseous Detectors". *Nucl. Instrum. Meth. A* 581 (2007). Ed. by Josef Hrubec *et al.* arXiv: 0706.3516 [physics.ins-det].

[11] Y. Giomataris *et al.* "MICROMEGAS: A High granularity position sensitive gaseous detector for high particle flux environments". *Nucl. Instrum. Meth. A* 376 (1996).

[12] Mingyi Dong *et al.* "CEPC Conceptual Design Report: Volume 2 - Physics & Detector" (Nov. 2018). Ed. by João Barreiro Guimarães da Costa *et al.* arXiv: 1811.10545 [hep-ex].

[13] Wei Liu *et al.* "WASA: a low power and high integration readout ASIC for TPCs in 65 nm CMOS". *JINST* 19.04 (2024), P04036.

[14] F Faccio *et al.* "Radiation-induced short channel (RISCE) and narrow channel (RINCE) effects in 65 and 130 nm MOSFETs". *IEEE Transactions on Nuclear Science* 62.6 (2015), pp. 2933–2940.

[15] Loukas Chevas *et al.* "Investigation of scaling and temperature effects in total ionizing dose (TID) experiments in 65 nm CMOS". *2018 25th International Conference" Mixed Design of Integrated Circuits and System"(MIXDES)*. IEEE. 2018, pp. 313–318.

[16] Dyi-Chung Hu *et al.* "Embedded glass interposer for heterogeneous multi-chip integration". *2015 IEEE 65th Electronic Components and Technology Conference (ECTC)*. IEEE. 2015, pp. 314–317.

[17] Haiyun Wang *et al.* "Simulation and Investigation of the Gaseous Detector Module for CEPC-TPC". *Springer Proc. Phys.* 213 (2018).

[18] Y. Chang *et al.* "Investigation of the avalanche fluctuations factor in a Time Projection Chamber detector using 266 nm UV laser". *JINST* 20.04 (2025), P04011.

[19] Z. Y. Yuan *et al.* "Performance of TPC detector prototype integrated with UV laser tracks for the circular collider". *Nucl. Instrum. Meth. A* 1040 (2022). arXiv: 2206.02375 [physics.ins-det].

[20] Wei Liu *et al.* "WASA: a low power front-end ASIC for time projection chambers in 65 nm CMOS". *Journal of Instrumentation* 15.05 (2020), P05005.

Comments from Ivan on Draft v0.4

- Anyhow, we may recommend including a subsection in the chapter mentioning the TPC response degradation issue, along with an overall strategy to mitigate it. This addition would send the message to the reader that they are aware of the importance of the issue and are actively working on how to resolve it. This section could be also fit in the TPC chapter, though.

As previously mentioned, we have added Section 6.3.2 (Ion back flow suppression), which outlines our proposed approach to mitigate ion back-flow effects in the TPC. This section explicitly addresses the TPC response degradation issue and our overall mitigation strategy.

ELECTROMAGNETIC CALORIMETER

Findings

- F-A-7-1: The high-granularity crystal ECAL is a recently proposed concept designed to be **compatible with particle flow algorithm (PFA)** reconstruction of jet energy within a **homogeneous** structure. The calorimeter is modular, with the fundamental detection units consisting of long orthogonal BGO crystal bars, read out at both ends by SiPMs.
- F-A-7-2: Achieving high granularity at an affordable cost requires making strategic choices and compromises, guided by specific performance benchmarks. The **team has made steady progress** in understanding the performance and optimizing the performance-cost balance, using the ECAL standalone energy resolution and PFA jet resolution as primary benchmarks.
- F-A-7-3: The baseline granularity was recently updated to 1.5×1.5×40 cm^3, resulting in a significant reduction in the number of readout channels and associated power needs. Simulations indicate that, even with this updated configuration, the calorimeter meets the target requirements for boson-mass resolution and standalone electromagnetic energy resolution. The **overall performance remains excellent**, despite some degradation in π^0/γ identification and two-photon separation; the latter may potentially be recovered through improvements in offline reconstruction methods.
- F-A-7-4: A **full-scale prototype** with the updated granularity is planned. Current simulation studies and experimental results from similar granularities provide confidence that the ECAL performance and component requirements are sufficiently understood, despite limitations in previous test beams due to electron beam spread. The team is also aware of the need for further progress beyond the reference TDR, particularly in **defining QA/QC aspects** for the components.

Recommendations

- R-A-7-1: Continue developing a **full-scale prototype** with the final geometry (using existing readout ASICs) and aim to confirm performance in an electron beam with low momentum spread.

- R-A-7-2: Further **refine calibration strategies** to ensure that necessary stability in transparency, linearity, and uniformity can be achieved in situ, without relying on a dedicated monitoring system.

- R-A-7-3: Advance preliminary engineering of the gaps between modules and fully assess their impact on reconstruction performance.

Feedback to IDRC Recommendations (1)

- R-A-7-1: Continue developing a **full-scale prototype with the final geometry** (using existing readout ASICs) and aim to confirm performance in an electron beam with low momentum spread.
  - Developing a full-scale prototype with the final geometry is planned for near future, by integrating crystals, readout boards (embedded with SiPMs and ASICs), light-weighted mechanics and cooling
    - **Covered in Chapter 16 "Timeline and Plans" (Section 16.2, page 615)**
  - International Collaboration in DRD-Calo (DRD6): subtask of WP3 (i.e. WP3.1.1 HGCCAL)
  - Electron beams with low momentum spreads: a stringent requirement for test beam facilities
    - First ECAL prototype shows EM resolution **better than 2%**, which requires beam momentum spread to be controlled **well below 1%** (or can be measured by tracker + dipole magnet)
  - Test beam facilities
    - CERN PS-T09 is the primary option (with best knowledge and hands-on experiences). Due to the Long-Shutdown 3 (LS3), we will also consider and investigate other options.
    - Options in China: need to investigate synchrotron radiation light sources (e.g. HEPS)
    - Option in Japan: 1-6 GeV electrons at KEK (momentum spreads appear significant, comparable to DESY)
      - DESY 1-6 GeV electron beams: momentum spread measured on the order of 10% at 1 GeV

Feedback to IDRC Recommendations (2)

- R-A-7-2: Further **refine calibration strategies** to ensure that necessary stability in transparency, linearity, and uniformity can be achieved in situ, without relying on a dedicated monitoring system.
  - **Covered in Chapter 7 (Section 7.2.6, page 231-234)** and **in Chapter 15 (Section 15.3.3, page 606)**
  - **Updates in Section 7.2.6 "Calibration and Monitoring"**
    - On-detector calibration: (1) pedestals and noises, (2) **SiPM non-linearity**, (3) channel-wise calibration per ASIC, (4) Beam-Induced Backgrounds
    - Collision data calibration: (1) Bhabha scatterings, (2) $Z \to ee$ decays, (3) π^0 decays, (4) MIPs from muons and "punch-through" hadrons, (5) other decays: $J/\psi \to ee$, $W \to e\nu$, $Z \to \mu\mu\gamma$
    - Calibration precision studies in simulation (Section 7.2.6.3)
    - Detailed calibration scheme on SiPM non-linearity (next page)

Feedback to IDRC Recommendations (2)

- Detailed calibration scheme on SiPM non-linearity effects
  - **Updates in Section 7.2.6 “Calibration and Monitoring”**
  - SiPM non-linearity effects are studied by including SiPM pixel recovery during the relatively slow BGO scintillation time (typ. 300 ns), which further increases the effective number of SiPM pixels (i.e. many pixels can be fired multiple times during this scintillation process)
  - Calibration is first done in an off-detector way, by extracting key parameters related to the SiPM non-linearity effects via the SiPM QA/QC database (e.g. breakdown voltage, interpixel crosstalk, etc.)
  - Apply these parameters to all SiPMs in ECAL after detector assembly and use them for commissioning
  - Use Bhabha events as an in-situ calibration source to monitor and calibrate SiPM non-linearity
- Plans beyond Ref-TDR scope
  - To **validate** the SiPM non-linearity simulation model either using laser or in beam tests
  - To **test batches of SiPMs** for non-linearity calibrations: to extract QA/QC parameters and to validate the proposed scheme mentioned above

Feedback to IDRC Recommendations (3)

- R-A-7-3: Advance preliminary engineering of the gaps between modules and fully assess their impact on reconstruction performance.
  - Engineering designs have been significantly updated in **Section 7.2.5 (page 224-230)**, including readout boards, mechanical structures, cooling pipes and plates
  - EM performance have been updated in **Section 7.3.4 (page 238-239)**
    - An energy-correction algorithm has been developed to correct cluster energy loss in module gaps
    - Incident photons are uniformly distributed around ECAL modules including module gap regions

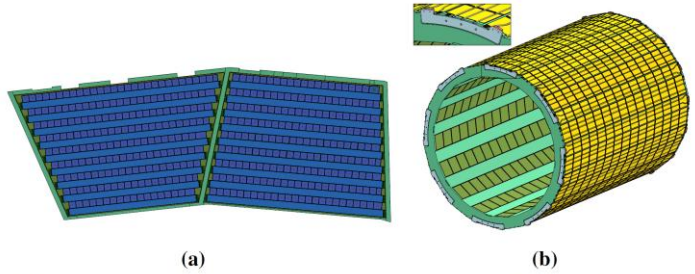

(a) (b)

Figure 7.11: The side view of two types of barrel ECAL modules (a); the stainless steel structure for inter-connecting the ECAL barrel to the barrel HCAL, which are embedded in the main carbon-fiber frame (b). The two module types are named "Type-A" for the trapezoid shape with its shorter side at the bottom and "Type-B" for the trapezoid shape with its longer side at the bottom. Detailed FEA results of the ECAL-HCAL inter-connections are described in Chapter 14 of Mechanics and Integration.

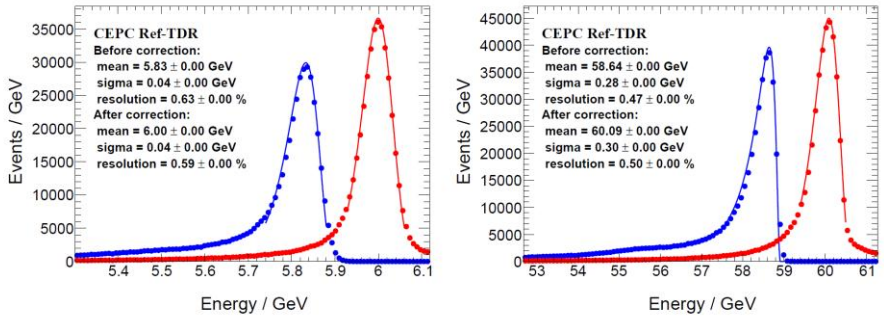

(a) 6 GeV **(b)** 60 GeV

Figure 7.22: Energy deposition of 6 GeV and 60 GeV photon with and without the energy correction. The directions of the photons are $\theta \in [40°, 140°]$ and $\varphi \in [0°, 360°]$.

Feedback to IDRC comments in April (1)

- C-A-7-1: The ECAL standalone energy reconstruction requires an energy threshold of 0.1 MIPs (as shown in Fig. 7.17), whereas the PFA jet reconstruction, based on fast simulation, adopts a higher threshold (Fig. 8.2). The ECAL team acknowledges the need to further develop and refine particle flow algorithms, photon identification at low energies, and π^0/γ separation to fully exploit the calorimeter's potential.
- Feedback
  - Updated CyberPFA for photon reconstruction
    - Descriptions are updated in **Section 7.3.2 (page 236)**
    - Achieved significant performance improvement, esp. in low-energy regions
  - π^0/γ separation: updates in **Section 7.5.1 (page 255)**

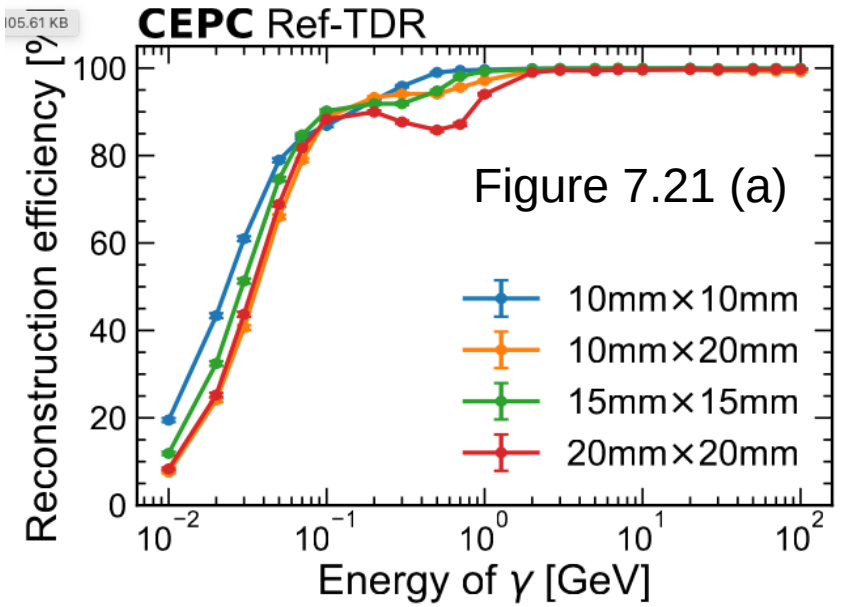

Feedback to IDRC comments in April (2)

- C-A-7-2: The timing specification of 0.5 ns for MIPs was not strongly motivated. This corresponds approximately to the time spread across a full bar and is insufficient to provide significant benefits for event reconstruction. Additionally, the current time resolution analysis appears suboptimal. The team acknowledges that a deeper understanding of timing response and its potential use is needed, although this is not a priority at this stage.
  - Updates in **Section 7.2.1 (page 219)**
  - A good timing resolution was initially motivated by the positioning precision to resolve ambiguities due to the arrangement crossed crystals. But test-beam results of long BGO crystal bars indicate that the timing resolution can not satisfy the positioning precision requirement.
  - Good timing performance (e.g. 0.2ns in EM shower cores) can also be motivated for better performance of PFA clustering, which requires further quantitative studies in PFA.

Feedback to IDRC comments in April (3)

- C-A-7-3: Crystal transparency variations are significant. While progress has been made toward developing a calibration plan using collision events, a quantitative demonstration that the precision and event rates are sufficient for monitoring response evolution across the detector is still missing.
  - Updates in Section **7.4.5.2 (page 251)**
  - BGO crystal transparency variations along with the TID dose was briefly discussed and a reference on TID-transparency measurements was added
  - Further quantitative studies will be performed in simulation and dedicated irradiation R&D studies.
- C-A-7-4: The non-linearity of the SiPMs poses a potential risk to the constant term in the energy resolution. Although compact photon detectors with more linear responses (such as APDs) were noted, SiPMs are preferred for cost and design uniformity reasons. However, SiPMs will require per-channel calibration, and possibly sorting during construction, along with continuous in-situ monitoring and corrections.
  - Updates in Section **7.2.6.1 (page 231)**
  - Key parameters of the SiPM non-linearity curve will be extracted from QA/QC protocols and recorded in database, along with in-situ monitored and corrections using collision data (e.g. Bhabha events).

Feedback to IDRC comments in April (4)

- C-A-7-5: Prototyping with close-to-final components is essential to confirm performance. Using existing readout ASICs can help decouple detector characterization from electronics debugging and allow parallel progress rather than sequential steps.
  - Details in the Feedback to Recommendation 1
  - New: beam tests of the first crystal ECAL prototype were performed at CERN during June-July in 2025, using existing readout ASICs, also with minimum possible materials in upstream at PS-T09 beamline
- C-A-7-6: The committee was pleased to see a substantial effort in understanding the impact of gaps between modules. However, the mechanical design and service layout within the gaps remains sketchy, and some components, such as the cooling plates, could be prone to underperformance.
  - EM performance updated in **Section 7.3.4 (page 238-239)**
  - Details in the Feedback to Recommendation 3 (updated engineering designs and performance results)
- C-A-7-7: From a stylistic perspective, the TDR would benefit from an upfront presentation of the key performance benchmarks and detector specifications, followed by a focused discussion of the performance-cost optimization supported by R&D and simulation evidence. The detailed discussion of alternative options currently in Section 7.2 could be summarized briefly and moved to an appendix.
  - Updates in **Section 7.6 (page 257-258)** : completely restructured, following up the IDRC suggestion

Feedback to IDRC Comments on Draft v0.4.1

- General comment
  - C-B-7-1: There is no mention of separation of showers or individual particle depositions. The parameters mentioned are energy resolutions without mentioning the segmentation (granularity) needed to achieve particle flow performance. We suggest adding mention of needed segmentation or granularity.
- Feedback: **Updates in Section 7.2.2 (page 219-220) and 7.3.2 (page 236-237)**
  - The two-particle separation performance (separation efficiency)
  - The required granularity of 15x15 mm is added in the updated version.

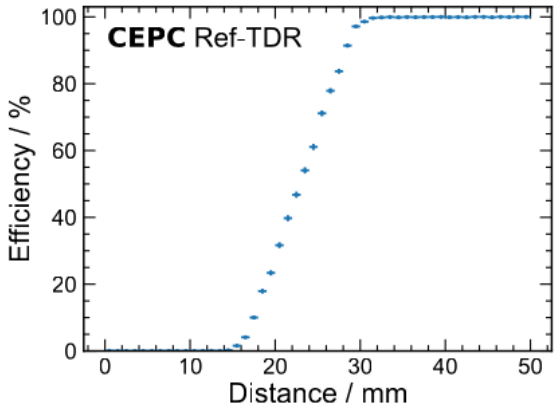

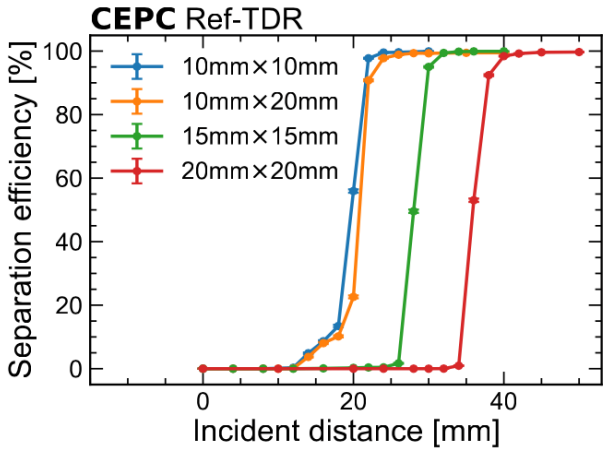

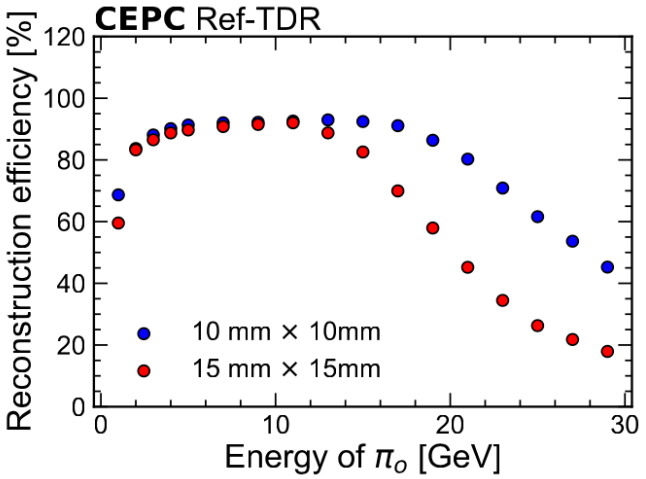

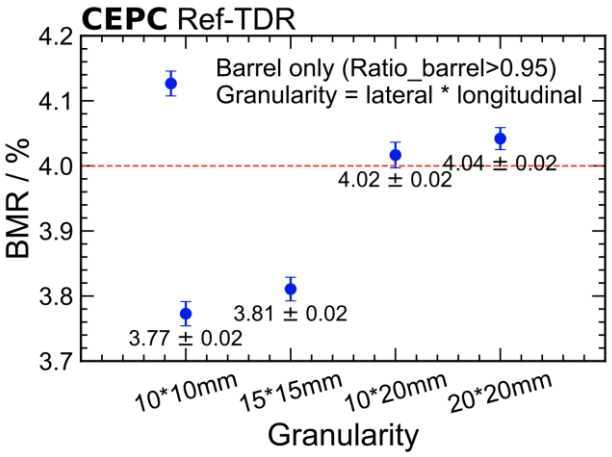

Feedback to IDRC Comments on Draft v0.4.1

- Detailed comment
  - C-B-7-2: The MIP requirement for the MIP light output has been raised from 200 to 300 p.e./MIP. While this makes the 0.1 MIP threshold for signal-to-noise ratio easier to achieve, it makes the requirement for the linearity up to 3000 MIPs (set by the maximum energy deposition from e showers for the CEPC operated at 360 GeV) more difficult to be met. Additionally, tests with prototypes show that the light yield of bars in the baseline bar configuration (1.5x1.5 x 40 cm3) are 400 pe/MIP (L.6527), thereby requiring linearity up to 106 pe and beyond. Simulation studies show that the linearity requirements are met (Section 7.3.5). However, these studies assume the nominal 300 pe/MIP and not the measured output of 400 pe/MIP for the baseline design choice for the BGO bars. Additionally, the study is limited to photons from the H → γγ decay for operation at 240 GeV, which have an energy deposition up to about 1500 MIPs (Fig. 7.5b). The SiPM dynamic range is further discussed in Section 7.4.2.2, with numbers that appear inconsistent with other parts of the TDR. For example, it is stated (L.6586) that a maximum deposition per bar of 45 GeV corresponds to 5x105 pe. However, at L.5984 it is stated that the MPV for a MIP is 13.3 MeV, which converts into 3383 MIPs for a 45 GeV energy deposition. At 300 pe/MIP, this gives already 106 pe. At 400 pe/MIP this is above 1.3x106. In summary, the effect of non linearity over the full range and up to 106 p.e. (or beyond) with SiPMs having 250k pixels does not appear to be sufficiently documented.
- Feedback
  - Updates in **Section 7.4.1 (page 242)** on the MIP Energy Response measurements with beam particles
  - Beam-test data: 307 p.e./MIP for 1x1x40cm BGO crystal bar rescaled with the target $3 \times 3\ \mathrm{mm}^2$ SiPM and the signal integration time of 300ns

Feedback to IDRC Comments on Draft v0.4.1

- Detailed comment
  - C-B-7-3: The specification about radiation hardness requirements has been dropped from the list (Table 7.1). A statement on the response stability of the BGO vs the ionization dose is needed in the section where the crystal choice is discussed, even if this is not translated into a specification.
- Feedback
  - Total Ionization Dose (TID) for BGO crystals: a reference and conclusions are added in Section 7.4.5.2 (page 251)
- Detailed comment
  - C-B-7-4: There are a few inconsistencies in the requirements about energy resolution. At line 5932 it is "$\sigma E/E \leq$ 2%/root(E)" while at L.1501 it is required an "energy resolution of <3%/root(E)". In other places the energy resolution is required to be less than 3% (Table 7.1) without specifying any energy dependency. Then there are instances where both the stochastic and the constant term are indicated (L. 6851 and L.1321, again with some inconsistency between 2% and 3%). Please clarify and distinguish clearly between the requirement and what is achieved. For example at L.6851, if the requirement is 3% and you achieve <2%, you can simply state that the requirement of <=3% is achieved.
- Feedback
  - Thorough updates in Chapter 7: descriptions of the EM energy resolution requirement ($\leq 3\%/\sqrt{\mathrm{E(GeV)}}\oplus 1\%$) are upated for consistency in the whole chapter

Feedback to IDRC Comments on Draft v0.4.1

- Detailed comment
  - C-B-7-5: The discussion about timing performance (Section 7.4.3) remains confusing. The time resolution is defined as “the standard deviation of the time difference of the time stamps of SiPM signals from the two ends of a crystal”. This quantity is not independent of the hit position and does not correctly quantify the precision with which the position of a deposition can be reconstructed. A deposition in the centre of the bar, would give a $\Delta t = 0$ with an RMS from the resolution of the device. A deposition near the ends of the bar would give a distribution with the same RMS centered at $\Delta t = +/- L/2v$, where L is the bar length and v the velocity of the light in the crystal. For a uniform hit distribution, the RMS will therefore get a contribution from the propagation path of $L/(v \sqrt{12}) \sim 0.6$ ns for L=40 cm, v = 1.5c. This should be added in quadrature to the genuine time resolution from the detector and readout. In Fig. 7.31 at L=40 cm, the resolution is 0.7 ns, which is consistent with 0.6 ns from propagation (+) 0.4 ns intrinsic to the detector, which you can read from the measurement with L=2 cm crystals. At L=60 cm, your measured resolution is almost 1 ns, which is again consistent with an $L/(v \sqrt{12}) \sim 0.9$ ns (+) 0.4 ns. So, while your data show the expected behaviour, your interpretation of the results is different. At L 6602, you conclude that at L=40 cm, the resolution is 700 ps (500 ps per end), while your data indicate a resolution is 400 ps/MIP (280 ps per end), which would scale to a resolution of 100 ps already at 200 MeV (per crystal). A better measure of the time resolution is provided by the RMS of the sum of the two timestamps, because the sum of the two propagation times is independent of the hit position. A plot of this quantity should clarify what is the actual resolution. You may still have some dependence on the bar length, because the light output is lower for longer bars.
- Feedback
  - Updates in **Section 7.4.3 (page 245-246)**
  - We have thoroughly re-analyzed the testbeam data using the definition in TDR (i.e. T1-T2) and the alternative definition suggested in the IDRC review (T1+T2). Plots are presented in the next page (also in the reference cited by the TDR).
  - Conclusions: (1) the 1-MIP timing resolution along the crystal length is uniform; (2) the 1-MIP timing resolutions using two definitions mentioned above are mostly the same.

Feedback to IDRC Comments on Draft v0.4.1

Timing Resolution vs Hit Position in BGO (testbeam data)

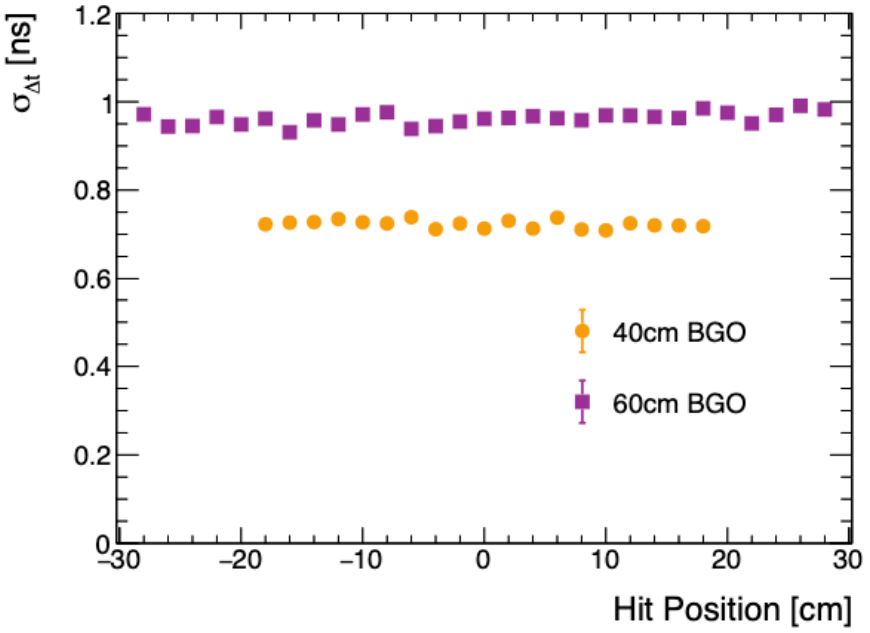

- ΔT=T1-T2: used in Ref-TDR
- Uniform sigma(ΔT) with hit positions

40cm BGO scan (testbeam data)

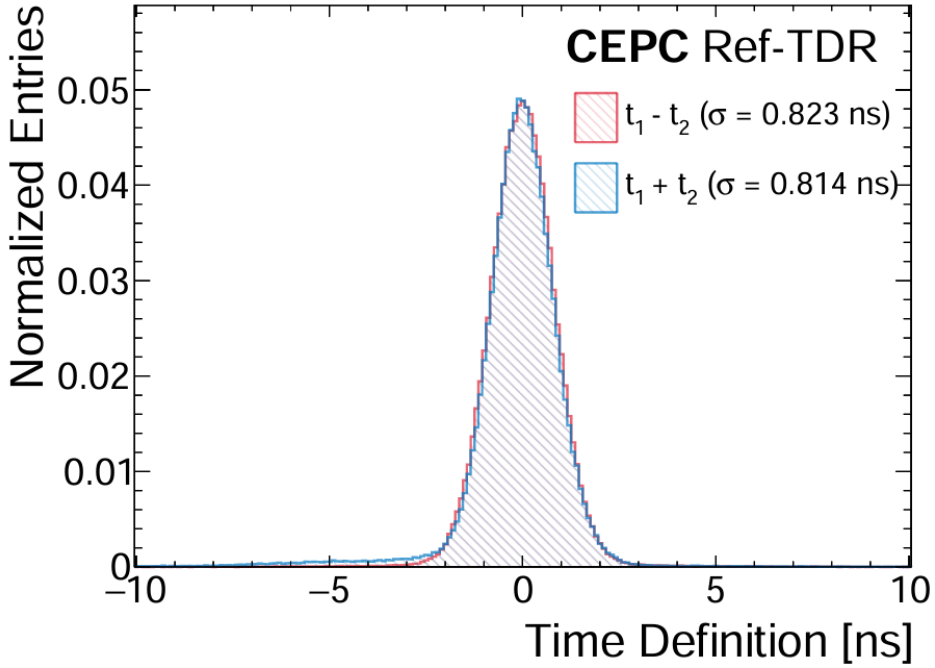

Two definitions of timing resolution compared: similar performance

- T1-T2 used in Ref-TDR
- T1+T2 suggested by IDRC: to eliminate position dependence

Feedback to IDRC Comments on Draft v0.4.1

- C-B-7-6: Line by line comments:
  - line 1475, 1481: - reference to just LEP for last gen e+e-. Suggest "LEP and SLD at SLC"
  - line 1490: "the key ingredient" I suggest "a key ingredient"
  - lines 1493-1494: We suggest expanding the sentence to "We propose to use BGO crystals as full absorption ECAL which will significantly improve energy resolution, which is essential for optimal H-> gamma gamma detection, for example."
  - line 1496: "18 longitudinal layers providing 24 radiation lengths" → "providing 24 or more radiation lengths", since there are more than 24 radiation lengths. for much of the barrel
  - line 1499: "fully contain electromagnetic showers." → "maximize containment of electromagnetic showers.", because, strictly speaking, there is still some leakage.
  - line 1524: "typical" would be better as "the typical" and "result" should be plural "results".
- Feedback
  - Changes were implemented in Chapter 2 by Haijun Yang (Editor of Chapter 2), which correspond to the lines mentioned above

Feedback to IDRC Comments on Draft v0.4.1

- Line by line comments (not exhaustive):
  - -line 5914 - "It also detects neutral pions $\pi 0$ ...." → "It detects neutral pions $\pi 0$ ...." The current formulation (with “also”) is a bit strange to me since it actually detects the gammas from neutral pions and those were already mentioned in the previous lines.
  - -line 5920 - "Moliere Radius" → "Moliere radius"
  - -line 5935 - "at two ends." slightly better would be "at both ends."
  - -line 5939+ and Fig 7.1: "contains over 400 long crystal bars”. It would be helpful here to re-state number of crystals in depth (18 specified much earlier on line 1496)
  - -line 5963 - "ers.`necessitating" looks like a typo ".`" should be ", "
  - -Figure 7.1: Here the "module" is shown as a "supercell". This is the first use of the term "supercell". Supercell is later referred to in section 12, but not until then. A clarification of these two different references should be added.
  - -Table 7.1 "EM energy resolution < 3%". Shouldn't this be energy dependent? Perhaps, add <3% above xx GeV.
  - -lines 6009 - 6010: "A typical 40 × 40 cm2 module employs 1.5 × 1.5 × 40 cm3 crystal bars". It would be helpful here to state there are 18 layers.
  - -lines 6861-6863: "~ 285,000 crystals" "571,000 SiPMs". As there are two SiPMs per crystal by design, make the two figures a factor two: either ~285,000 and ~570,000 or 285,500 and 571,000.
  - -line 6851 "to achieve an EM energy resolution of $\sigma E/E$ ≤2%/root(GeV) ⊕1%" should be root(E(GeV)). Please correct also the requirement on line 1321 "$\sigma E/E$ ≤ 3%/ root(E(GeV)) ⊕ 1%," (and make them consistent)
  - -lines 11299-11301: "The ECAL supercells, mentioned in Section 7.2, are used for the preliminary trigger studies.". We don’t find mention of supercells in section 7.2, where discussion of ECAL elements are modules. If the ECAL supercells are identical to "modules" the terminology used in Section 7, it would be helpful to state that here.
- Feedback
  - Changes were implemented in Chapter 7 accordingly

HADRONIC CALORIMETER

Findings

- F-A-8-1: A key innovative feature of the Hadronic Calorimeter (HCAL) is the large sampling fraction achieved through the use of heavy scintillating glasses (GS). The proposed layout offers the potential to significantly improve the PFA resolution by enhancing the stochastic term of the single-particle energy resolution. The committee acknowledges that the team is highly motivated and is making steady progress toward this ambitious design.

Findings

- F-A-8-2: The proposal is reasonable but aggressive. Detector specifications and performance benchmarks are clearly defined; however, considerable work is needed to bring the GS-HCAL baseline choice from its current R&D phase to a full-scale detector.

- --The primary objective of this section is to validate that the GS-HCAL design meets the CEPC physics program's core performance criteria. Leveraging extensive simulation studies in the absence of prototype data, we demonstrate the design's compliance with these requirements. In the new version in **Section 8.5 (** simulation and performance).

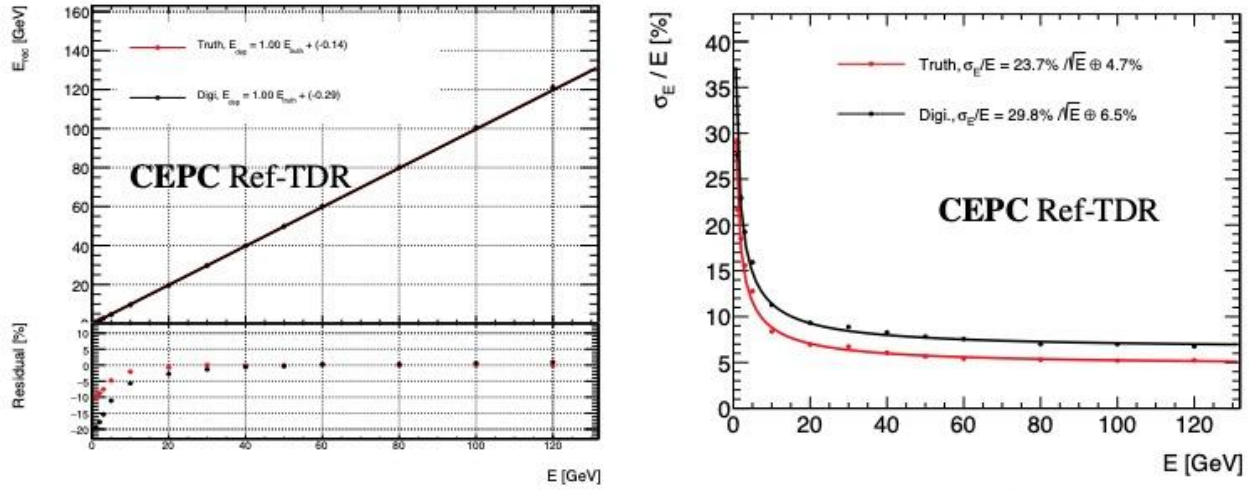

(a) (b)

Figure 8.24: (a) Energy linearity and (b) energy resolution of GS-HCAL with the digitization model.

The estimated energy resolution of $\sigma E\ /E$ = 29.8%/$\sqrt{E} \oplus$ 6.5% and an energy linearity within 2% before calibration, outperforms the stochastic term of traditional HCALs.

Findings

- F-A-8-3: For instance, during the review, the team was uncertain about the origin of the constant term observed in the hadronic energy resolution, a result obtained from idealized simulations with only limited hardware effects included.

- --To verify the hypothesis that longitudinal leakage was the cause of the observed discrepancy, we increased the depth of the GS-HCAL from 48 layers (6 λ_I) to 80 layers (10 λ_I) in **Section 8.5.2 Hadron Energy Resolution**. When the calorimeter depth was extended to 80 layers, this tail decreased significantly, and the constant term dropped to around 2.9%. The significant improvement in the constant term upon increasing the depth of the GS-HCAL supported the hypothesis that shower leakage, rather than an intrinsic design flaw.

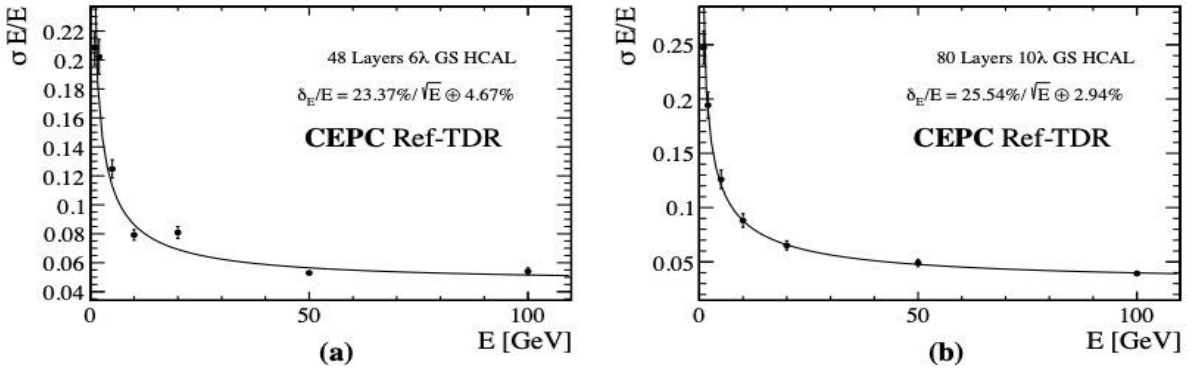

Figure 8.27: Comparison of two GS-HCAL configurations with different depths. A shallower setup with 6 λ_I (a) yields a pronounced high tail in the energy resolution and a large constant term. A deeper setup with 10 λ_I (b) effectively contains the showers, reducing the tail and lowering the constant term to a more typical value.

Findings

- F-A-8-4: The committee is pleased to note that the next step is the construction of a large-scale prototype.

- --Yes, in the new version of the HCAL-TDR, the new design of the prototype has already described, as in the **Section 8.4.8 Prototype**. The construction and testing program proceeds in phases. A 3×3×7 mini-prototype is currently under construction for initial beam tests at CERN in October 2025. The full 8112-channel prototype is scheduled for completion by end-2026.

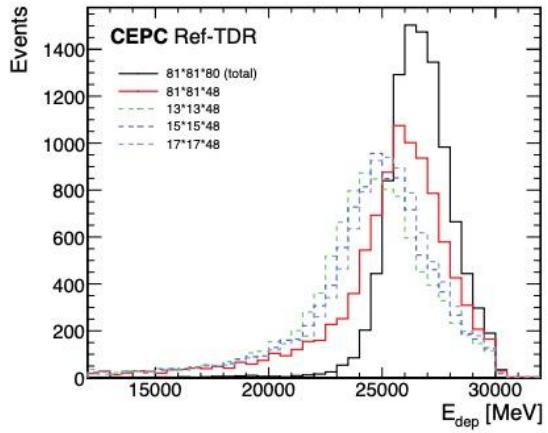

Figure 8.22: Distribution of deposited energy in prototype with different size using 80 GeV π for simulation.

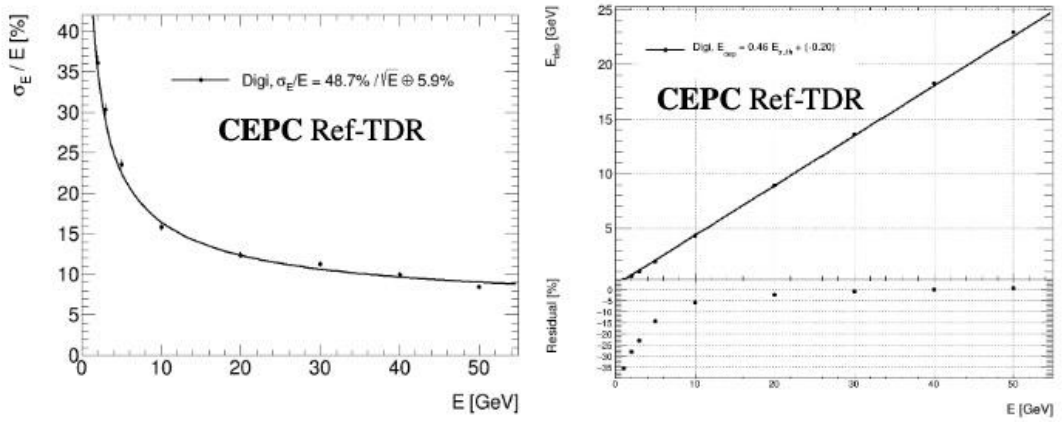

(a) (b)

Figure 8.23: (a) Energy resolution and (b) energy linearity of GS-HCAL prototype based on simulation.

Findings

- F-A-8-5: In this prototype, each tile will be read out by four SiPMs, whereas in the final detector only one SiPM per tile is foreseen for cost reasons.

- --It is clear that there is only one SiPM for tile for the design and cost, as show in **Figure 8.2**, and detialed describe could be found in **section 8.2.1** (Single layer structure). In the **Section 8.4.5** (Measurements of GS with SiPM), it is shown the cosmic ray test result of the 4cm*4cm*1cm glass cell coupling with 1 piece of 3mm*3mm SiPM.

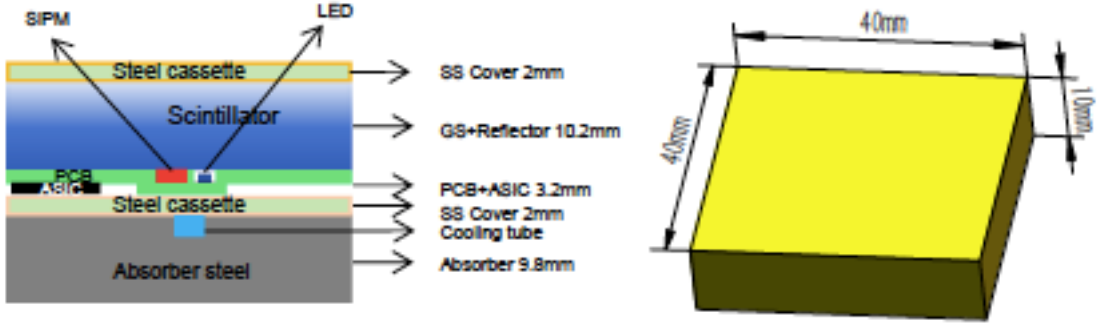

Figure 8.2: (a) Single layer structure of GS-HCAL. (b) One GS cell.

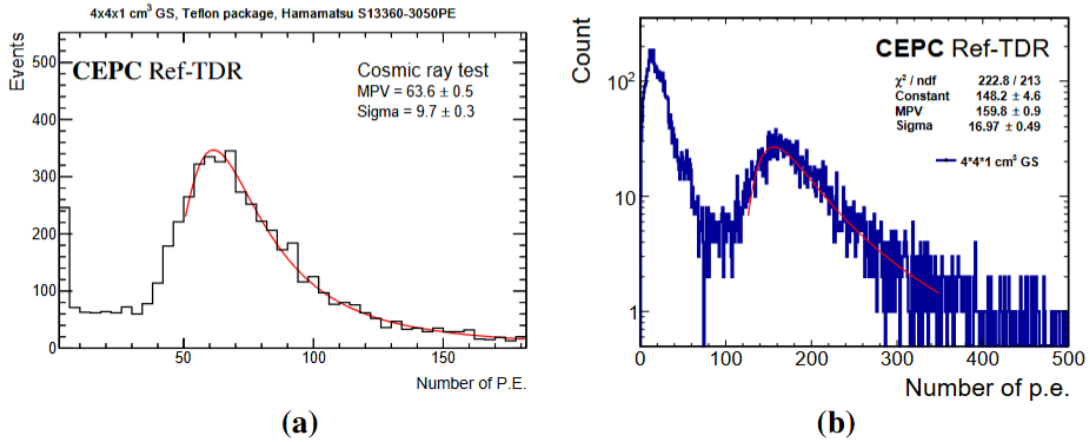

Findings

- F-A-8-6: Regarding costs, the committee notes that the current cost estimate does not include the cost of PCBs, which experience shows can become a significant item for granular calorimeters due to the complexity of design and production.
- --the cost of PCBs has already included in the electronics part.

Findings

- F-A-8-7: It was also acknowledged that a sampling calorimeter based on plastic scintillator (PS-AHCAL), which is more mature and better understood, remains a viable fallback option. The committee encourages the team to continue pursuing the GS-HCAL option, while maintaining the PS-HCAL as a backup.

- --Yes, the GS-HCAL and PS-HCAL are both the options of the HCAL. the size of the GS or PS tile are the same as 4cm*4cm, has the same photon readout SiPM and the electrinics, the same size Box and Prototypes. If the GS R&D was falled, it will be easy go back to the PS-HCAL design. There is also a special **Section 8.6 (**Alternative HCAL options) introduce the R&D results of the RPC-SDHCAL and PS-HCAL.

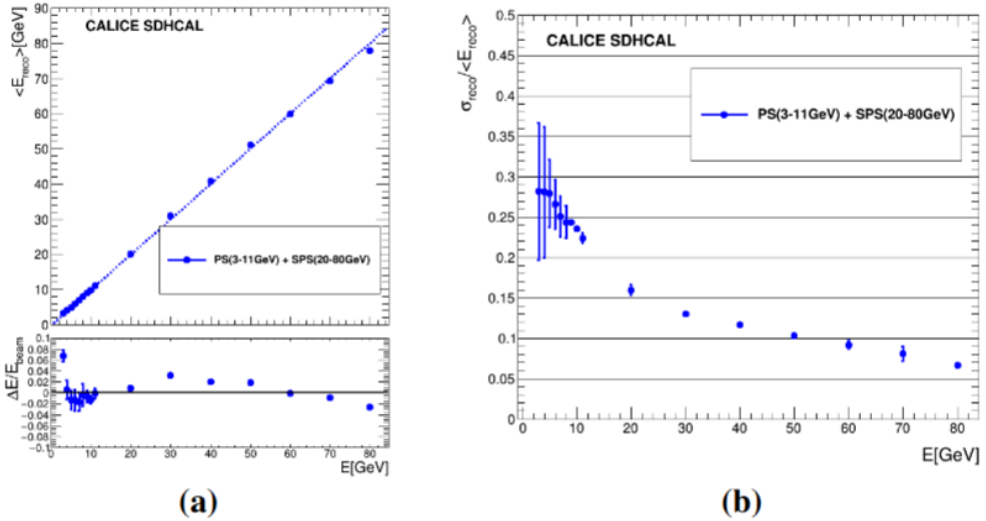

RPC-SDHCAL

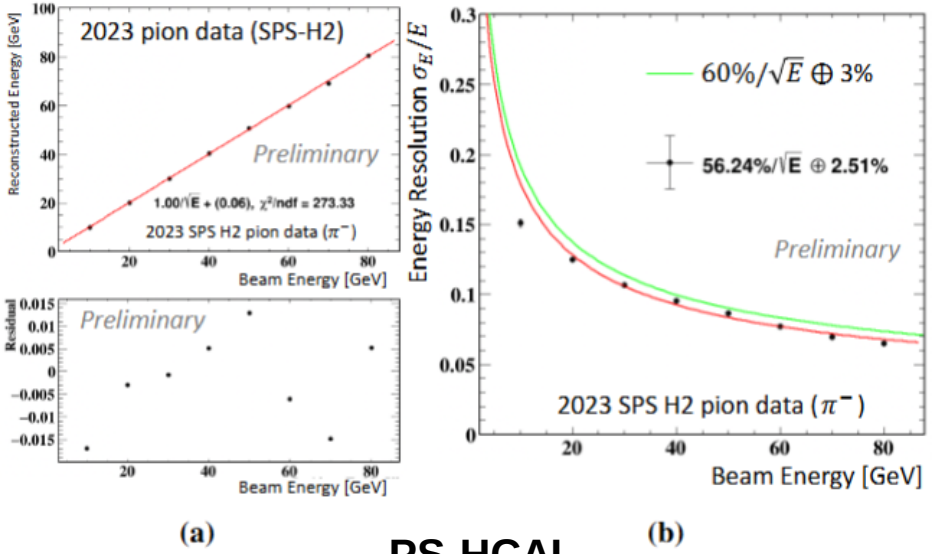

PS-HCAL

Comments

- F-A-8-8: Scintillating glasses represent new territory for hadronic calorimetry. The material properties, such as radiation length and hadronic interaction length, are not yet fully characterized. Although the decision to adopt this technology is well justified, it carries significant risk. Therefore, extensive prototyping and simulation studies are mandatory to validate the concept.

- --Yes, the study of the GS-HCAL option is only start in two years ago, and choise to be the baseline option on Aug.2024, there are lots studies need to do. And the new design o

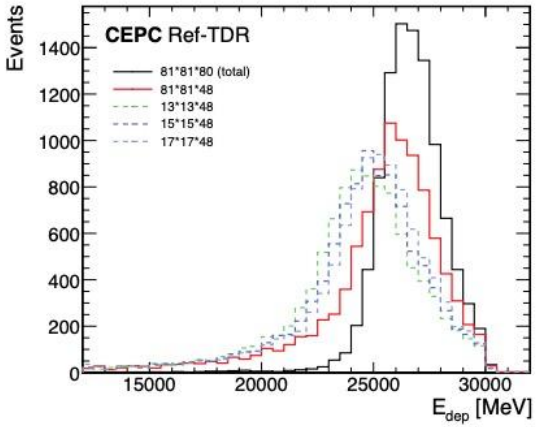

Figure 8.22: Distribution of deposited energy in prototype with different size using 80 GeV π for simulation.

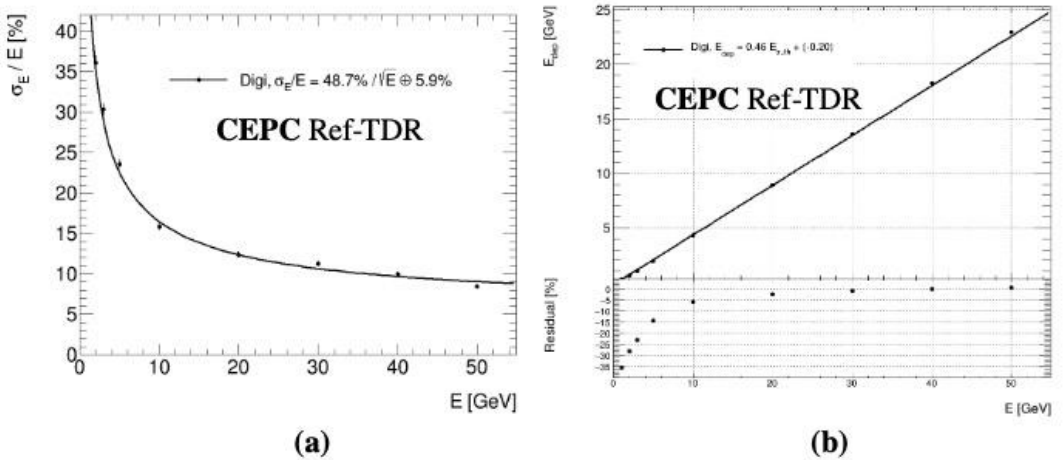

Figure 8.23: (a) Energy resolution and (b) energy linearity of GS-HCAL prototype based on simulation.

Comments

- C-A-8-1: A deep understanding of the response to hadrons is essential, including clarification of the constant term origin, study of the e/h ratio (software compensation), validation of GEANT4 physics lists, and accurate characterization of material properties such as quenching (Birks' law).

- --The new version of the TDR ahs already update the simulation work and the group also did more study for the design. In **Section 8.5 simulation and performance**. The energy linearity and resolution of the GS-HCAL are estimated using Geant4 simulation within the CEPC Software (CEPCSW) framework.

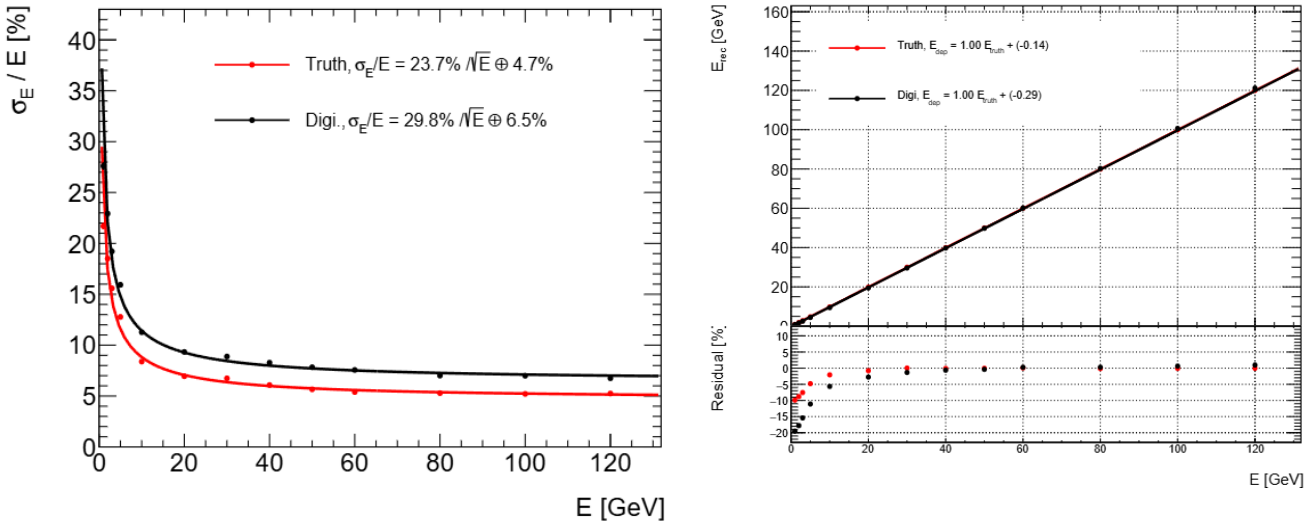

The estimated energy resolution of $\sigma E\ /E$ = 29.8%/$\sqrt{E}$ $\oplus$ 6.5% and an energy linearity within 2% before calibration, outperforms the stochastic term of traditional HCALs.

Comments

- C-A-8-2: The introduction of the TDR currently lacks references to important developments such as the CALICE AHCAL, built by German, Czech, and Japanese groups, which served as a foundation for the scintillator section of the CMS HGCAL.

- --The refs has already marked in the new version. Especially in the **Section 8.6 (Alternative HCAL options)**, it is introduced the developments of different option for HCAL. Multiple technological approaches of the CEPC calorimeters have been investigated to achieve the required jet energy resolution. These include gaseous detector-based approaches like the Digital HCAL (DHCAL) [29, 30] and SDHCAL [5, 31], as well as plastic scintillator tile designs (AHCAL) [10–13].

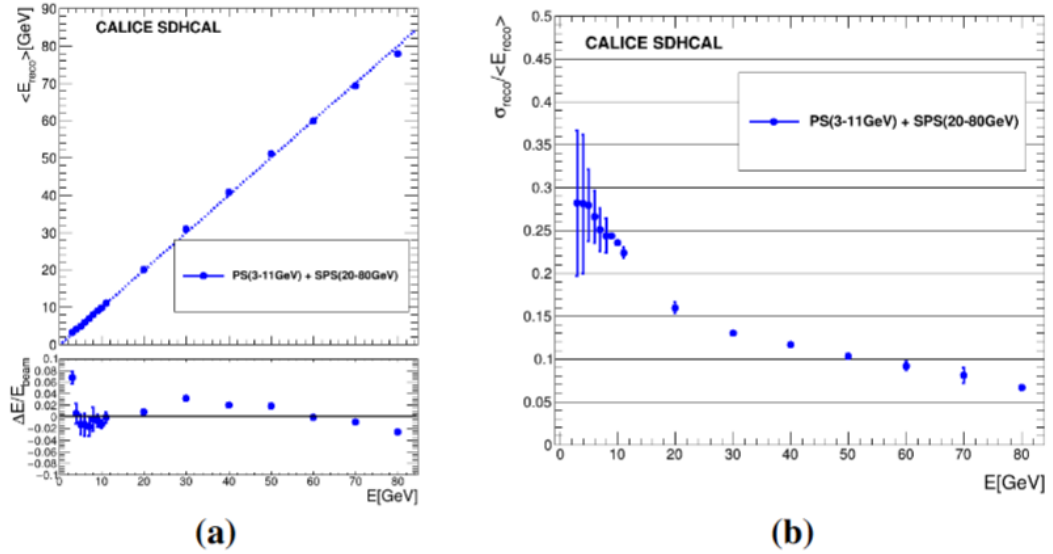

RPC-SDHCAL

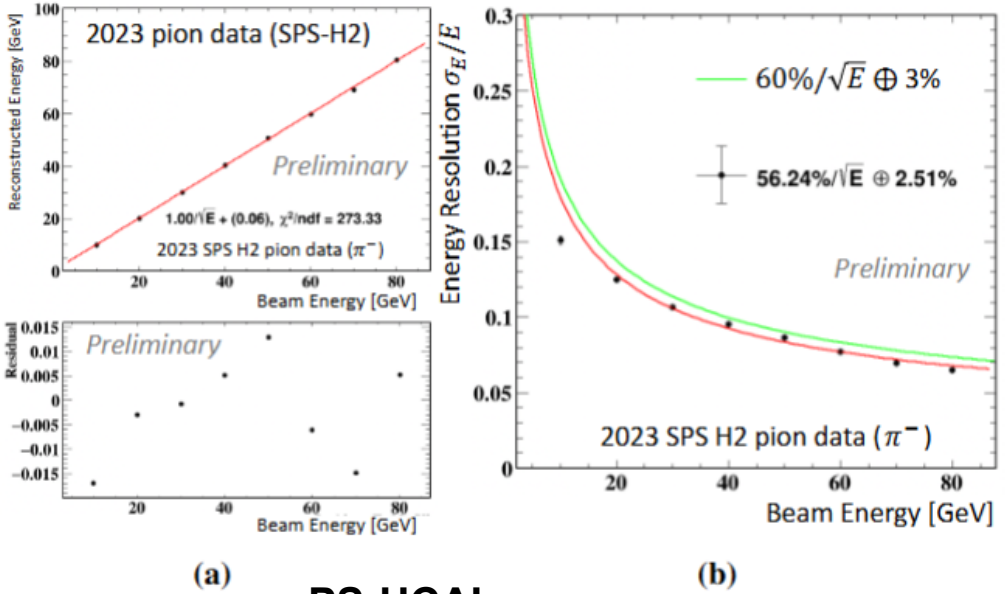

PS-HCAL

Comments

- C-A-8-3: The process of down-selecting technology options should be better explained in the text. Statements such as "excessive power consumption" should be supported with quantitative arguments for clarity and transparency.

- --The quality of the language has already improved a lot in the new version. In this new version, only one person (Li Hengne) represents the whole HCAL team to write documents and hold discussions with others, maintaining the uniqueness of the writing style.

Recommendations

- R-A-8-1: Develop a detailed plan to validate the choice of GS-HCAL technology in a timely manner. This plan should include the development of glass samples with reproducible and controlled quality, along with a detailed understanding of single-particle and jet energy resolution.

- --Yes, in the new version, there is a new **section 8.4 (**Technology R&D to demonstrate technologies and prototypes) introduced the technology of HCAL as GS, SiPM, Simulation and Calibration. To verify the performance stability of the GS, a batch of 150 glass samples were produced, and corresponding performance tests were conducted.

- In **Section 8.5.2** （Hadron Energy Resolution）introduce the energy linearity and energy resolution of GS-HCAL with the digitization model.

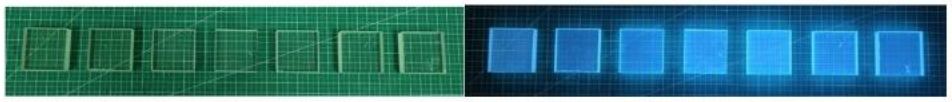

(a) (b)

Figure 8.11: GFO glass cells with the size of $40 \times 40 \times 10$ mm^3 under (a) natural light and (b) ultraviolet light.

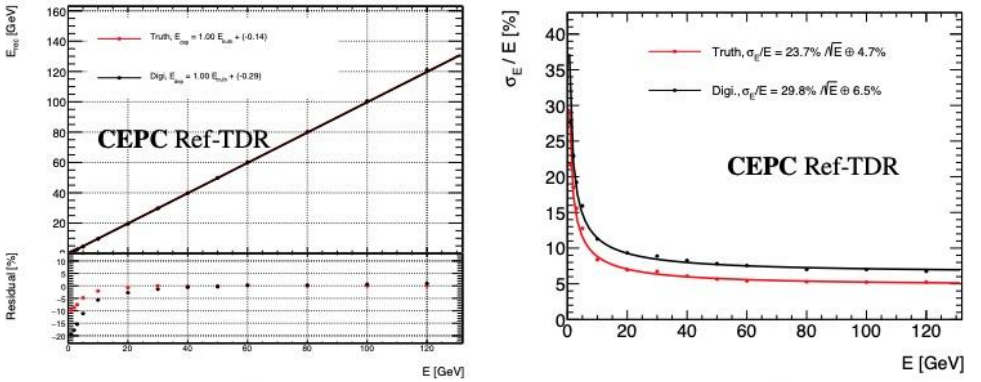

(a) (b)

Figure 8.24: (a) Energy linearity and (b) energy resolution of GS-HCAL with the digitization model.

Recommendations

- R-A-8-2: Prioritize the construction of a full-scale prototype. This prototype should incorporate the preliminary selection of glass tiles and ideally include a first version of both the readout ASIC and the PCB. Decide early on the final configuration regarding the number of SiPMs per tile and implement this choice in the prototype.

- --Good suggestion, the final prototype will use the GS,ASIC and PCBs, which will be used in the HCAL-CEPC in the future. A 3×3×7 mini-prototype is currently under construction for initial beam tests at CERN in October 2025. This mini-prototype will use the DT5202 from CAEN (https://www.caen.it/products/dt5202/)for electronics. But the full 8112-channel prototype scheduled for completion by end-2026, with include the readout ASIC and the PCB by our electronics group in CEPC. The full 8112-channel prototype is scheduled for completion by end-2026, with cosmic ray tests planned at IHEP and subsequent beam tests preferably at CERN in 2027. This prototype implements a steel-scintillator sandwich structure in a compact 0.6 m^3 volume (52 cm × 52 cm × 130.6 cm).

- R-A-8-3: Organize the group's work such that the prototype is simultaneously implemented into the simulation framework, including a complete digitization chain, to enable rapid feedback from test beam campaigns.

- --Yes, These will be the next steps to focus on.

The Mini-Prototype for beam tests at CERN in October 2025

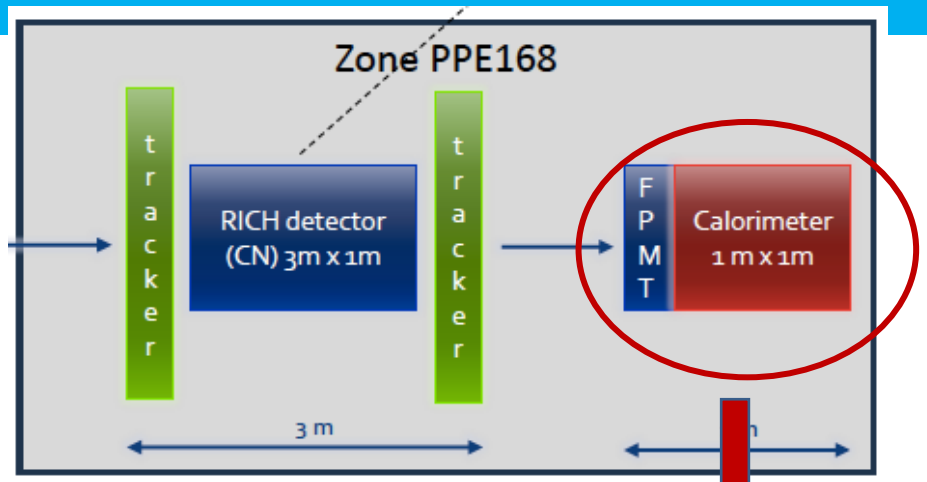

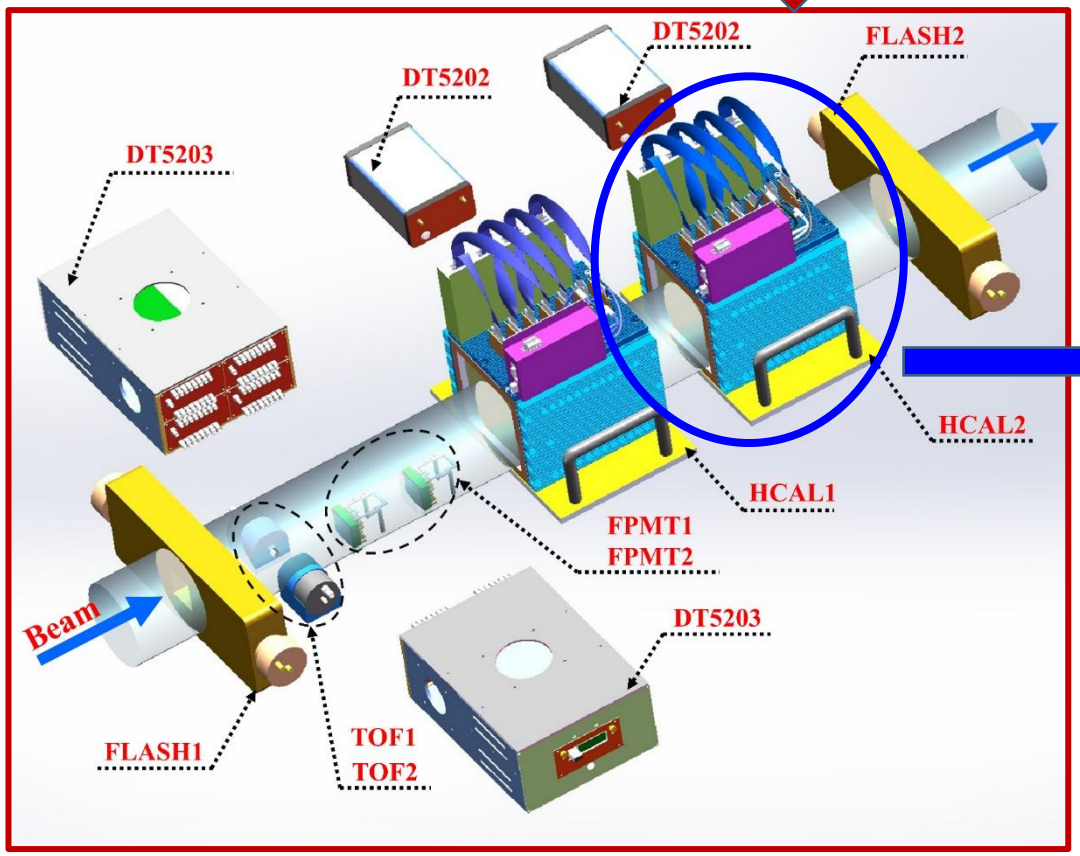

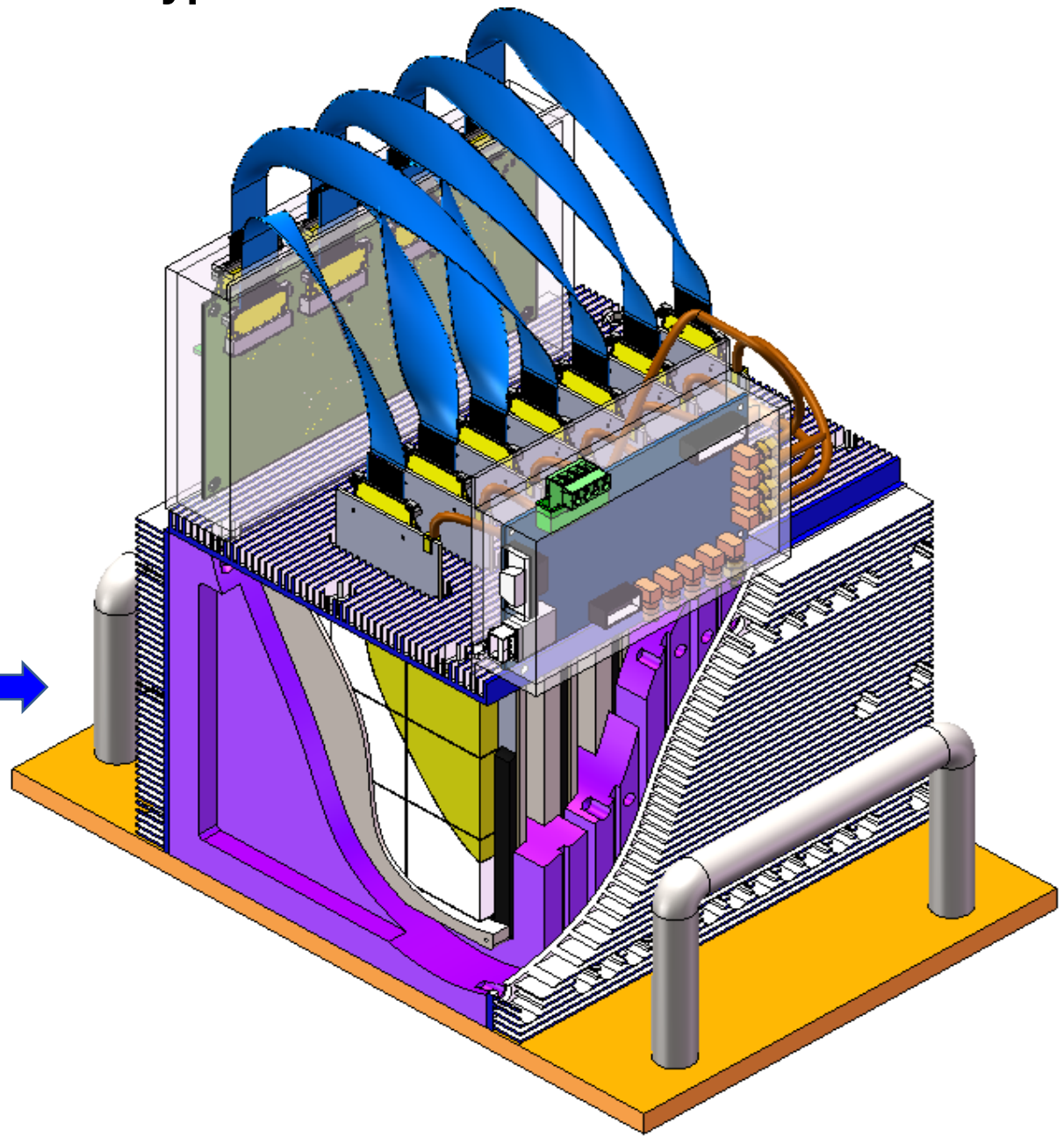

Comments in backup

HCAL

- C-A-8-4: The authors are encouraged to make the text more concise where possible, while still providing sufficient detail where necessary.
  - o C-A-8-4-1: Captions such as that for Fig. 8.12 ("The real AHCAL prototype") are inadequate and should be made more informative.

  --the outline of the HCAL in new version has changed, this types of pictures were deleted.
  - o C-A-8-4-2: The authors should carefully review the text to ensure that all figures are properly motivated, and that the overall argumentation is logical and coherent.

  --the outline of the HCAL in new version has changed.
  - o C-A-8-4-3: For example, it is unclear why the emission spectrum shown in Fig. 8.52 is included—is it representative or used for digitization? This should be explicitly explained.

  --this figure was deleted. Totally about 91 figures aere deleted, and all the figures in the new version TDR were modfied with high quality.

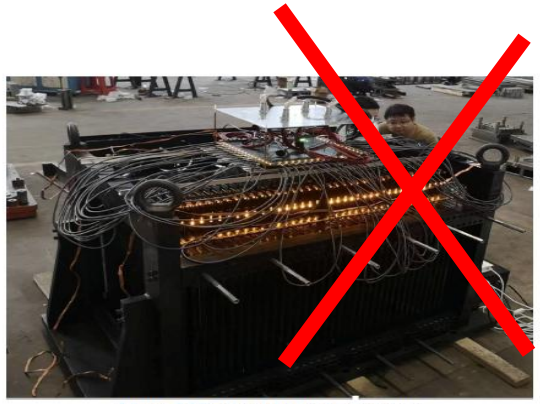

Figure 1.12: The real AHCAL prototype.

Fig. 8.12 in old version

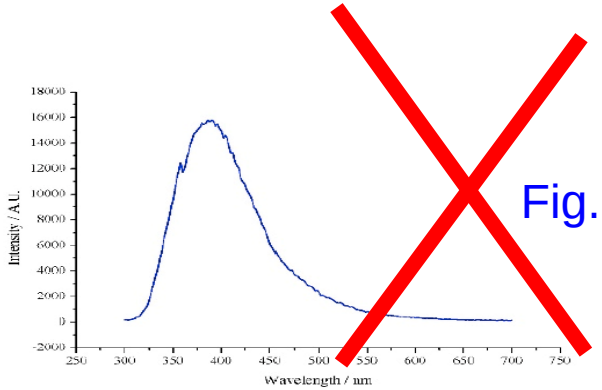

Figure 1.52: The emission spectrum of GS.

Fig. 8.52 in old version

Comments in backup

- C-A-8-5: The authors are encouraged to make the text more concise where possible, while still providing sufficient detail where necessary.
- As with other sections, the presentation was significantly better than the corresponding document and should serve as a guideline for revising the written material.
- -- the old version of the HCAL TDR has about 122 pictures and 70 pages, after the IDRC review, we have rewrite the new version with only 30 pictures and 40 pages without the reference.

Comments in backup

HCAL

- C-A-8-6: Section 8.5 contains an extended discussion of SiPMs, mixing general background information with results from the collaboration's own R&D. This section should be streamlined to separate general background from specific experimental achievements.--.
- --this part was deleted in HCAL. The introduction of SiPM could be find in ECAL part. In the new version part, there is small **subsection 8.4.3** (Photon detector) about the SiPM, as other key technologies include in the **Secion 8.4** (Technology R&D to demonstrate technologies and prototypes).

- C-A-8-7: Since SiPMs are used extensively across the calorimeter and muon systems, it would be more effective to consolidate the discussion of SiPM R&D into a single section. This would avoid redundancy and present a more coherent overview of the topic.
- --this part was deleted in HCAL. It could be find in ECAL part **Section 7.4.2** SiPM.

Comments in backup

HCAL

- C-A-8-8: Mechanical integration aspects, currently occupying much of Section 8.7, could be better placed within a general "Detector Integration" section. The authors should use their judgment to decide which integration details are most relevant to retain in the specific HCAL section, while moving broader topics to a centralized discussion.
- --there is the new section about the mechanical part at the begin of the HCAL as 8.2 Design part. The Outline of the HCAL part are the same an other Detector, first the design, then the Key technologies, both the major challenges and the R&D results. Then the simulation and performance. The Alternative HCAL options are to be a special section to overview the other group's work for the HCAL.

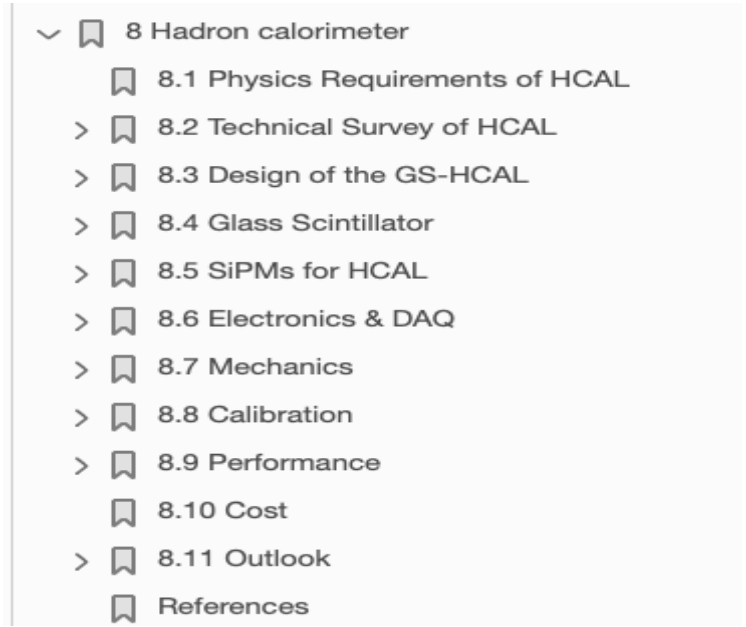

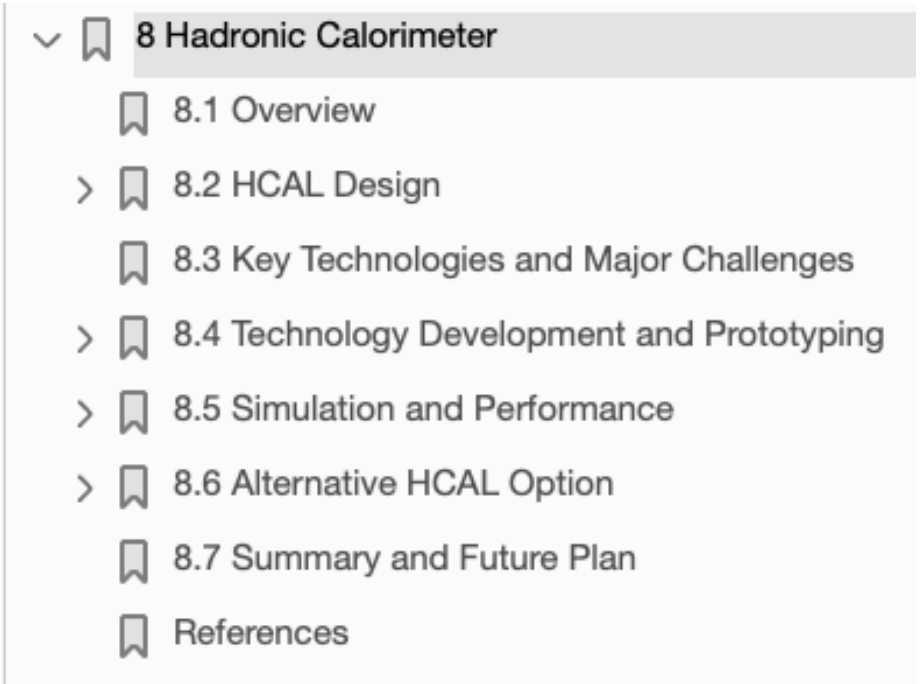

Comments on Draft v0.4

- General comment
- Let us first congratulate them for the huge amount of interesting work that is presented. As already observed for the Eca part also the HCal part has been restructured. It also presents directly the design choice and comments on alternatives at the end of the chapter, meeting therefore a comment made during the review in April. In the following a few high level comments and a non-exhaustive list of line-by-line comments. An annotated pdf file of the HCal put has been put at the disposal of the project members.

Comments on Draft v0.4

- C-B-8-1: Still the main problem is that a technology is proposed that is at the very beginning of the R&D cycle
  - C-B-8-1-1: From our point of view It will take at least five years with full resources before this calorimeter will reach the TDR level
  - C-B-8-1-2: We note however that the authors show awareness of this (major) shortcoming
  - C-B-8-1-3: The project matches perfectly a strategic R&D topic in DRD Calo but is too early for a TDR.

--The answer from Imad.

1） several components of the is technology are similar to ones used in the AHCAL technology like SiPM and readout systems as well as calibration techniques. All this is integrated in the new technology

2） although future extensive tests will confirm it, the simulation used to produce the TDR results seems to be corroborated by the first beam tests and cosmic benches.

3) the strong collaboration with local industries allow us to be confident that new generation of scintillanting glass will provide even higher performances in terms of light yield and attenuation length leading to even much better performances than the ones put in the TDR.

- **--The answer from Hengne & Sen.**
- Agree. In deed we well accept this glass scintillator technoligy is still at its early stage . however, given it's valuable potential (e.g. cheap, easy modeling, etc.) we chooose to boost it in the future CEPC HCAL application. For this reason We did the following updates in the text accordingly:
- 1.Updated the preamble part before "Overview" Section, explicitly mention that we fully aware the GS technology is at its early stage and still need at least 5 years of R&D to be a TDR-Level technology.
- 2.Update corresponding sections, to clearly present what R&D have been done, what haven't yet. And trying to make a clear and solid plan towards a mature technology at the time scale of 5 - 10 years, i.e. before the construction of the CPEC detector.

Comments on Draft v0.4

○C-B-8-1-4: How critical is the non availability of CERN (i.e. a high energetic hadron beam) between the middle of 2026 and ~2029.

---May be in KEK or the Proton beam in CSNS in China.

-- A clear proposal of using CERN high energy hadron test beams for the R&D of the GS-HCAL is presented.

●C-B-8-2: The document lacks a clear plan toward construction

--please see the **section 8.4.8** Prototype, the **section 8.7** Summary and Future Plan.

The GS-HCAL development follows an aggressive yet realistic timeline:

- **2024–2025**: Finalize $40 \times 40 \times 10\,\mathrm{mm}^3$ glass tile design and initiate mass production of 10,000 prototype tiles;
- **2026**: Complete $0.6\,\mathrm{m}^3$ prototype assembly (8,112 tiles) and begin beam tests at CSNS or CERN;
- **2027**: Full-scale module integration and performance validation with cosmic-ray/beam tests.

Comments on Draft v0.4

- C-B-8-3: What are design parameters (on e.g. cell S/N) of the system?

-- we are expecting a 10% of MIP value as the S/N cut threshold.

- C-B-8-4: At the moment only a handful of tiles have been tested
  - C-B-8-4-1: How to ensure mass production?
  - C-B-8-4-2: In this context how to ensure homogenous tiles and what are the criteria?

--No matter what. We must trust the production capabilities and quality control of Chinese enterprises.

--the successfull example is the 20 inch MCP-PMT for JUNO. We get the small number of prototypes at Lab in 2015, and the factory setup the mass production line in 2016, and start the mass production from 2017 to 2020, finished 15000 pics 20 inch MCP-PMTs for JUNO.

--for the Glass Scintiallator and SiPM, the situation right now are really much better than the PMTs at that time. When the CEPC will be supported by the goverment, the factories will do the mass production by themeslves.

--for the SiPM, the chinese company ZJGD (www.zjgd.com.cn) has already finished the mass production line on June 2025, and produce the SiPM with 40% PDE and acceptiable price. **The news will be publish in The Innovation will introduce it.**

A significant breakthrough achieved in the production of high-performance SiPMs with epitaxial quenching resistors

S. Qian[a,b,c,*], P. Hu[d], Z. Liu[e], J.F. Han[f], X.L. Wang[g,h]

[a]Institute of High Energy Physics, Chinese Academy of Sciences, Beijing, 100049, China.
[b]State Key Laboratory of Particle Detection and Electronics, Beijing, 100049, China.
[c]Key Laboratory of In-fiber Integrated Optics, Ministry Education of China, Harbin Engineering University, Harbin 150001, China
[d]China Nuclear (Beijing) Nuclear Instrument CO.,LTD, Beijing, 100176, China.
[e]Paul C. Lauterbur Research Center for Biomedical Imaging, Shenzhen Institutes of Advanced Technology, Chinese Academy of Sciences, Shenzhen 518055, China
[f]Key Laboratory of Radiation Physics and Technology of the Ministry of Education, Institute of Nuclear Science and Technology, Sichuan University, Chengdu, 610064, China.
[g]Key Laboratory of Nuclear Physics and Ion-beam Application (MOE), Fudan University, Shanghai, 200443, China
[h]Institute of Modern Physics, Fudan University, Shanghai, 200443, China

1. News

Recently, a significant breakthrough has been achieved in the production of high-performance Silicon Photomultipliers (SiPMs) with epitaxial quenching resistors (EQR) [1]. The EQR SiPM packaging production line, developed by CGN Capital Photonics Technology (Tianjin) Co., Ltd., has been successfully launched with a product yield exceeding 90%. This breakthrough has sparked new growth in China's semiconductor optoelectronic device industry.

The SiPM is a solid-state photon detector known for its high sensitivity and compact structure. It is a silicon chip that is composed of a series of miniature avalanche photodiodes (APDs), each operating in Geiger mode by being reverse-biased above the breakdown voltage to realize the avalanche multiplication of photoelectrons. A special resistor is connected with each

*Corresponding author.
Email address: qians@ihep.ac.cn (S. Qian)

Preprint submitted to Innovation *August 10, 2025*

GS Cell Batch Test Results --20250810

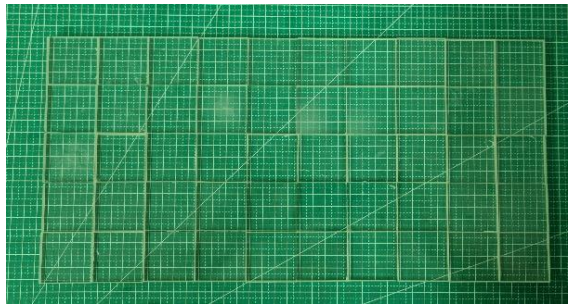
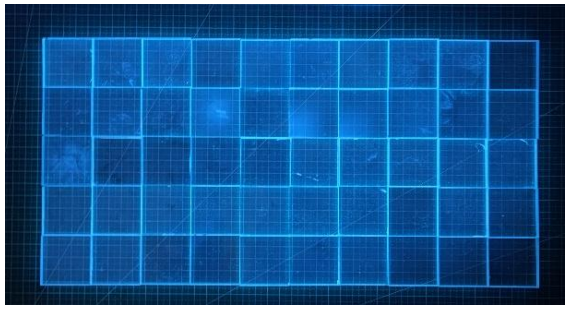

BGRI

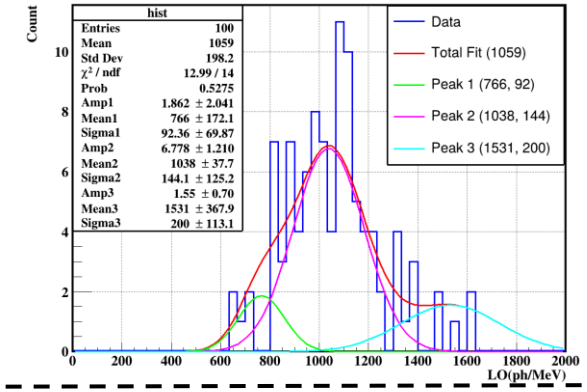

- The light output of 60.0% of GS is ≥1000 ph/MeV (60/100)
- The light output of 21.0% of GS is ≥1200 ph/MeV (21/100)

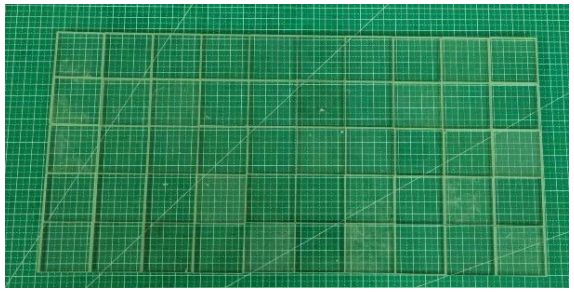
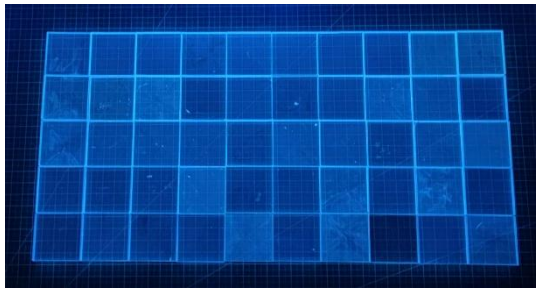

SIOM

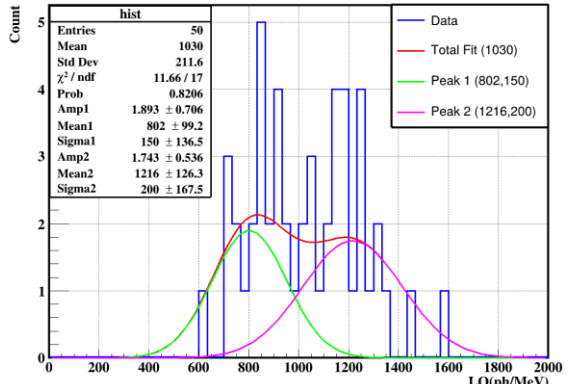

- The light output of 54.0% of GS is ≥1000 ph/MeV (27/50)
- The light output of 20% of GS is ≥1200 ph/MeV (12/50)

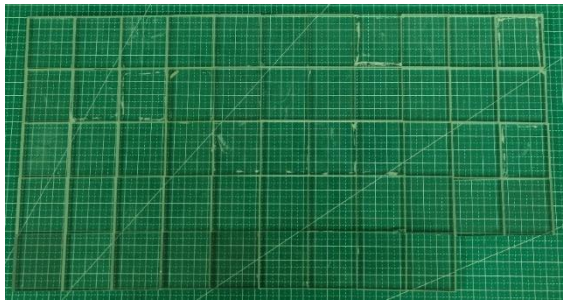
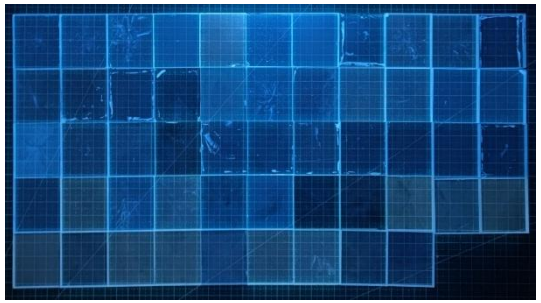

CBMA

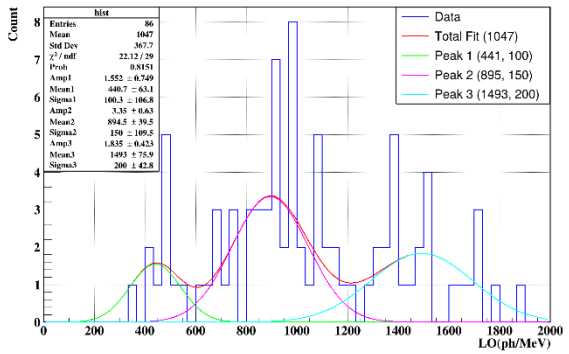

- The light output of 46.5% of GS is ≥1000 ph/MeV (40/86)
- The light output of 31.4% of GS is ≥1200 ph/MeV (27/86)

GS Cell Batch Test Results --20250819

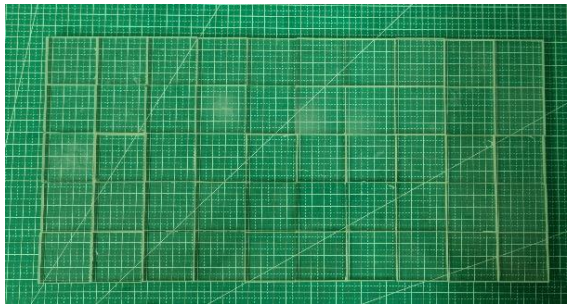

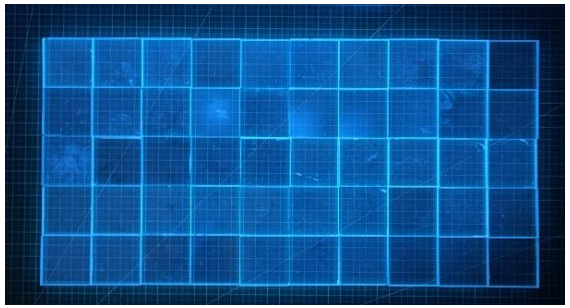

BGRI

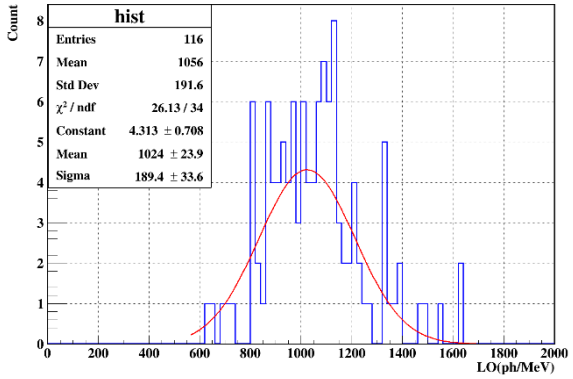

- The light output of 60.3% of GS is ≥1000 ph/MeV (70/116)
- The light output of 20.7% of GS is ≥1200 ph/MeV (24/116)

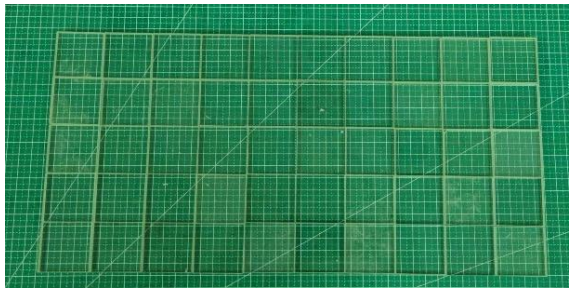

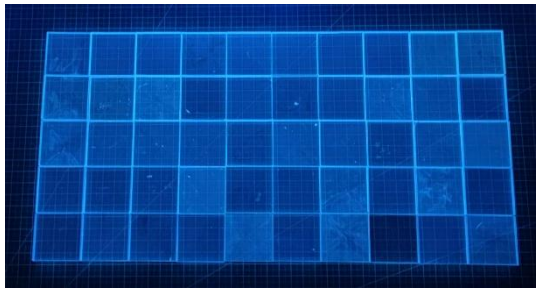

SIOM

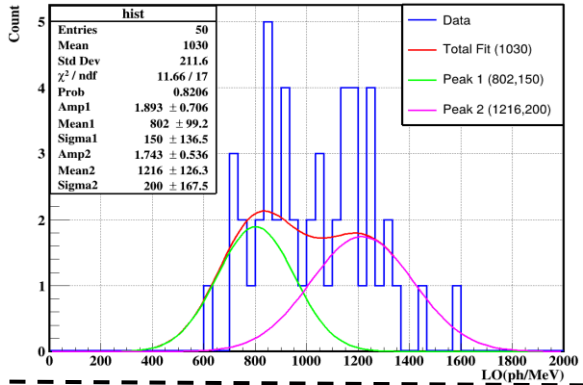

- The light output of 54.0% of GS is ≥1000 ph/MeV (27/50)
- The light output of 24.0% of GS is ≥1200 ph/MeV (12/50)

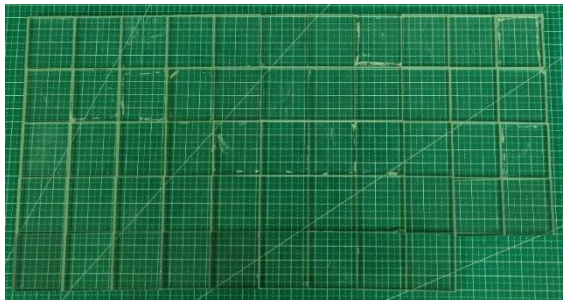

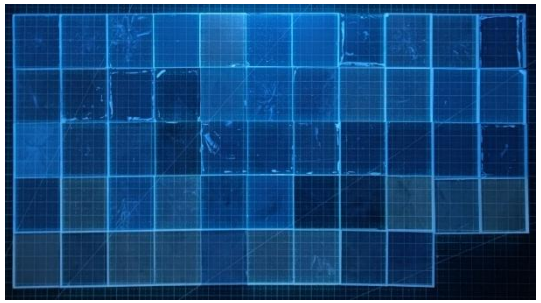

CBMA

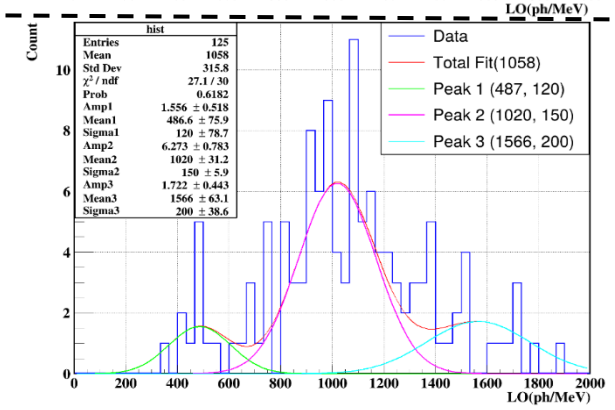

- The light output of 55.2% of GS is ≥1000 ph/MeV (69/125)
- The light output of 30.4% of GS is ≥1200 ph/MeV (38/125)

Comments on Draft v0.4

C-B-8-4-3: In the draft we don't see the results of all the (few) tiles that have been e.g. tested beam or in the cosmic stand

--In Fact， in the Section **8.4.2 Glass Scintillator**, the **Figure 8.12**: the transmission and XEL spectra of large GFO glass, the Energy spectra of GFO GS and the Scintillation decay curve of the GFO.

there is the new version for the **8.4.5 Measurements** part, the **Figure 8.17**: Measurement results of the GS cell with SiPM readout, using 137Cs radiation source and Cosmic ray.

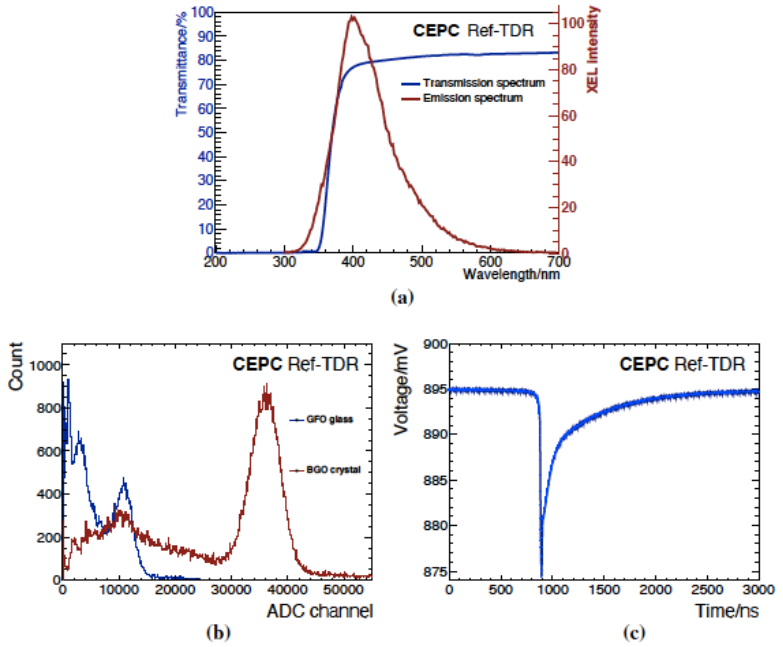

Figure 8.12: (a) Transmission and XEL spectra of large GFO glass, (b) Energy spectra of GFO GS and BGO crystal with same dimension. (c) Scintillation decay curve of the GFO glass.

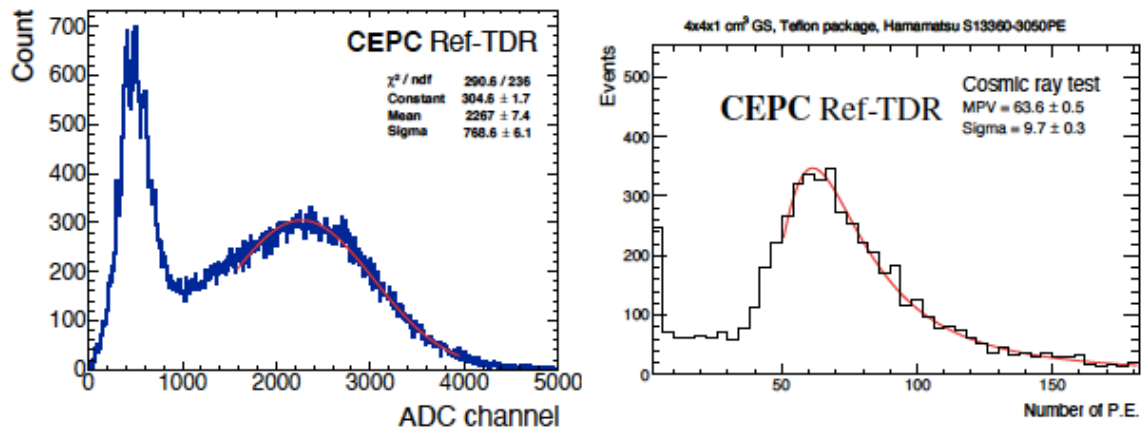

Figure 8.17: Measurement results of the GS cell with SiPM readout, the same GS cell size of $40 \times 40 \times 10$ mm^3 is used. (a) The measured ADC spectrum of GS cell with a SiPM (HPK S14160-3050HS) using ^{137}Cs radiation source. (b) Cosmic ray test results measured using HPK S13360-3050PE SiPM, resulting a light output about of 64 p.e./MIP.

Comments on Draft v0.4

- C-B-8-5: There are inconsistencies; examples (non exhaustive)
  - ○C-B-8-5-1: All SiPM tests in 8.4.4 were carried out with HPK SiPMs however for the prototype NDL SiPMs will be used

    --all changed, not fix the SiPM for HCAL.

  - ○C-B-8-5-2: Is the pre-amp tested in Sec. 8.4.6 the same that will be used in SIPAC?

    --not yet. The pre-amp was combined in ASIC, which has not designed for using right now.

- C-B-8-6: On Page 290 the authors raise concerns about the radiation hardness.
  - ○ C-B-8-6-1: The tiles will not withstand 10 years of operation. Is this a fundamental problem and if yes how will this be systematically addressed?

-- radiation section is removed. it is not an issue. According to the existing TDR data, during the 10-year Higgs run (with a luminosity of 8×10^{34} $cm^{-2}s^{-1}$), the irradiation dose reaches 100 Gy.For the Z run, the luminosity is 192×10^{34} $cm^{-2}s^{-1}$, so a rough estimate suggests that 1 year of Z running would result in an irradiation dose of 240 Gy. However, since the Z-peak energy is 91 GeV (lower than the Higgs production energy), **the actual dose is expected to be somewhat lower.**

indeed, you correctly pointed out adiation hardnes is not a fundamental problem. Previously we spent many text discussing radiation damage but in fact it is not really an issue. We have receved comments from several experts that the radiation damage is actually not an issue in electron-positrom machine such as CEPC, we agree on that and re-evaluated the situation, we deceided to remove a large fraction of the radiation damage discussion.

-- from 8.4.2.3 Radiation Tolerance

This version of ref-TDR is aiming at Higgs and low lumi-Z modes. Current there is no technical bottleneck for CEPC Phase-I TDAQ. High lumi-Z mode is Phase-II of CEPC. The requirement of technical for High lumi-Z is not included in this version.

Comments on Draft v0.4

C-B-8-7: The description of the cooling system (Page 279) is insufficient.

-- agree, adding more text and a figure to better describe the cooling system. More detialed could be seen in Section 8.2.2 Barrel and Section 8.2.3 Endcap.

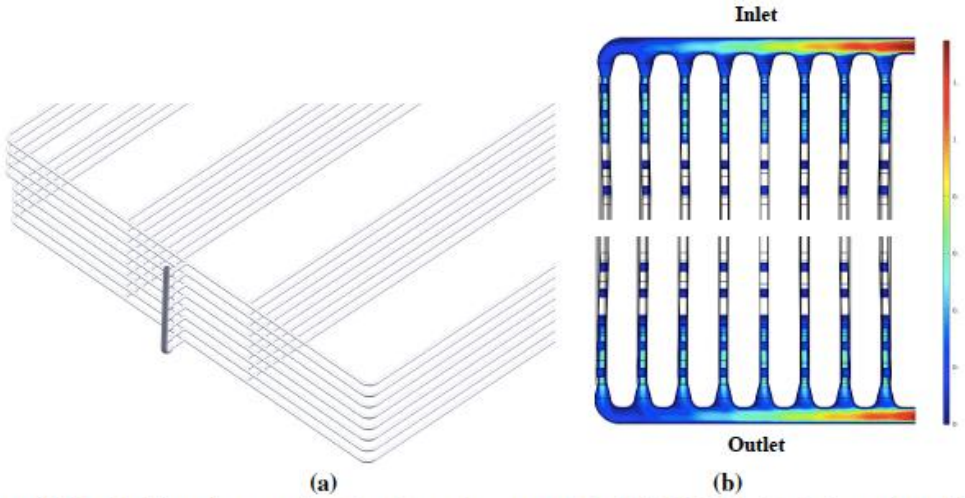

Figure 8.6: Cooling pipe routing for a barrel sector of the GS-HCAL. (a) Schematic of the eight-in-one pipeline design. (b) Simulated flow velocity (m/s) distribution of the coolant along the pipeline, with inlet and outlet positions indicated.

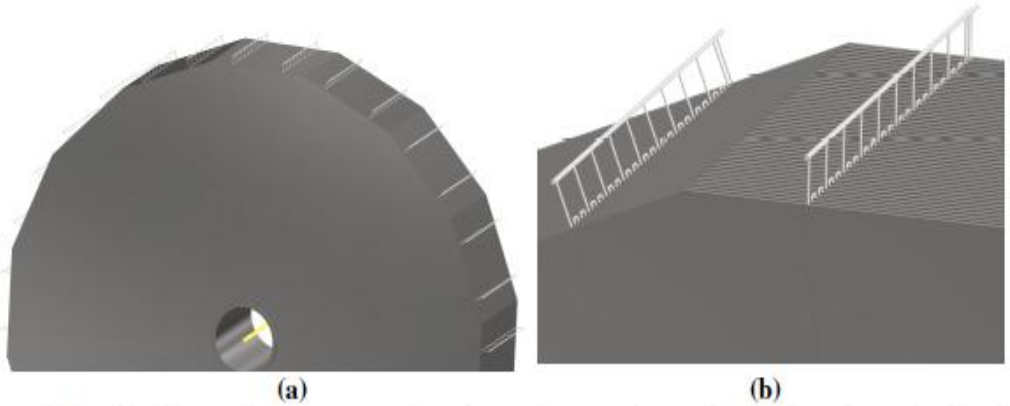

Figure 8.8: Cooling pipe structure for the endcap, where (a) is showing a half of the endcap, and (b) is showing a zoomed in corner of the endcap.

Comments on Draft v0.4

- C-B-8-8: Think to shorten the introduction to 8.4
- --The Part 8.4 have to change as follows:
- keep the 8.4.1 Historical review; 8.4.3 Photon detector; 8.4.4 Simulation Study of Attenuation Length
  8.4.6 Calibration;8.4.7 Readout electronics for R&D; 8.4.8 Prototype

- rename 8.4.5 Measurements of GS with SiPM as 8.4.5 Measurements

- **rewrite the 8.4.2 Glass scintillator;**

8.4.2.1 Light Yield,

8.4.2.2 Light Attenuation Length;

8.4.2.3 Radiation Tolerance

- **rewrite the 8.4.2 Glass scintillator; (1) light yied,**
- delate the result of the electron beam result;
- remove cosmic ray test result to 8.4.5 Measurement

8.4.2.1 Light Yield

Figure 8.11 shows the pictures of GFO glasses with a size of $40\times40\times10$ mm^3 under natural (such as regular room light) and ultraviolet light. Figure 8.12(a) shows the X-Ray Excited Luminescence (XEL) spectrum and transmission spectrum of a GFO glass,The transmittance in the visible light range exceeds 80%. Combined with the XEL spectrum, it can be observed that there is a certain self-absorption effect in the glass [20]. Additionally, as the glass thickness increases, its transmittance in the visible spectrum decreases from approximately 80% to around 75%. The measurable light output of GFO glass is a critical factor for HCAL applications. Extensive γ-ray testing has demonstrated that the light yield of GFO glasses can consistently exceed 1000 ph/MeV. When measured with an XP2020 (2 inch) Photomultiplier Tube (PMT), the detected photo-electron number reaches 1/3 that of BGO crystals with identical dimensions [21], as shown in Figure 8.12(b). Figure 8.12(c) presents the scintillation decay profile of GFO glass under γ-ray excitation. While maintaining a light yield of 1000 ph/MeV, the decay time of the slow component can be controlled to below 500 ns. Although achieving faster decay time remains challenging, the large-scale GFO glass successfully maintains an optimal balance between density, light yield, and scintillation decay characteristics.

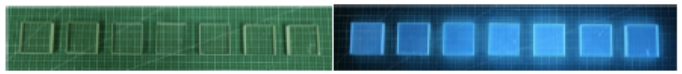

(a) (b)

Figure 8.11: GFO glass cells with the size of $40\times40\times10$ mm^3 under (a) natural light and (b) ultraviolet light.

To verify the performance stability of the GS, a batch of 150 glass samples were produced, and corresponding performance tests were conducted. Additionally, the radiation resistance characteristics of GFO glass under proton and γ-ray irradiation were tested. With proton beam irradiation at 800 Gy, the 400 nm transmittance showed a 60% reduction from its original value, the cumulative reduction further arrived at 87% for a dose of 8100 Gy. While for light yield, when the dose reached 400 Gy, it decreased to 34% of its original value [22]. The light yield dropped to 71% under γ-ray irradiation of 100 Gy, corresponding to ten years of data taking of the CEPC GS-HCAL.

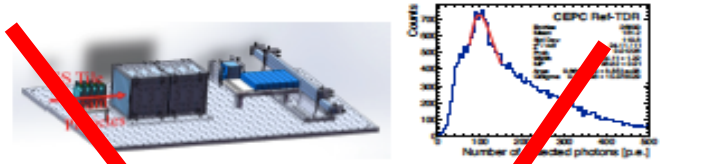

Figure 8.8: DESY electron beam test of the GFO glass tiles in 2023. Left figure shows the experimental setup, right figure shows the measured p.e. distribution.

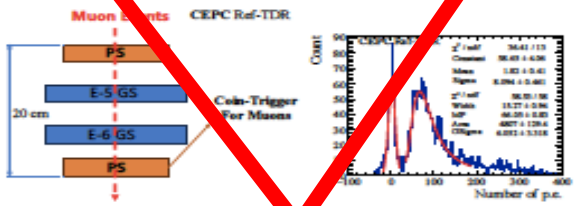

Figure 8.9: IHEP cosmic ray setup performed in 2024 of GFO glass tiles (left), and the measured p.e. distributions for MIPs (right).

To independently validate the MIP response, a second measurement was performed using cosmic muons in a vertical stack configuration at IHEP in 2024. Two Plastic Scintillator (PS) paddles provide coincidence triggers above and below the GS tiles (labeled E-5 and E-6) to ensure clean muon tracks. This setup is schematically shown in the left panel of Figure 8.9. The readout is using Hamamatsu S13360-6025CS SiPM. A longer integral gate of 4 μs was employed to fully collect the slower scintillation components. The measured MIP response of the E-5 tile reached an MPV of approximately 67 p.e./MIP, corresponding to an inferred light yield of $\sim$750 photons/MeV, which is consistence with the DESY results.

Both measurements confirm the feasibility of using GS tiles for high-granularity HCAL applications. A summary of the results is presented in Table 8.4. These results validate the promising performance of GS tiles and provide critical input for optimizing the calorimeter design for CEPC.

Table 8.4: Summary of GS tile beam test and cosmic ray measurements.

Test Setup	Integral Gate	Light Yield	MIP Response
DESY Electron Beam	1 μs	600–700 ph/MeV	90–100 p.e./MIP
IHEP Cosmic Ray (E-5)	4 μs	$\sim$750 ph/MeV	65–70 p.e./MIP

- **rewrite the 8.4.2 Glass scintillator; (2) Light attenuation length,**
- delate the test result of the data by the light output in our lab published in Ref[18];
- retest the samples by the transmittance data and give the new results and also the ref.23

R. Y. Zhu et al. “A Study on the properties of lead tungstate crystals”. Nucl. Instrum. Meth. A 376 7517 (1996), pp. 319–334..

Light attenuation length

The attenuation length (L_0) is a critical parameter for evaluating light transmission performance in scintillators. Multiple batches of GFO glass samples with cross-sectional dimensions of $5 \times 5\,\mathrm{mm}^2$ and thicknesses ranging from 1–15 mm were prepared for systematic measurements (Fig. 8.10). The best-performing GFO glass sample currently available achieves an attenuation length of 6.2 cm at 400 nm. This value is used as the standard reference in the TDR, and all performance results are based on it.

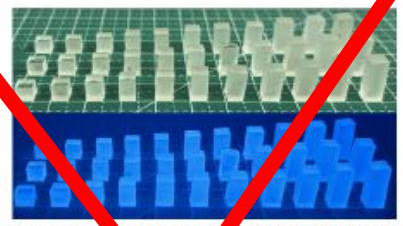

Figure 8.10: GFO glass samples under natural light (top) and ultraviolet light (bottom).

The light attenuation follows the exponential relation is given by $Y = Y_0 \cdot \exp(L/L_0)$, where Y_0 is the initial photon yield, Y the yield after propagation distance L, and L_0 the characteristic attenuation length. Initial measurements yielded $L_0 = 2.3 \pm 0.01$ cm [18], limited by glass matrix defects and Ce^{3+} self-absorption.

Through process optimization, the light yield of GFO glass increased from 1000 to over 1500 ph/MeV, suggesting corresponding attenuation length improvements. Figure 8.11 (a) illustrates the γ-ray spectral method for determining the light attenuation length. The method involves measuring the ratio of the initial light yield (Y_0) to the light yield after transmission through varying glass thicknesses (Y). By fitting this ratio as a function of thickness, we extract the attenuation length, yielding a value of $L_0 = 2.3$ cm and $L_0 = 3.4$ cm for two batches of glass samples before and after optimization, respectively.

A more accurate method determines L_0 through thickness-dependent transmittance (T) can be written as $L_0 = (L_2 - L_1)/\ln(T_{L_1}/T_{L_2})$, where T_L is the transmittance at thickness L. This method accounts for full-volume light penetration, eliminating position uncertainty. Figure 8.11 (b) shows the improved attenuation length of 6.2 cm at 400 nm (emission peak), with consistent 5.8–6.2 cm performance across the visible spectrum - a 100% improvement over previous samples (3.1 cm at 400 nm). These results confirm that γ-ray methods systematically underestimate L_0, while verifying GFO's about 6 cm attenuation length enables efficient light collection.

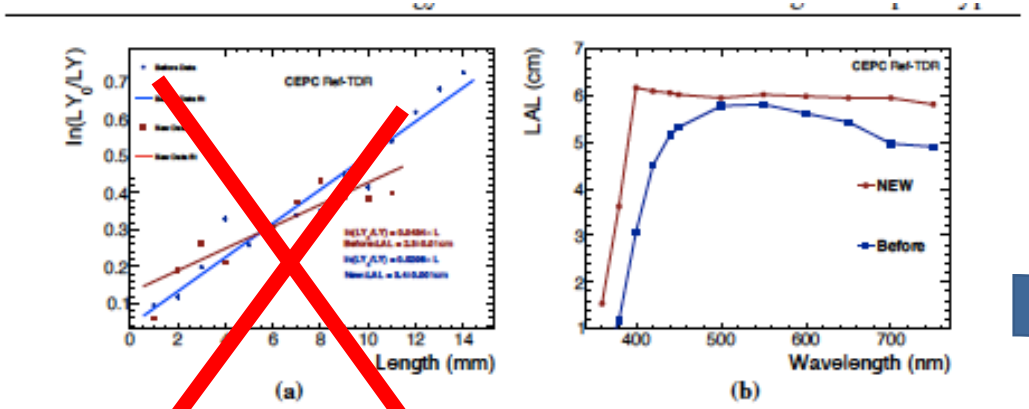

Figure 8.11: (a) Light yield ratio $\ln(Y_0/Y)$ as a function of the thickness of the glass is fitted to extract light attenuation length (LAL). (b) Attenuation length spectrum from transmittance measurements (“New”: current GFO; “Before”: previous samples).

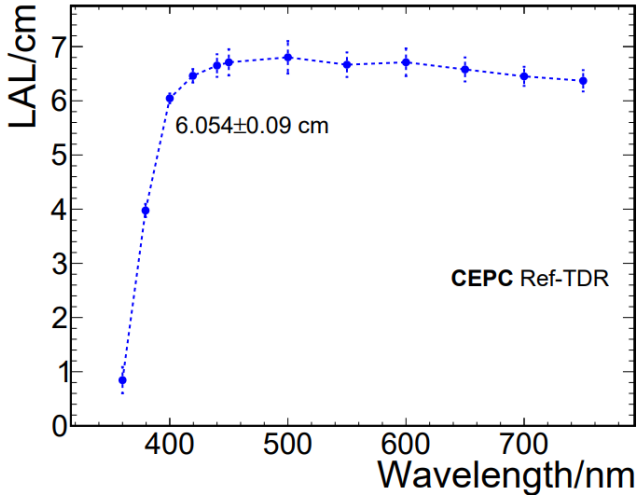

- **rewrite the 8.4.2 Glass scintillator; (3) Radiation resistance ,**
- just delate this part and give the result in (1) Light Yield part. and ref the papaer published in NIMA about this result right now (suggested by Imad).
- **Ref**［**22**］S.H. Yin et al. “Radiation resistance study of Gd-Al-B-Si-Ce3+ glass scintillators using 80MeV proton beam irradiation”. Nucl. Instrum. Meth. A 1081 (2026), p. 170869. issn: 0168-9002.

Radiation resistance

The radiation resistance of glass scintillators is crucial as their performance degrades after irradiation. The GFO glass samples were studied using an 80 MeV proton beam at the Associated Proton Beam Experiment Platform (APEP) [19] across a wide dose range (400 Gy to 4.1×10^4 Gy). Proton flux for this test is 4.86×10^9 (p/cm²/s), and the beam spot size is 50×50 mm². Seven 5×5×10 mm³ pieces (labeled #1–#7) were used for this test, using different radiation time to obtain corresponding radiation dosage as shown in Table 8.5). Sample #1 kept as an unirradiated reference.

The scintillation properties were characterized through transmission spectra, XEL, light output, and decay time measurements (Table 8.5). Unirradiated sample showed 78% transmittance at 400 nm, while transmittance of irradiated samples dropped to 31% with a dose of 800 Gy, and further dropped to 10% for a dose of 8100 Gy, consistent with visible color changes indicating defect formation. The Ce^{3+} emission peak (386 nm in unirradiated samples) shifted slightly to 376–384 nm after irradiation. Figure 8.12 displays the visual changes in samples #1 to #7 under progressively higher radiation doses, with increased dosage correlating to decreased transparency and darker color.

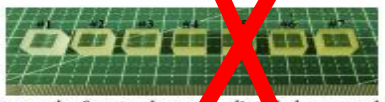

Figure 8.12: The photograph of proton beam irradiated glass samples. From sample #1 to #7, the radiation dosage progressively increases, resulting in darker color with decreased transparency.

In contrast to proton irradiation, gamma irradiation tests evaluate performance degra-

16

Draft v0.3.1

8.4 Technology R&D to demonstrate technologies and prototypes

Table 8.5: Performance summary of the glass tiles after proton irradiation test.

Sample	Dose (Gy)	Transmittance @ 400 nm (%)	XEL (nm)	Light Output (ph/MeV)	Decay Time (τ) (ns)
#1	0	77.9	386	552	87, 985
#2	400	37.4	376	187	89, 980
#3	800	31.3	380	–	–
#4	2000	13.7	384	–	–
#5	4100	10.4	376	–	–
#6	8100	8.3	380	–	–
#7	41000	5.8	376	–	–

dation at lower doses (10–400 Gy). A ^{60}Co point source (3.656×10^{11} Bq) was used, emitting gamma rays at 1.1732 MeV and 1.3325 MeV. The absorbed dose rate follows the inverse square law relative to the source distance. Six 5×5×5 mm³ glass samples were irradiated simultaneously for 37.5 hours at varying distances (10–63 cm) to achieve different dose rates, slight yellowing (darkening in color) for samples with higher radiation dosage can be observed.

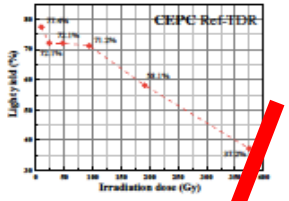

Figure 8.13: Gamma irradiation results showing the relative light yield of the scintillator as a function of irradiation dose. The light yield decreases gradually with increasing dose, reaching 71.2% at 100 Gy.

Scintillation performance was characterized through transmission spectra, XEL, light output, and decay time measurements. The maximum transmittance degradation was 14% - significantly less severe than proton irradiation at comparable doses (400 Gy). This difference likely stems from the lower dose rate and reduced ionization damage in gamma irradiation, as protons have higher linear energy transfer. The emission peaks remained stable (380-386 nm), consistent with proton irradiation results. Light output measurements using the same ^{137}Cs/PMT setup showed progressive degradation: 71% retention at 100 Gy and 37% at 375 Gy, matching proton irradiation trends. Decay times exhibited minimal variation, 87-89 ns fast component, 978 ns slow component, again consistent with proton irradiation observations. The gamma irradiation test results of the scintillator samples, showing the relative light yield as a function of accumulated dose, are shown in Figure 8.13. A significant degradation in light yield is observed with increasing dose,

17

Draft v0.3.1

8.4 Technology R&D to demonstrate technologies and prototypes

with the yield dropping to about 71.2% at 100 Gy. This corresponds to an expected total dosage (about 100 Gy of CEPC HCAL after 10 years of data taking.

The comparative analysis reveals that while both radiation types cause similar qualitative effects, gamma irradiation induces less severe degradation at equivalent doses. This suggests that the damage mechanism depends not only on total absorbed dose but also on radiation type and dose rate, with proton irradiation causing more severe ionization damage due to higher linear energy transfer.

Nuclear Instruments and Methods in Physics Research A 1081 (2026) 170869

Contents lists available at ScienceDirect

Nuclear Inst. and Methods in Physics Research, A

journal homepage: www.elsevier.com/locate/nima

Technical notes

Radiation resistance study of Gd-Al-B-Si-Ce^{3+} glass scintillators using 80 MeV proton beam irradiation

S.H. Yin [a], P. Hu [a,*], S. Qian [b,c], [**], H. Cai [d], D.P. Chen [e], J.F. Han [f], D.B. He [e], C. Hu [g], Z.H. Hua [b], S.Q. Li [d], W.C. Li [e], S. Liu [h], L.S. Qin [i], J. Ren [j], Z.X. Sui [b,j], X.Y. Sun [k], G. Tang [l], Z.L. Wang [l], Y.F. Wen [k], D. Yang [h], M.H. Zhang [g], Y. Zhu [j]

[a] China Nuclear (Beijing) Nuclear Instrument CO., LTD, Beijing, 100176, China
[b] Institute of High Energy Physics, Chinese Academy of Sciences, Beijing, 100049, China
[c] State Key Laboratory of Particle Detection and Electronics, Beijing, 100049, China
[d] China building materials academy, Beijing, 100024, China
[e] Shanghai Institute of Optics and Fine Mechanics, Chinese Academy of Sciences, Shanghai, 201800, China
[f] Institute of Nuclear Science and Technology, Sichuan University, Chengdu, 610064, China
[g] Shanghai Institute of Ceramics, Chinese Academy of Sciences, Shanghai, 201899, China
[h] Beijing Glass Research Institute, Beijing, 101111, China
[i] College of Materials and Chemistry, China Jiliang University, Hangzhou, 310018, China
[j] College of Physics and Optoelectronic Engineering, Harbin Engineering University, Harbin, 150001, China
[k] Department of Physics, Jinggangshan University, Ji'an, 343009, China
[l] Research Center for Space Optical Engineering, Harbin Institute of Technology, Harbin, 150001, China

ARTICLE INFO

Keywords:
Glass scintillators
Radiation resistance
Proton beam
Scintillation performance

ABSTRACT

High-density Ce^{3+}-doped Gd-Al-B-Si glass scintillators have been developed by the Glass Scintillator R&D Collaboration (GS Collaboration) for applications in nuclear and high energy physics. One of the critical factors in these applications is the radiation resistance of the glass scintillator. The impacts of proton irradiation on Ce^{3+}-doped Gd-Al-B-Si glass samples have been investigated at doses up to approximately 4×10^4 Gy, utilizing the 80 MeV proton beam on the Associated Proton Beam Experiment Platform (APEP) located at the China Spallation Neutron Source (CSNS). The optical and scintillation properties, including emission, transmittance, light output, decay time and their degradation after proton irradiation, have been measured. Blue shifts of emission peaks were observed in X-rays excited luminescence (XEL) spectra after proton irradiation. Additionally, a red shift in the cut-off wavelength and a decrease of approximately 50% in transmittance at 400 nm were also observed after proton irradiation. The light output decreases by approximately 2/3 after 400 Gy proton irradiation, without significant alteration in the decay time constants of fast and slow components. This research serves as an important reference for evaluating the radiation resistance of high-density Gd-Al-B-Si-Ce^{3+} glass scintillators and can guide their practical applications.

1. Introduction

Over recent decades, significant progress has been made in high performance scintillation materials due to increasing demand. Among solid-state scintillators, glass scintillators distinguish themselves through tunable scintillation performance and physicochemical properties, which can be customized by modifying the glass matrix composition and dopants to meet application-specific requirements. Furthermore, glass scintillators are advantageous due to their relatively simple preparation process, low cost, excellent moldability, and scalability for mass production [1]. These features provide glass scintillators with great potential for application in various fields, including high-energy physics experiments [2–4], nuclear radiation monitoring [5,6], nuclear radiation imaging [7–9] and other fields [10,11].

In comparison to plastic and crystal scintillators, glass scintillators with high density, moderate light yield, and fast decay time present notable advantages in the design of calorimeters for large colliders, such as the CEPC (Circular Electron-Positron Collider) [12]. These properties enable excellent detection performance in a cost-effective

* Corresponding author.
** Corresponding author at: Institute of High Energy Physics, Chinese Academy of Sciences, Beijing, 100049, China.
E-mail addresses: hupeng6550575@163.com (P. Hu), qians@ihep.ac.cn (S. Qian).

Comments on Draft v0.4

- C-B-8-9: **The constant term is still an issue.**
  - C-B-8-9-1: Line 7867: "Both approaches led to a reduction in the fitted constant term". What was the fraction of the events that were selected?
  - C-B-8-9-2: We propose to show the linearity in addition to the resolution
  - C-B-8-9-3: Please comment on the expected e/h ratio
  - C-B-8-9-4: We understand "all inner sub-detectors are removed" in this study.
  - C-B-8-9-5: Since there will be an ECAL before the HCAL in the actual experiment, the effective depth of calorimetry will be larger and the selection and constant term (with and without selection) will be different. It is also interesting to investigate how the different responses in the ECAL and the HCAL will impact the constant term in the integrated detector.
  - C-B-8-9-6: The AHCAL prototype discussed in Sec. 8.6.2 has a depth (from memory) of 4-5 interaction lengths but a constant term of only 2.59%. Thus, the depth cannot be the only reason for the large constant term of the GS HCAL

  -- we agree with your suggestions above, we are implementing them one by one, as you have correctly pointed out, this section have already rewriten with these comments in the new version in **Section 8.5.2** Hadron Energy Resolution and in **Section 8.5.3** Energy Response e/h Studies.

Comments on Draft v0.4

- The constant term is still an issue.
  - C-B-8-9-1: Line 7867: "Both approaches led to a reduction in the fitted constant term". What was the fraction of the events that were selected?

it is less than 20%, the selection requires the shower starts in the first 60mm, corresponding to the first two layers, about 0.25 nulcear interaction length, which agrees with the calculation usign the simplified formula P = 1-exp(-0.25) ~ 0.2 . Attached is the eff. (fraction of starting showin in first two layers) vs each energy points in the simulation.

the text modified to be "The other required the hadrons to initiate their first interaction within the first two layers of the \gls{GS-HCAL} (corresponding to the initial $0.25\lambda_\mathrm{I}$), though such events constituted less than 20\% of the total sample."

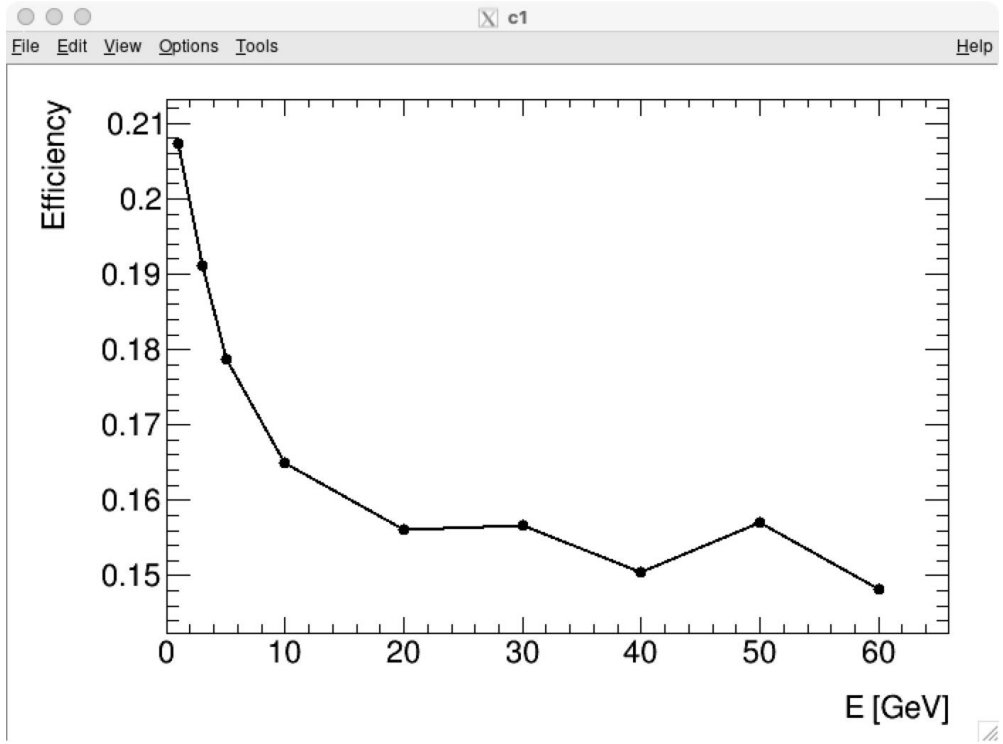

Comments on Draft v0.4

- The constant term is still an issue.
  - C-B-8-9-2: We propose to show the linearity in addition to the resolution

--As shown in Fig. 8.24, conparing linearity and resolution between with and without digitisation, the linearity does not show a apparent issue, i.e. the leackage, or the hadronic shower longitudinal profile is not expected to depend on the energy of the incident hadrons, e..g.

accroding to some previous studies such as [Y.A. Kulchitsky, V.B. Vinogradov/Nucl. Instr. and Meth. in Phys. Res. A 413 (1998) 484—486], where Longitudinal profiles of the hadron showers of 20 GeV (crosses), 50 GeV (squares), 100 GeV (open circles) and 140 GeV (triangles) energies as a function of the longitudinal coordinate x in units j

I for the conventional iron-scintillator calorimeter do not show apparent difference in the shape.

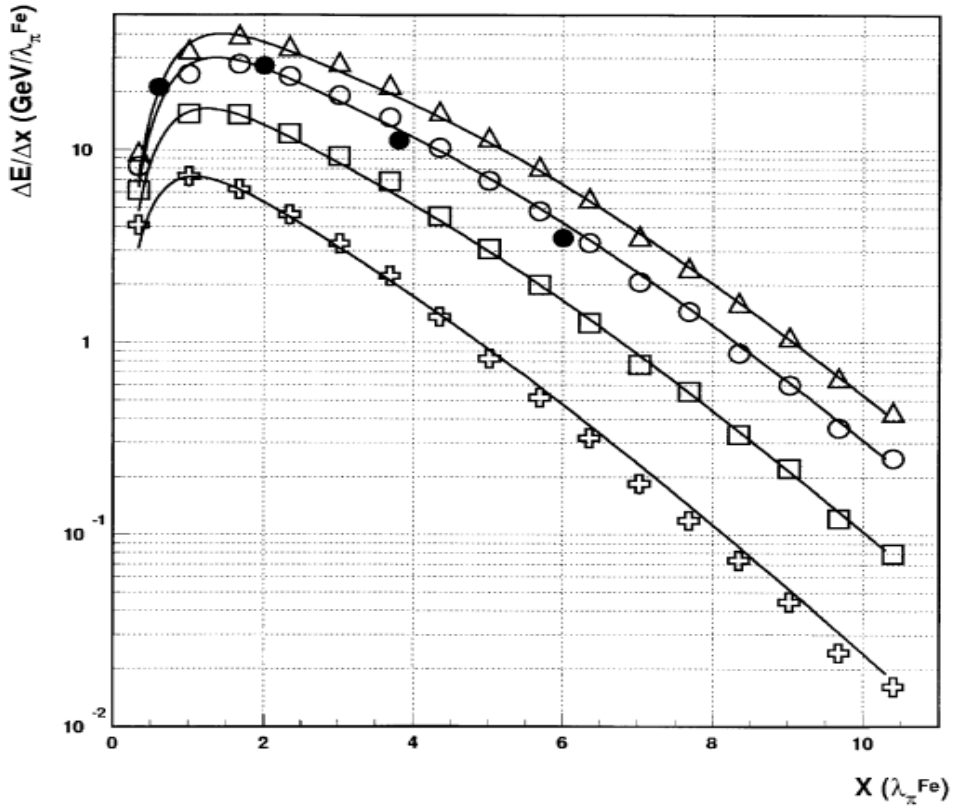

Fig. 1. Longitudinal profiles of the hadron showers of 20 GeV (crosses), 50 GeV (squares), 100 GeV (open circles) and 140 GeV (triangles) energies as a function of the longitudinal coordinate x in units λ_I for the conventional iron-scintillator calorimeter [4] and of 100 GeV (black circles) for the tile iron-scintillator calorimeter [8]. The solid lines are calculations by function (3) with parameters from Ref. [4].

Comments on Draft v0.4

- The constant term is still an issue.
  - C-B-8-9-3: Please comment on the expected e/h ratio

--We added a new subsection based on previous samples describing e/h results " 8.5.3 Energy Response e/h Studies."

By fitting the energy responses of electron and pion, kion...etc, the e/h is derived to be from 1.02 to 1.14, exhibits a non-compensation at the level of 9–14%,

  - C-B-8-9-4: We understand "all inner sub-detectors are removed" in this study.

-- indeed, added this information in the following setence in the pretty beginning of this section. :

“In initial studies of the \gls{GS-HCAL}, the energy resolution yielded a constant term (b) of approximately 5–6\% based on Geant4 full simulations with all inner sub-detectors (e.g., \gls{ECAL}) removed. ”

Comments on Draft v0.4

- The constant term is still an issue.
  - C-B-8-9-5: Since there will be an ECAL before the HCAL in the actual experiment, the effective depth of calorimetry will be larger and the selection and constant term (with and without selection) will be different. It is also interesting to investigate how the different responses in the ECAL and the HCAL will impact the constant term in the integrated detector.

  -- Indeed, agree, with the ECAL infront of HCAL the overall ECAL+HCAL PFA results will largely reduce the impact of the leagage, and therefore smaller constent term. A through study is needed as the next step after TDR, but we already added this point here:

  "As mentioned before, the leakage studies were performed with \gls{HCAL}-only. In the full \gls{CEPC} detector configuration, the \gls{ECAL} with about $1.2\lambda_\mathrm{I}$ will cause approximately 70\% of hadrons to initiate showers before reaching the \gls{GS-HCAL}.

  This upstream shower development is expected to significantly reduce leakage effects and consequently lower the constant term in the combined \gls{ECAL} and \gls{HCAL} system."

  - C-B-8-9-6: The AHCAL prototype discussed in Sec. 8.6.2 has a depth (from memory) of 4-5 interaction lengths but a constant term of only 2.59%. Thus, the depth cannot be the only reason for the large constant term of the GS HCAL

  --After verify this point we learned that the beam test results onf the AHCAL prototype showing 2.59% constant term is after a selection of events showing interactions (with energy deposition) in the first several layers to keep sufficient containment in the AHCAL, and avoid leakage from the back.

Comments on Draft v0.4

- Line-by-Line Comments
- C-B-8-10-1: Line 6952 - "The HCAL is a key component in achieving the jet energy resolution". One may could argue it is THE key component

--agree, indeed, Re-written the beginning of the chapter, and provided justification and discussion why HCAL is "THE key component", e.g. HCAL is responsible for the reconstruction of >70% of jet energy....etc.

- C-B-8-10-2: Lines 6962-6964 "plastic scintillators and gaseous detectors, with readout based on SiPMs or other photon sensors.". This is confusing. Maybe "plastic scintillators, with readout based on SiPMs or other photon sensors, and gaseous detectors."?

--agree, fixed, Re-written the beginning of the chapter.

- C-B-8-10-3: Line 6983 "$W$and Zdecays" - spaces missing - "W and Z decays"

--agree, fixed, re-written the beginning of the chapter.

- C-B-8-10-4: Lines 7042-7043: "851.34 mm" and "1367.56mm" are unnecessarily precise (10 microns). Could this be rounded off to mm? --agree, fixed.
- C-B-8-10-5: Figure 8.3: "851.34 mm" and "1367.56mm" are unnecessarily precise (10 microns). Could this be rounded off to mm? --agree, fixed.
- C-B-8-10-6: Lines 7570-7574: Could some example distributions be shown? --Added.
- C-B-8-10-7: Line 8066 "measure hadronic jets energy" I believe jet should be singular. "measure hadronic jet energy" line 8068 "GS and SiPMs'. We suggest spelling these out again when first mentioned in the summary ----agree, fixed.
- C-B-8-10-8: Line 8082 "This can be achieved" -> may be achieved? -> "This may be achieved" -----agree, fixed.

---Agree, the pointed out parts have already update in the new version.

Comments on Draft v0.4.1 from Roman

The comments from Roman on 29th.July. 2025.

- ----all the comments are replayed one by one within the PDF file.
- **<CEPC_Ref_TDR_v0.4.1_BarcelonaEdition-Roman_reply.pdf>**

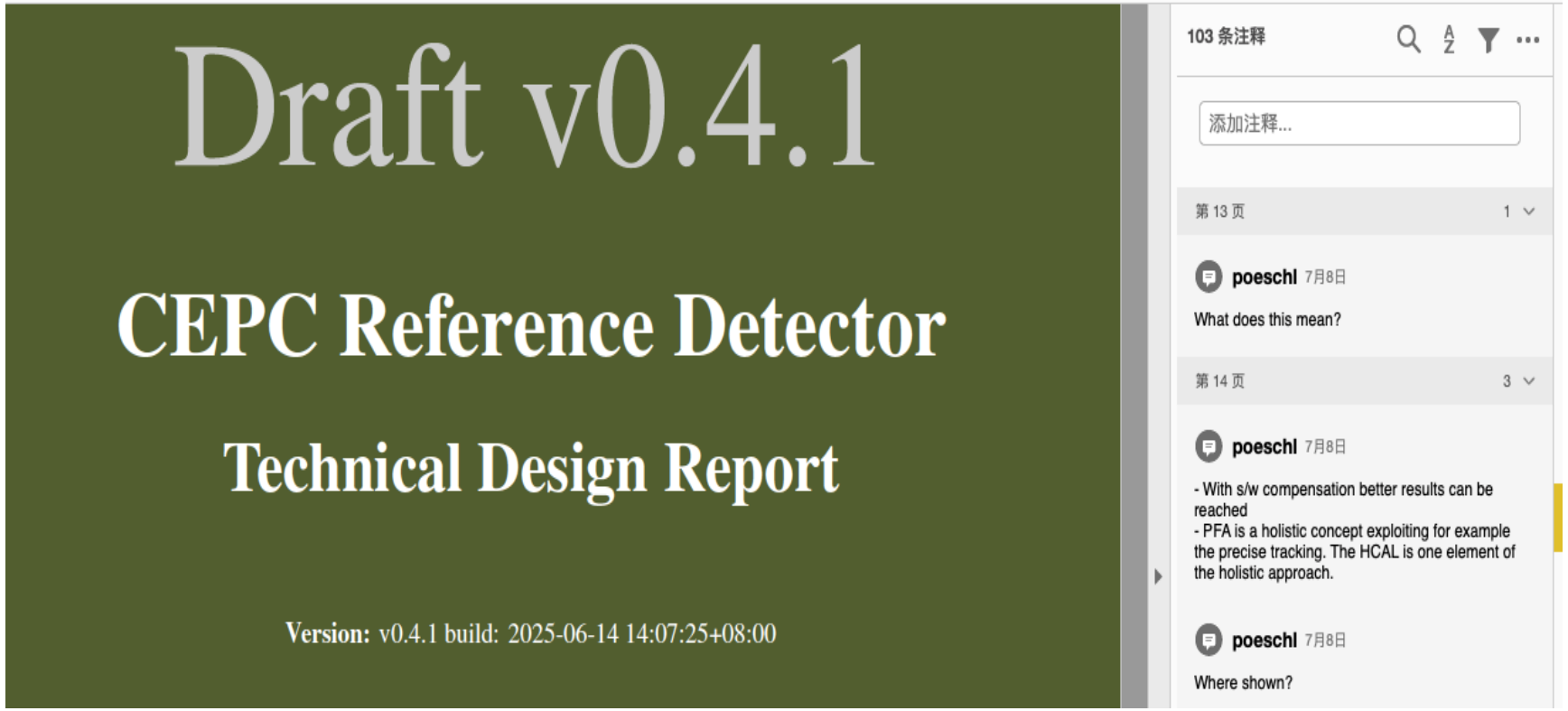

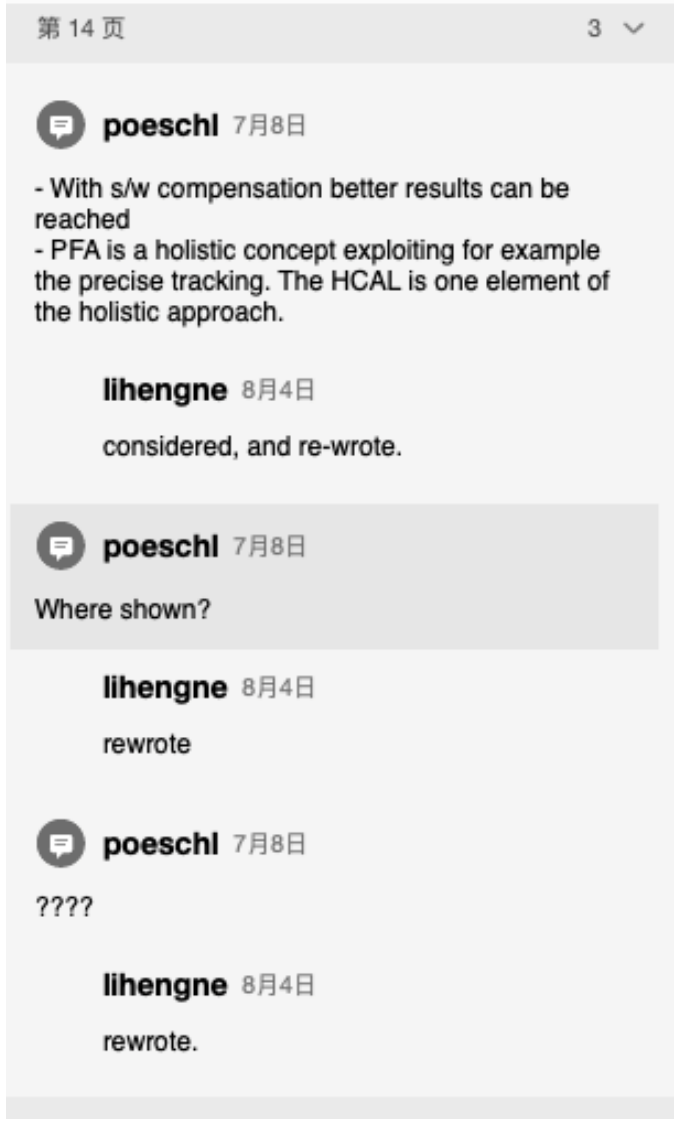

Comments on Draft v0.4.1 from Roman

C-B-8-11: Origin of four emission lines in GFO spectrum (is the multiline structure a problem?

- ----no, it's not the background noice, it is the usefull signals. They are the ADC pedestal,
- the 32keV peak,
- the 180keV peak,
- and the 662keV full-energy peak.

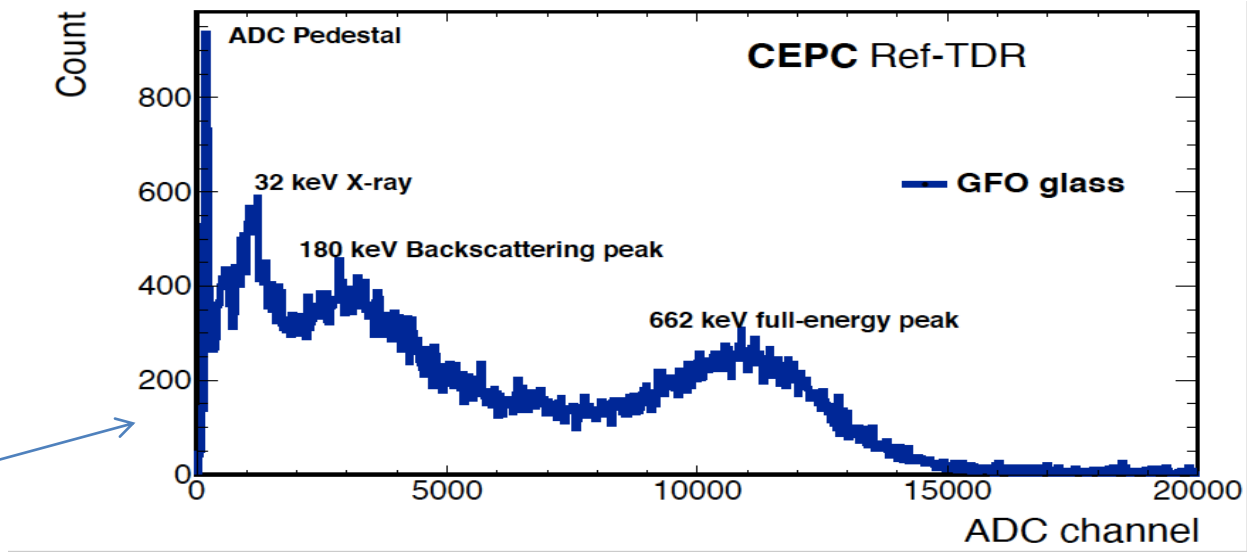

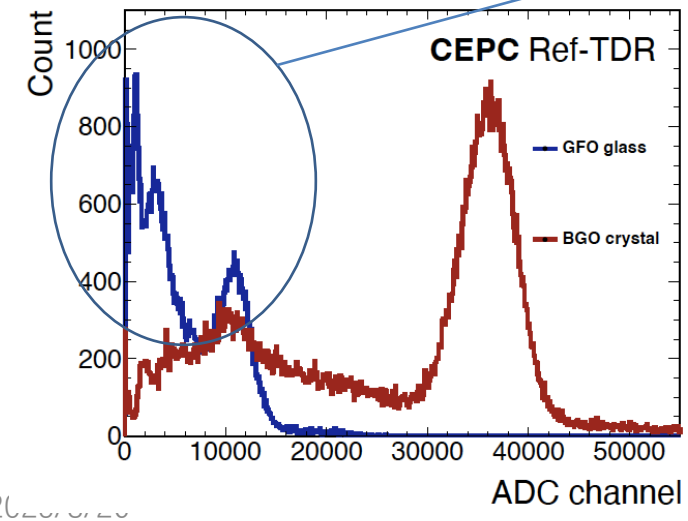

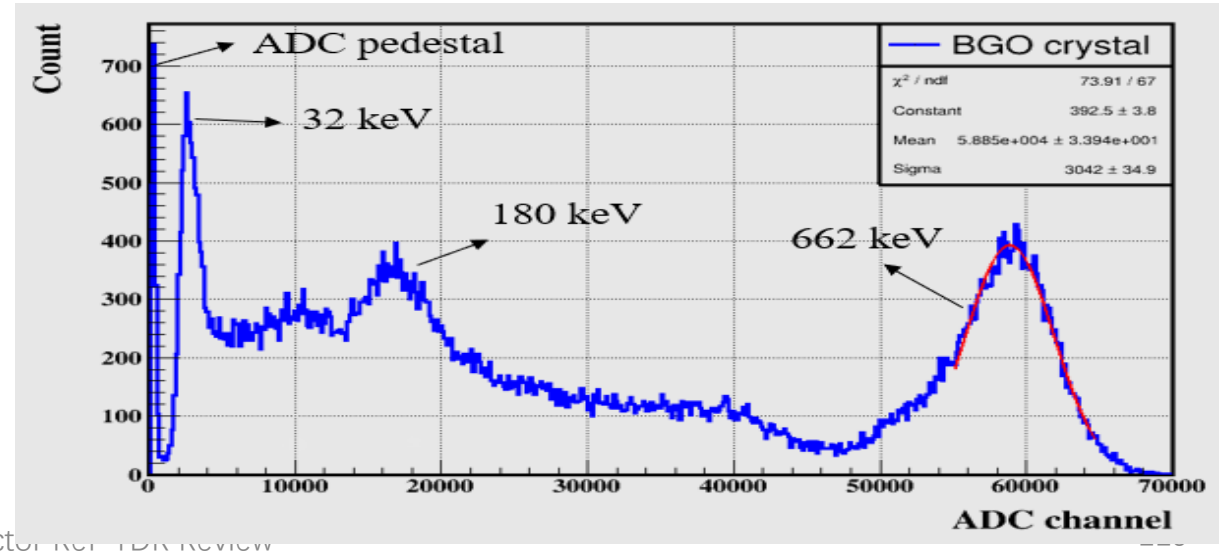

MUON

Findings

- F-A-9-1: The TDR presents a baseline design for the Muon Detector based on extruded plastic scintillator (PS) bars, coupled with WLS fibers and SiPMs. This approach is cost-effective, and the primary objective is to demonstrate that the system can meet stringent performance requirements across the detector's large active area.

- F-A-9-2: The Muon Detector will consist of six superlayers in both the barrel and endcap regions. It uses long scintillator strips, 4 cm wide, with lengths exceeding 4 meters. Due to WLS fiber routing, effective optical lengths can be even longer, making attenuation length a critical parameter, directly impacting timing resolution and detection efficiency. Enhanced light collection strategies are thus essential.

- F-A-9-3: The readout system adapts designs from the ECAL and HCAL and includes uSiPMs, front-end boards (uFEBs), and management boards (uMBs), tailored specifically for the Muon Detector. 14 Background studies show a maximum hit rate of ~2 Hz/cm^2, comfortably below the system's rate capability.

- F-A-9-4: The Muon Detector supports trigger functionalities, including tagging long-lived particles (LLPs), although integration into the full CEPC TDAQ system remains preliminary. RPC technology, using environmentally friendly gases, is also under consideration via the DRD1 collaboration.

Comments

The TDR chapter and the review presentation show significant technical progress with clear physics motivation and encouraging prototype results. However, several areas need further development:

- C-A-9-1: Testing of full-length bars (4.2–5 m) must be completed, fully implementing optimized light collection methods.
- C-A-9-2: Standardized procedures for optical glue application (thickness, curing time) and validation of coating quality at scale are still required. A detailed system-level comparison between NDL and MPPC SiPMs is lacking. Given the Muon Detector's lower light yield and tighter timing requirements compared to calorimeters, selecting the optimal SiPM is critical.
- C-A-9-3: Consolidated detector specifications (spatial and time resolutions) must be validated through simulations and trigger performance studies

Comments

- C-A-9-4: Testing of full-length bars (4.2–5 m) must be completed, fully implementing optimized light collection methods.
  - Prototypes incorporating 5m long PS bars have been successfully developed and tested, as depicted in Fig. 9.12 of the TDR v0.6.0. These new PS bars exhibit a 50% enhancement in fluorescence yield. The prototypes utilize WLS fibers with a diameter of 2.0 mm, and the coupling between the WLS fibers and the sensitive area of the SiPMs being improved. However, due to the technical challenges associated with applying optical glue uniformly along the 5m PS bars, no optical glue was used to optimize the coupling between the PS bars and the WLS fibers. Testing of the 5-meter prototypes at their far ends demonstrated an average nPE of ~35, a time resolution of ~1 ns, and an efficiency of ~97% at an nPE threshold of 15. The prototypes achieved the required performance without the use of fill glue within the PS strip's hole, validating the design's effectiveness under these conditions. Filling optical glue in a 5m bar to enhance the light collection is implemented into the future R&D.

Comments

- C-A-9-5: Standardized procedures for optical glue application (thickness, curing time) and validation of coating quality at scale are still required. A detailed system-level comparison between NDL and MPPC SiPMs is lacking. Given the Muon Detector's lower light yield and tighter timing requirements compared to calorimeters, selecting the optimal SiPM is critical.

  The primary challenge in optical glue application lies in uniformly filling the glue in PS bars exceeding 4m in length. This process remains under a further R&D, and we are collaborating with the company to establish a test procedure for validating the quality of the coating.

  We have completed a system-level comparison between NDL and MPPC SiPMs, and the results have been documented in the TDR, as illustrated in Fig. 9.11 of v0.6.0. The NDL SiPMs demonstrate consistent quality and stability in mass production. Testing of a 5m prototype yielded an average nPE of approximately 35 at the far end, with the nPE consistently exceeding the threshold of 15 for signals from MIPs in cosmic ray tests. Although the NDL SiPMs exhibit lower gain, DCR, and increased cross-talk compared to MPPC SiPMs, both types perform equally in terms of efficiency and time resolution. NDL SiPM has a large advantage in cost.

  Additionally, we have identified a new WLS fiber from Kuraray, which features a significantly shorter decay time. This fiber is currently under evaluation, and we anticipate improved performance in time resolution as a result of its enhanced characteristics.

Comments

- C-A-9-6: Consolidated detector specifications (spatial and time resolutions) must be validated through simulations and trigger performance studies

  Currently, the software and simulation focus on standalone muon identification and pion fake rate analysis. The spatial and time resolutions depend on standalone track reconstruction within the muon detector, which has not yet been implemented. This will be addressed in the next step, along with the trigger performance study.

Recommendations

- R-A-9-1: Complete comprehensive tests on full-length bars using final SiPM configurations and 2.0 mm WLS fibers, measuring timing, light yield, and efficiency.

Prototypes utilizing 5-meter-long plastic scintillator bars, 2.0 mm-diameter wavelength-shifting (WLS) fibers, and EQR-20 SiPMs have been tested. The results demonstrate a time resolution of 1 ns, an average nPE of approximately 35, and an efficiency of 97% at a threshold of 15 photoelectrons.

- R-A-9-2: Define standard application procedures and conduct studies addressing mechanical stability, aging, radiation resistance, and refractive index.

We have outlined the standard procedure for assembling a plastic scintillator unit (PSU), constructing a detector module, and installing the module into the muon detector in the TDR. The process is designed to minimize mechanical complications. In the near future, we plan to build detector modules to evaluate mechanical stability.

We recently completed research and development for 5-meter-long scintillator bars, focusing on enhancing fluorescence. Using these new samples, we will soon conduct studies on mechanical stability, aging, radiation resistance, and refractive index.

Recommendations

- R-A-9-3: Systematically assess MPPC and NDL SiPMs (including new 20 μm pixel versions), focusing on gain, DCR, cross-talk, and operating thresholds under realistic conditions.

We conducted a systematic comparison between MPPC and NDL SiPMs, specifically the MPPC S14160-3050 and the NDL ERQ20-11-3030. The results are detailed in Section 9.3.1 and Figure 9.11 of the TDR v0.6.1. The tests focused on key parameters such as gain, DCR, cross-talk, and breakdown voltage.

- R-A-9-4: Expand simulation studies to include full event samples, especially displaced vertex signatures, to validate and refine time resolution requirements.

This study has not yet been conducted, as the current focus remains on muon identification and reducing the pion fake rate. We plan to carry out the recommended analysis in the near future. Achieving excellent time resolution is critical, as it not only facilitates the identification of signals from displaced vertices but also enhances background suppression, eliminates ghost tracks in cases of multiple tracks within a detector sector, and improves the search capabilities for LLPs. For these purposes, we aim for the best possible time resolution.

- R-A-9-5: Clearly state detector performance requirements linked to physics goals. Move Muon ID algorithm discussions to the global TDR Performance chapter and focus this chapter on local and standalone performance. Ensure consistent technical terminology and improve figure referencing.

In accordance with the recommendation, we have moved the discussion on the overall muon ID algorithm from the TDR. The current discussion now focuses on the standalone muon ID for the muon detector. Additionally, we have updated the figures in Section 9.4 of the TDR v0.6.1.

Findings on Draft v0.4.1

- The updated Muon Detector chapter in the CEPC Reference TDR (Barcelona version) shows clear improvements over the previous iteration:
  - The chapter is better structured and easier to navigate.
  - A performance summary table is now included early in the chapter.
  - Key technologies—such as SiPMs, long scintillator strips, and optical coupling—are described more clearly.
  - The new EQR-20 SiPM (20 μm pixel, higher gain, lower DCR) is introduced, and preliminary test results are presented.
  - Initial prototype results for long strips (up to 4–5 m) are now included.
- These updates are welcome and demonstrate tangible progress. However, several important technical and editorial issues remain only partially addressed or unresolved.

Comments on Draft v0.4.1

1. Long-bar prototype test results

- C-B-9-1-1: The inclusion of tests for 4–5 m strips is a positive step, but the presented information lacks clarity and context.
- C-B-9-1-2: Figures (e.g., Fig. 9.12) are not well integrated into the text and sometimes captions are confusing.
- C-B-9-1-3: The intended target threshold remains undefined, despite reporting signal yields at various p.e. levels.
- C-B-9-1-4: Results from IHEP and Fudan differ in setup (SiPM type, fiber), and the comparison lacks explanation.
- C-B-9-1-5: Dual-ended readout is briefly mentioned but not quantified or discussed.

The long-bar prototype test was incomplete in Draft v0.4.1, as the results from both IHEP and Fudan did not align with the design of the plastic scintillator unit. We have since completed the test using new prototypes, which feature 5m-long plastic scintillator bars, NDL EQR20 SiPMs, and 2.0mm-diameter WLS fibers. Additionally, there was the test conducted with dual-ended readout. All new results are presented in Section 9.3.3 and Fig. 9.12.

Comments on Draft v0.4.1

2. SiPM characterization (NDL vs. MPPC)

- C-B-9-2-1: While pixel size and gain differences are noted, the comparison remains superficial.
- C-B-9-2-2: Critical performance aspects—such as timing, noise, cross-talk, and behavior under temperature or radiation—are not evaluated.
- C-B-9-2-3: There is no final decision or validation plan for SiPM selection.

We conducted a systematic comparison between MPPC S14160-3050 and NDL EQR20-11-3030 SiPMs. While the MPPC demonstrates advantages in gain, dark count rate (DCR), and cross-talk, these characteristics do not significantly enhance performance in the PSU application. On the other hand, the NDL EQR20 offers benefits in terms of operating voltage and cost. Based on these findings, we clearly state that the NDL SiPM is the preferred option.

Comments on Draft v0.4.1

3. Readout architecture and threshold definition

- C-B-9-3-1: The readout chain is inherited from ECAL/HCAL but lacks justification for its use in the Muon Detector.
- C-B-9-3-2: Lower light yield and tighter timing constraints raise concerns about its suitability.
- C-B-9-3-3: Thresholds shown in figures are not linked to a defined operating point or noise model.

(Difficult to answer from muon group.)

4. Trigger strategy

- C-B-9-4-1: Trigger concepts are mentioned (e.g., LLP tagging), but no logic, architecture, or latency assessment is included.
- C-B-9-4-2: No integration plan with the CEPC trigger system is presented.

(Difficult to answer from muon group.)

Comments on Draft v0.4.1

5. Simulation studies and background

- C-B-9-5-1: Beam background simulations are provided and show manageable occupancies.
- C-B-9-5-2: Section 9.4.3 suffers from language issues (tense shifts, awkward phrasing).
- C-B-9-5-3: No physics-driven simulation studies (e.g., low-pT muons, displaced vertices) are presented.
- C-B-9-5-4: Detector performance specs (e.g., timing, granularity) are not explicitly linked to physics goals.

We have revise the section for simulation studies and backgrounds. As discussed before, we need more studies on software and simulation.

Comments on Draft v0.4.1

6. Structure and editorial issues

- C-B-9-6-1: Figure referencing is sometimes incomplete.
- C-B-9-6-2: Section 9.3.3: The last paragraph of this section is duplicated, likely due to a copy-paste error. This repetition should be removed. In addition, the text would benefit from a general language revision to fix grammatical issues (e.g., subject-verb agreement, article usage) and improve clarity.
- C-B-9-6-3: Section 9.4.3: The background paragraph conveys relevant information, but the English requires significant improvement. Verb tenses are inconsistent, and some expressions are unclear or incorrect. A thorough revision is needed to improve clarity and readability.
- C-B-9-6-4: Terminology and language quality vary across the chapter and require final editorial revision.

We have made extensive revisions to the structure, figures, and language, as detailed in TDR v0.6.1.

Recommendations on Draft v0.4.1

Considering that the TDR is near completion, we do not expect extensive new studies. Nonetheless, to improve clarity and completeness, we recommend:

R-B-9-1: Clarify prototype study objectives

- Explicitly state the performance targets (e.g., threshold, signal yield, efficiency, timing) for long-strip tests and explain how the results support detector requirements.
  Threshold and noise strategy
  Even if a final threshold is not yet fixed, describe the criteria and expected noise level. Justify the thresholds used in figures and explain how they relate to realistic detector conditions.

In a realistic detector condition, the threshold can be adjusted according to the background level. Typically, the threshold is nPE~8.

Recommendations on Draft v0.4.1

R-B-9-2: Readout chain evaluation

- Acknowledge the differences between the Muon and ECAL/HCAL environments. Outline how the current electronics will be validated or adapted to meet the Muon Detector's demands.

We will add the related discussion in the next version of the TDR.

R-B-9-3: SiPM selection process

- Describe the performance metrics which will drive SiPM selection (e.g., dark noise, gain, radiation tolerance) and outline upcoming R&D needed for final validation.

To date, the tests have demonstrated that both the MPPC and NDL SiPMs meet the required performance specifications for the muon detector.

Recommendations on Draft v0.4.1

R-B-9-4: Trigger implementation

- Provide at least a minimal scheme and indicate how integration with the CEPC trigger system will be assessed.

(Difficult to answer from muon group. It may require a standardalone track reconstruction, which has not been done.)

R-B-9-5: Simulation roadmap

- Include plans to simulate full physics events and connect detector specs to the physics motivation (e.g., LLP, muon ID performance).

We will add this into the research plan in the TDR.

R-B-9-6: Final editorial revision

- Ensure all figures are referenced in the text, remove the duplicated paragraph in Section 9.3.3, and revise language in Section 9.4.3 for clarity.

This has been done, see TDR v0.6.1.

SUPERCONDUCTING SOLENOID

Findings

- F-A-10-1: The CEPC Ref-TDR superconducting solenoid design has made significant progress. The solenoid provides a central magnetic field of 3T (for $t\bar{t}$, Higgs, and W runs) and 2–3T (for Z runs), with an inner bore diameter of 7.07 m and a cryostat/yoke half-length of 4.53 m. It is enclosed within an iron yoke that also houses the muon detector. The variation of the solenoid magnetic field in the central tracker (TPC) region is currently calculated to be approximately 10%.
- F-A-10-2: The solenoid coil design is based on four layers of Al-stabilized superconductor, supported by an aluminum-alloy outer support cylinder and cooled using a two-phase helium thermosiphon system. This general design concept is well established, drawing on the reliable design experience of the CERN-LHC CMS detector.
- F-A-10-3: A key technology development effort focuses on Al-stabilized superconductors, with two approaches to mechanical reinforcement:
  - Option A: Double-layered, two-step co-extrusion process.
  - Option B: Single extrusion with micro-alloying for reinforcement, followed by a cold-work process.
- F-A-10-4: Further R&D is planned for 2025.
- F-A-10-5: The maximum von Mises stress on the Al-stabilizer during magnet excitation is evaluated at 96 MPa, which is close to the current yield strength of the Al-stabilizer material (105 MPa). Further mechanical evaluation is necessary to ensure an adequate safety margin, including the mechanical integrity of the NbTi/Cu superconductor itself.
- F-A-10-6: Remaining technical challenges primarily concern the production of large-scale, high-strength Alstabilized superconductors, as well as ensuring the reliability of the numerous aluminum-pipe welds required in the thermosiphon cooling system

Comments and Recommendations

SYSTEM MAGNET

- C-A-10-1: Field uniformity in the TPC region is a fundamental boundary condition for detector performance. The current 10% field variation must be carefully assessed to ensure it is acceptable for the required TPC performance. It is important to note that the ALICE detector has a different configuration, and that the ALICE magnet is much larger resulting in significantly better field quality in its TPC region compared to CEPC.
- R-A-10-1: Carefully verify that the magnetic field uniformity of the CEPC Ref-TDR solenoid meets the TPC performance requirements without introducing unacceptable distortions to particle drift paths. If the current configuration proves insufficient, consider alternative design modifications—such as the addition of compensation windings in the forward and backward regions, as explored in ILD studies, or adjustments to the shape and configuration of the magnetic iron poles.

Impact on tracking: **Ref TDR: 349-352**

- The impact of non-uniform magnetic field on the momentum measurement can be minimized if the track fitting algorithm (i.e. Kalman filter) can deal with the non-uniform magnetic field with the measured magnetic field map.

The key issue is whether we use a right field map in software. Two requirements

- Measurement precision of the magnetic field map is good enough.
- Gradient of the field small enough (The map is smooth, without big fluctuation within small area)

CEPC magnetic field gradient of the TPC region:

The gradient of TPC region is around $5.4*10^{-5}$ T/mm, which is small enough and meets the requirement

Measurement precision:

If the measurement precision is 10^{-3} (i.e., position error during measurement is around 1mm), the deviation of B is around $5.4*10^{-5}$ T according the gradient, which meets the requirement of momentum resolution (~0.1%)

An example of BESIII

- NUMF in BESIII is 5%, and measurement error of B is around 0.3%
- The momentum resolution is good as the expected after the track fit with Kalman filter and track-based calibration. No significant impact from NUMF is observed.

Comments and Recommendations

- C-A-10-2: The committee recognizes the remarkable progress achieved in developing Al-stabilized superconductors, achieving a yield strength of 105 MPa at 4.2 K using micro-alloying (Ni + Be). However, further R&D is required to demonstrate the full mechanical performance of the conductor and the successful fabrication of full-scale Al-stabilized superconductor segments.
- C-A-10-3: It is critical to demonstrate that the full conductor (NbTi/Cu + Al-stabilizer) can withstand mechanical stress up to 135 MPa. This threshold is about 50% higher than the maximum von Mises stress (~90 MPa) expected during operation at 3T. If achieving this mechanical strength proves difficult, increasing the thickness of the support cylinder could be considered, although this would be undesirable. As a last resort, if necessary, a reduction in the operating field strength may need to be discussed.
- C-B-10-5: The mechanical stress analysis is advanced. However, the results have not been clear enough and the mechanical safety design has not been clearly described. It would be very important to determine necessary mechanical strength of the Al-stabilized superconductor with the box-type design and to be consistent with the performance test results from the conductor development. It must be critically evaluated.

The stress issue can be addressed by the development of Box-type conductor, which has a better mechanical performance.

Secondary co-extrusion **Box-type** Cable size and structure: **56mm*22mm (Box type)**

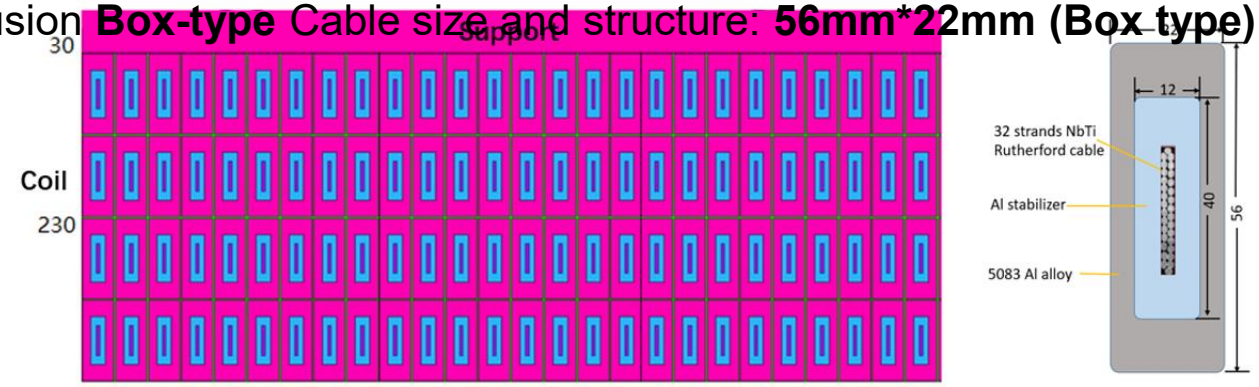

Ref TDR: 352-353

Comments and Recommendations

Ref TDR: 352-353

The maximum stress on the coil is 246 MPa, located in the NbTi/Cu cable. The high-purity aluminum stabilizer experiences a maximum stress of 22.5 MPa, while the aluminum alloy and aluminum alloy support reach maximum stresses of 137 MPa and 127 MPa, respectively. The maximum shear stress in the epoxy glass fiber is 10.6 MPa.

The average Von Mises stresses in this turn are 132 MPa for NbTi/Cu, 16.6 MPa for the aluminum stabilizer, and 65.9 MPa for the reinforcement.

Maximum stresses in all coil materials remain within allowable limits, providing sufficient safety margins for stable coil operation.

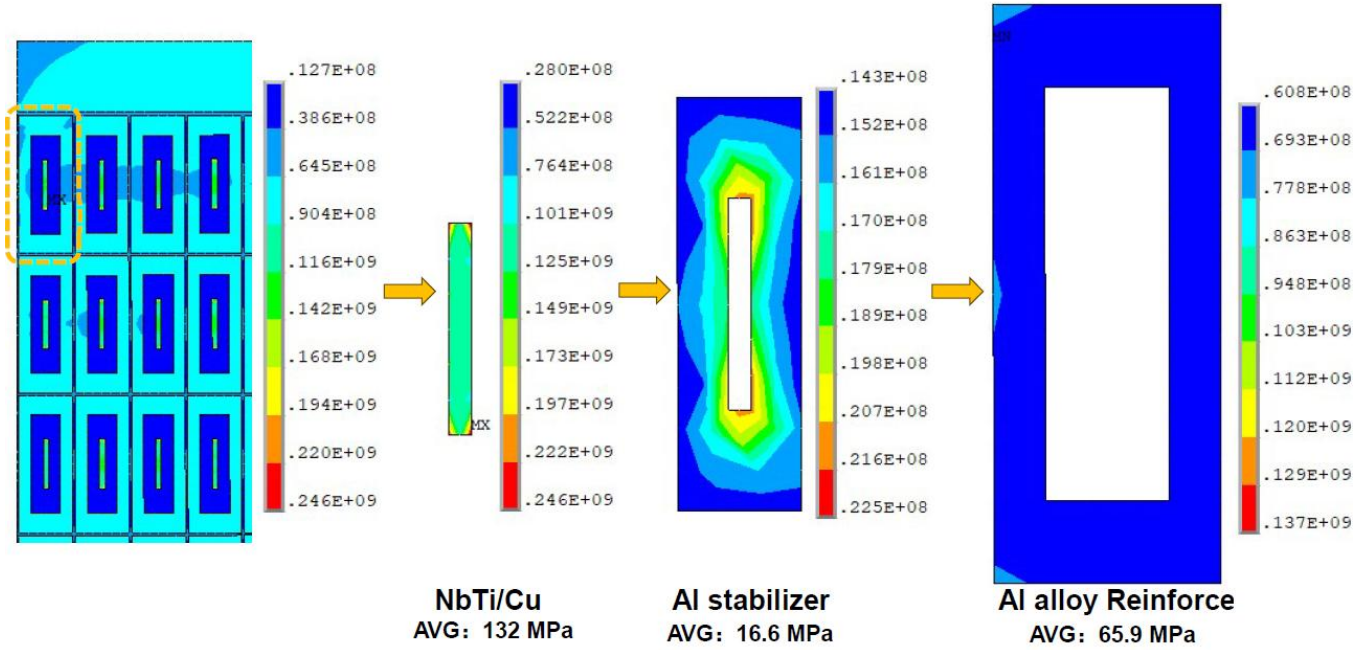

Materials	Peak stress/MPa	Rp0.2@4.2 K/MPa	Safety margin
NbTi/Cu	279	>800	**65%**
4N8 Al	22.5	~34	**33.8%**
5083 Al alloy	137	>500	**72.6%**

Comments and Recommendations

- R-A-10-2: Maintain the highest priority for the R&D of the Al-stabilized superconductor, aiming to demonstrate full-scale conductor fabrication, production of sufficient lengths, and mechanical performance that meets the required safety margins.
- C-B-10-8: Proceed the ‘box-type’ Al-stabilized superconductor as the highest priority, aiming to demonstrate full-scale conductor fabrication, and to verify the superconducting and mechanical performance that meets the required safety margins. It will be important to demonstrate a sufficiently continuous length, at least, enabling to realize a superconducting model coil to be fabricated and the superconducting magnet performance demonstration. In parallel, backup solutions shall be continued to prepare for the case of the ‘box-type’ not to be practical.

The full-scale conductor is very important. The box-type conductor remains the primary focus, with parallel R&D on backup solutions. We are developing the full-scale Box-type conductor with sufficient length (100 m).

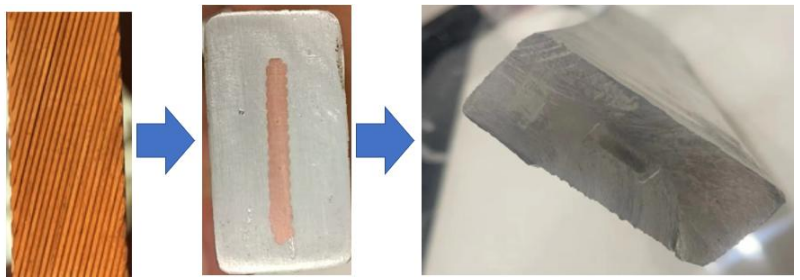

32 strands Rutherford cable

First co-extrusion

Second co-extrusion

Ref TDR: 373-345, 369-371

Comments and Recommendations

- C-A-10-4: Developing a scaled model coil, including full cooling and excitation tests, will be an important step. Without such a demonstrator, confidence in the readiness of the solenoid technology for CEPC will be limited.
- R-A-10-3: Develop a detailed plan for the construction and testing of a superconducting model coil, including demonstrations of cooling and excitation. Achieving this milestone is essential for progressing toward full-scale magnet construction.
- C-B-10-6: The SC coil winding design with a four-layer coil is to be wound by using an 'inner coil winding technology', and it sounds reasonable and promising. The demonstration by using a dummy conductor has been successfully made in cooperation with industry. It needs to be recognized as a preparation step for a SC model coil to be developed and SC performance to be demonstrated.

Establishing a scaled model coil is really a necessary step before the processing of the detector magnet. We are doing the design of scaled model coil.

Comments and Recommendations

- C-A-10-5: Two cooling channel designs are under consideration:
  - Vertical Al-pipe channels, as used in CMS.
  - Sloped or tilted serpentine channels, which may reduce the number of welds and save cryostat space.
  - The latter option could be advantageous for construction reliability
- R-A-10-4: Finalize the cooling system design based on the thermosiphon concept, with particular attention to the reliability and quality assurance of aluminum-pipe welding procedures during construction

We are optimizing the cooling system from two aspects: Design and Welding Technology

(1) We are doing the simulation of sloped serpentine cooling path, meet the requirements of temperature distribution, and reduce the number of welds.

(2) Regarding the welding of aluminum tubes, we had experience in welding small model coils, but we have not yet had experience in welding such a large number of pipes in a large-scale cooling structure. We are conducting verification experiments to ensure reliability and quality assurance.

Ref TDR: 362-366

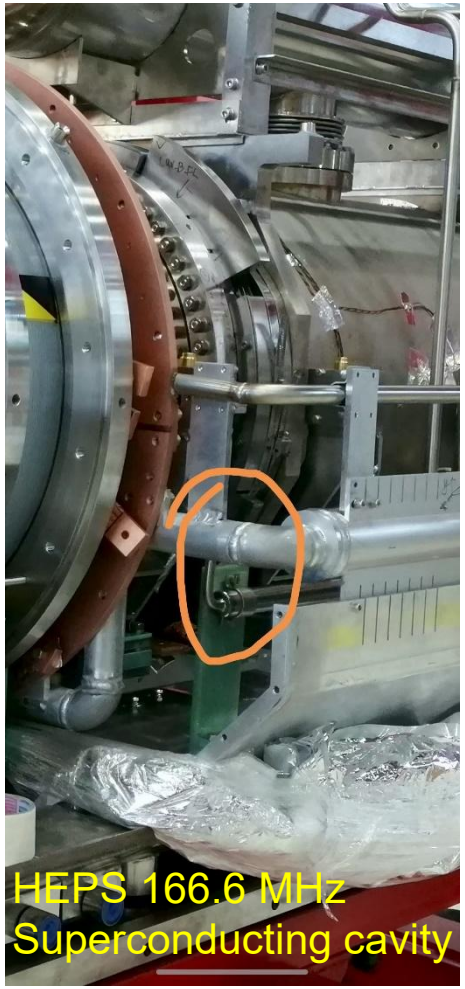

Comments and Recommendations

- C-B-10-7: The quench protection and safety design is based on two technologies of ‘partial energy extraction’ by using an external dump resister and ‘quench back’ inductively induced by the external support cylinder, functioning a single-turn secondary circuit. On the other hand, an expected energy extraction fraction of > 80% may need to be confirmed or updated. If the coil temperature would be increased to ~ 60 K on average after switching off the circuit, a half of the stored energy might be already dumped in the coil. The energy extraction ration would be more reasonable with a level of ~ 50%. The quench protection study may be further improved.
- C-B-10-9: Advance/improve the quench protection and safety study that reach a reasonable estimate for a balance of the coil temperature rise after the quench and the energy extraction ratio. It is a fundamental balance to be well understood.

We are optimizing the quench-protection system and refine the simulation process to confirm the reliability of the results. At the same time, we will adjust the quench protection in line with the progress of conductor development.

Ref TDR: 357-359

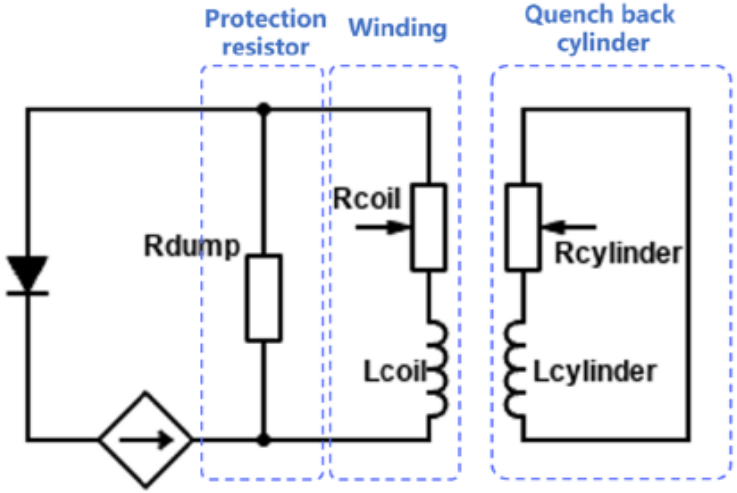

Fast dump discharge

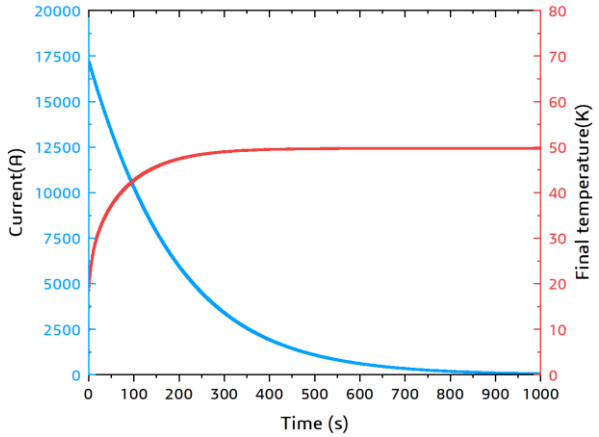

Quench Parameters

Parameter	Value
Breaker delay time	2 s
Delay time	0.03 s
Dump resistance	50 mΩ
Terminal voltage	923 V
Coil internal voltage	64.86 V
Final temperature	40.15 K
Extracted energy ratio	91.19%
Decay time*	171 s

**time when the current is $I = I_0/e = 6340\,A$.*

Finding and comments on Draft v0.4.1

SYSTEM MAGNET

- C-B-10-1: The superconducting (SC) solenoid design for the CEPC Reference Detector Technical Design Report (Ref-TDR) has significantly progressed. Congratulations!
- C-B-10-2: The solenoid provides a central magnetic field of 3T (for $t\bar{t}$, Higgs, and W runs) and 2–3T (for Z runs), within an inner bore diameter of 7.07 m and a cryostat/yoke length of 9.06 m. As a fundamental number, the SC magnet stored energy (E) is 1.5 GJ with the coil mass (M) of 145 tons with E/M = ~ 10 kJ/kg. It is assembled with an iron yoke, helically assembled, also with muon detectors. The profile and uniformity of the solenoid magnetic field in the central tracker (TPC) region is expected to be approximately 7%. It would be OK, if the TPC may accept this field variation.
- C-B-10-3: The solenoid coil is composed with four layers coils wound with Al-stabilized superconductor, supported by an outer support cylinder made of Al-alloy and cooled by using a two-phase helium natural convection flow with a thermo-siphon scheme. This design concept has been well experienced and established with previous collider detector programs, such as the CERN-LHC CMS detector and others.
- C-B-10-4: The ‘box-type Al-stabilized superconductor’ with two step co-extrusion has been uniquely proposed, and the development is in progress. It is expected to successfully demonstrate the full-scale box-type conductor within 2025. It shall be a very important milestone and strongly encouraged. However, it is also important to keep backup solutions to be prepared for the box-type conductor development not to be successful.

This aligns with our development roadmap: the box-type conductor remains the primary focus, with parallel R&D on backup solutions.

Magnet Cost Comparison

- The TDR quotes a magnet cost of about 22 MCHF, compared to around 130 MCHF for the more complex ILD system (which includes the yoke). A cross-check should be performed to understand and justify the difference between these two estimates.

System	Option	Cost [MILCU]	Mean Cost [MILCU]
Vertex			3.4
Silicon tracking	inner	2.3	2.3
Silicon tracking	outer	21.0	21.0
TPC		35.9	35.9
ECAL			116.9
	SiECAL	157.7	
	ScECAL	74.0	
HCAL			44.9
	AHCAL	44.9	
	SDHCAL	44.8	
FCAL		8.1	8.1
Muon		6.5	6.5
Coil, incl anciliaries		38.0	38.0
Yoke		95.0	95.0
Beamtube		0.5	0.5
Global DAQ		1.1	1.1
Integration		1.5	1.5
Global Transportation		12.0	12.0
Sum ILD			391.8

Item	Cost [kILCU]	Item	Cost [kILCU]
Coil		**Yoke**	
Conductor and winding	12900	Steel, including machining	80400
Internal Cryogenics	1000	Support	1700
Suspension system	560	Moving System	3500
tooling, assembly	10000	Assembly	6700
Qualification, testing	1100	Survey	500
Ancillaries			
Cryogenics, vacuum	6800	Integration	933
Electrical installation	1700	Field Mapping	560
Control and Safety system	350	Engineering	2200
Sum	131000		

Item	**CEPC (kCHF)**	**ILD (kCHF)**	
Conductor and winding	10,128	10397	Cable length (km) 33 vs 31.2
Internal Cryogenics	1008	806	Cryostat
Suspension system	242	451	Coil and Shield Suspension System
Tooling, assembly	1024	8060	Assembly Jigs and Tools
Qualification, testing	1103	887	Liquid helium, testing Dewar, machine
Cryogenics, vacuum	4144	5481	Refrigeration System 1000W@4.5K
Electrical installation	2589	1370	Power source, dump resistor, Circuit breaker
Control and Safety system	131	282	Interlock and control
Integration	640	752	Installation
Field Mapping	269	451	
Engineering	688	1773	
Total	**21,966**	**30,711**	

ELECTRONICS

Findings

- F-A-11-1: The reference TDR provides a clear and accurate description of all on-detector and off-detector electronic systems required for the readout of the various detectors, along with their associated 17 requirements—many of which are critical to the overall experiment performance. Since the last committee meeting, several important decisions have been taken, most notably the adoption of full data transmission (streamed readout), which is now firmly established.
- F-A-11-2: The nine different ASICs, currently at various stages of development, are clearly summarized, with an assessment of their maturity ranging from level 2 (initial design) to level 4 (prototyped) on a 1-to-5 scale. Three of these are common service ASICs used for power distribution and data transmission. The required manpower for the ASIC developments and future steps is well detailed and appears realistic.
- F-A-11-3: The shared back-end architecture and power distribution scheme are also well described, building upon the solid experience gained from large-scale operational experiments such as JUNO.

Comments

•The committee is very impressed with the progress made and the thorough implementation of previous recommendations. In particular, the decision to adopt a data streaming readout is a major step forward, significantly impacting the ASIC architecture. The handling of data rates and the application of safety margins are well managed.

•C-A-11-1: The ASICs are well documented, and several key building blocks have already been successfully prototyped, demonstrating the strength and efficiency of the teams involved. The progress is remarkable; however, as the complexity of the chips increases, substantial work still lies ahead. It would be helpful for each ASIC to clearly identify the lead responsible person(s) and the contributors to the various blocks and development tasks.

- •The responsible persons have been assigned for each new chip.
- •Data Link: FEDA, FEDI, OAT – Di Guo (CCNU)
- •Power: PAL – Jia Wang (NPU)
- •SiPM – SIPAC (ECAL, HCAL, MUON): Huaishen Li (IHEP)
- •OTK – LATRIC: Xiongbo Yan (IHEP)
- •For existing chips, development will follow with the current team:
- •VTX - Taichupix: Wei Wei (IHEP)
- •TPC – TEPIX: Zhi Deng (THU)

Comments

- C-A-11-2: Verification of the ASICs is critical, especially for large chips that include substantial digital logic (e.g., tracking ASICs). Verification should be conducted by individuals independent of the design teams and should use state-of-the-art tools and methodologies.
- C-A-11-3: Testing of ASICs can never be too extensive: it should involve not only the designers but also multiple user teams wherever possible. Chips should be characterized across a range of temperatures and supply voltages to detect weaknesses early. As larger volumes become available, systematic analysis of failing or underperforming chips (“bad chips”) will be essential.
  - Part of the verification has been done during the design phase by the design team. However, more verification work should be done while lack of manpower
  - Independent verification work will be done during the test phase by independent teams, for which it is not so high-level tech required
- C-A-11-4: From a stylistic standpoint, the SIPAC chip (common to three detectors) is extensively described within this chapter, while other ASICs are detailed within each detector’s respective section. For improved readability, it may be preferable to move the SIPAC description to the calorimeter section, retaining in the electronics chapter only a general overview of all ASICs and a detailed view of the shared service chips (e.g., for power and data transmission). For the front-end ASICs, detailed schematics could be reduced in favour of presenting more relevant simulation results, such as pulse shapes or noise versus input capacitance.
  - We have done exactly as suggested.
  - SIPAC part has been moved into the ECAL chapter, and shrunk for the length and details, only the main specs and scheme were kept.

Comments

- C-A-11-5: The back-end electronics are comprehensively described and benefit from the team's previous experience with large-scale systems. However, the availability of high-performance FPGAs could pose a risk. Maintaining a dual-source strategy for critical components would be a prudent mitigation measure.
  - Yes, that is also our current idea. We have kept eyes on backup resources for the key components. Almost all of them have found extra vendors or substitutes.
- C-A-11-6: Identify the teams responsible for testing each ASIC, ensuring they are different from the design teams. Bugs are often discovered late in development, and broader involvement in chip evaluation improves characterization and helps uncover potential weaknesses.
  - See the answer for the comment 1.
  - We have assigned the teams and responsible persons for each chip.
- C-A-11-7: Begin detector testing with available “sister chips” where feasible. This parallel approach can advance both detector and chip development and provide valuable benchmarks for comparison.
  - This is the idea during previous R&D for detector prototypes, like for the ECAL.
  - We will follow this way for the future R&D for the early prototypes for sub-detectors. “Sister chips” (like the ROC chip series) will be evaluated to make the chip development in parallel (to some extent) with the detector R&D.

Recommendations

- R-A-11-1: Minimize power dissipation at every stage. Each milliwatt of consumption should be justified by a specific performance requirement.
  - We are continuing optimize the scheme.
  - Currently we have several consideration:
    - Optimize the OTK detector design, so that the power may be saved.
    - Optimize the electronics design for HCAL, according to the new design from the detector side. Channels will be saved, and frontend will be reconsidered with less dynamic requirements.
- R-A-11-2: Proceed with system development in parallel with chip development. System-level issues can often be addressed early at the chip design stage if identified promptly.
  - We will keep that in mind.
  - Actually we already have a prototype design of the common backend board, which works well and has been verified. We will optimize the design for the following prototypes of sub-detector R&D.

Comments on Draft v0.4

- C-B-11-1: However, I regret that the overview of the ASICs has also been removed and it only figures as the "next steps" in section 11.10, squeezed in a table which is actually difficult to read. The previous version which was detailing the different ASICs, their number, number of channels, level of maturity, existence of a "sister chip"... was very important and helpful. As in many experiments, they are likely to be a corner stone of the project and they should not become stumble stones !
  - **We have added this table in the Ref-TDR, to describe the maturity of all related ASICs and similar chips. The table can be found below**:

Name	Application	Functionality	Maturity	Similar chips
FEDI	Common Elec	Data Link	2~3	lpGBT[17]
OAT	Common Elec	Optical	3~4	VTRx[42]
FEDA	Common Elec	Data Aggregation	2	lpGBT[17]
PAL	Common Elec	DC-DC	2	bPol[43]
Taichu	VTX	VTX-Stitching	2~3	MOSAIX[44]
TEPIX-TPC	TPC	Pixel TPC	3~4	Gridpix[45]
COFFEE	ITK	HVCMOS	3	MightyPix[46]
LATRIC	OTK	LGAD-TOF	2	ALTIROC[47]
SIPAC	SiPM ASIC	ECAL, HCAL, Muon	2~3	HGCROC[48]

TDAQ

Findings

TDAQ

- F-A-12-1: The TDAQ system is based on the full transmission of data from the front-end electronics to the back-end electronics (BEE), with the trigger operating at the BEE level. Data rates from each subsystem are provided for the different CEPC operational scenarios; however, the underlying assumptions behind these estimates should be discussed more explicitly in some cases.
- F-A-12-2: The TPC represents a special case due to its long drift time, and a more detailed discussion of the implications of this extended integration time is necessary.
- F-A-12-3: The first stage of the trigger is planned to operate on the BEE boards, generating trigger primitives from the calorimeter and muon systems, with the possible addition of primitives for a track trigger. The trigger architecture has evolved to include BEE-resident primitive algorithms alongside a three-layer L1 hardware system. The CEPC team has demonstrated that simple requirements on calorimeter and muon primitives effectively reduce background rates while preserving high efficiency for the primary physics processes of interest, addressing a key recommendation from the previous review.
- F-A-12-4: It was noted that some exploratory work on a fast-track trigger has been conducted, though no results were presented. A silicon-based fast track trigger remains of high interest, as it would complement calorimeter and muon primitives and provide stronger separation between collision and non-collision backgrounds.
- F-A-12-5: This review focuses primarily on the ZH production and low-luminosity Z-pole running planned for the first ~10 years of CEPC operations. Nevertheless, the overall TDAQ design appears appropriate for other planned running modes as well.
- F-A-12-6: The Ref-TDR chapter should first describe the proposed baseline trigger system before presenting proof-of-concept studies for the trigger primitive algorithms.

Comments

TDAQ

- C-A-12-1: The background event rate and event size are critical inputs to defining the TDAQ system dataflow requirements. Assumptions used should be explicitly stated and consistently referenced across all relevant chapters (some inconsistencies were noted in the current draft).

- >>The detail information for the event rate and event size are summarized in table 12.3 and 12.4. The event size is calculated based on the information from the electronic chapter, and the time windows for each sub-detector.

Table 12.3: Time windows for each subdetector and the event size calculation for both Higgs and Z mode. The "Full Data" is calculated by multiplying the Ave. Hit Rate, from Table 3.7, by the detector area, safety factor 1.5, and the bit width from Table 11.1. The data size per bunch is derived by dividing the "Full Data" by the none-empty bunch crossing rate, with the Higgs mode rate being 1.34 MHz and the Z mode 12 MHz. The data size per event is obtained after accounting for the impact of the time windows of each sub-detector plus the trigger uncertainty (20 ns) on individual events.

	VTX	ITK	OTK	TPC	ECAL	HCAL	Muon	Total
Time windows (ns)	69	69	69	34500	69	1000	69	
Higgs mode Full Data (Gbps)	48.7	15.6	61.7	19.8	558	19.9	<1	725
Data size / bunch (kB)	4.54	1.46	5.76	1.84	52.1	1.86	<0.1	67.7
Data size / event (kB)	4.54	1.46	5.76	230	52.1	7.44	<0.1	301
12.1MW Z mode Full Data (Gbps)	142	28.4	105	42.9	901	20.4	<1	1241
Data size / bunch (kB)	1.48	0.296	1.09	0.446	9.39	0.213	<0.1	12.9
Data size / event (kB)	2.96	0.592	2.18	223	18.8	3.2	<0.1	251
50MW Z mode Full Data (Gbps)	886	168	639	264	5698	129	<1	7785
Data size / bunch (kB)	2.81	0.533	2.03	0.836	18.1	0.409	<0.1	24.7
Data size / event (kB)	11.2	2.13	8.12	1255	72.4	18.8	<0.1	1368

Table 12.4: Trigger rate estimation table for different run conditions. The physical event rate is introduced in Section 12.1.1.1. The detailed readout rates of each sub-detector are shown in Table 12.12. The total DAQ storage rates are calculated based on the corresponding raw event size which could be compressed with full reconstruction and detailed RoI analysis at HLT.

Operation phase		**I**		**II**	**III**
Condition	**Higgs**	**Z (12.1 MW)**	**W**	**Z (50 MW)**	**$t\bar{t}$**
Non-empty bunch crossing rate(MHz)	1.34	12	6.5	39.4	0.17
Luminosity (10^{34}/cm^2/s)	8.3	26	26.7	192	0.8
Physical event rate (kHz)	0.5	10	1.1	77	0.057
L1 triger rate (kHz)	50	120	65	400	2
DAQ readout rate (Gbyte/s)	6.04	8.70	-	78.1	-
HLT rate (kHz)	1	20	2	154	1
Raw event size (kbyte)	301	251	500	1368	500
DAQ storage rate (Gbyte/s)	0.301	5.02	1	50.4	0.5

Comments

- C-A-12-2: The safety factors applied in system design should be made explicit, clearly motivated, and documented to allow for easy updates and assessment of their impact on different subsystems.
- >>A safety factor "1.5" is applied when estimating the event size, mentioned in section 11.2: "During the calculation, a safety factor of 1.5 was considered for the background rate.". Another safety factor "10" is applied when estimating the trigger efficiency, as mentioned in section 12.4.1: "For both the Higgs and the Z mode, each beam background event includes 10 bunch crossings, corresponding to a safety factor of 10.“
- C-A-12-3: Section 12.4 should be moved after Section 12.6 to improve the logical flow of the chapter.
- >>Done.

Recommendations

- R-A-12-1: Clearly motivate the data bandwidth requirements into the L1 trigger, between trigger layers, and specify the number of links needed. Provide details on the expected trigger primitives from each BEE type and the associated data volumes. Similarly, describe the output products of the local trigger layers and provide data bandwidth estimates into the global trigger layer.

- R-A-12-2: Update the design of the common trigger board—particularly the bandwidth and input link capacities from the BEEs—to reflect the information presented. Explain the rationale behind the estimated number of trigger boards required at each of the three L1 levels.

- >> These part is added in "resource estimation" section as following. In the resource estimation, the trigger primitives for ITK, OTK, ECAL and HCAL are cluster information, which includes cluster position, size, energy information and time information; The muon detector provides hit counting information, including hits number, hit position and timing information. For TPC detector participating in trigger further research is needed. Currently only preliminary estimates are made based on its' data volume. The estimation of global trigger part of each detector is based on the divisions of sector. All trigger primitives information is obtained from off detector electronics. Trigger primitive transmission to trigger system from back end electronics is based on 10Gbps line rate, 8Gbps bandwidth removing the encoding overhead of 8B/10B. In the Level-1 trigger system, 16 channels of optical will be used for connection with off-detector electronic boards or previous level trigger boards. Based on the data volume of trigger information which calculated based on background simulation of each detector, trigger optical links to each detector's sub-trigger and number of trigger boards can be estimated. In trigger system installation, one ATCA crate can install up to 10 trigger boards and at least one DCTD board. According to this calculation approach, a rough scale of trigger system was estimated as shown in table 12.5.

Table 12.5: L1 Trigger resource estimation table. The number in parentheses represents the resources required for track trigger additional, in which VTX, ITK, OTK and TPC will be used.

Detector	BEE Board Num	TP Bits	Fiber num to trg/BEE	Trigger Board	ATCA Crate	DCTD Boards
VTX	6	–	–	(6)	(1)	(1)
TPC	32	–	1	(2)	(1)	(1)
ITK-Barrel	24	64	1	(2)	(1)	(1)
ITK-EndCap	6	64	1	(2)	(1)	(1)
OTK-Barrel	55	64	1	(4)	(0)	(0)
OTK-EndCap	34	64	1	(3)	(1)	(1)
ECAL-Barrel	60	48	3	12	1	1
ECAL-EndCap	28	48	3	6	1	1
HCAL-Barrel	346	48	1	22	3	3
HCAL-EndCap	192	48	1	12	2	2
Muon-Barrel	2	–	1	—	—	—
Muon-EndCap	1	–	1	1	1	1
Global Trigger	–	–	–	18+(12)	2+(2)	2+(2)
TCDS	–	–	–	1	1	1
Sum	–	–	–	72+(31)	10+(7)	10+(7)

Recommendations

- R-A-12-3: Provide a detailed description of how the TPC data stream will be handled, especially considering its long drift times.
- >>A new paragraph for the TPC data stream detail information is added in section 12.1.2. It can still utilize L1 to pack TPC data whatever all raw data need be read out with more than 30 kHz L1. Data is packed in blocks by multiple Trigger ID for parallel processing. TPC data is easily located via Trigger ID, enabling joint analysis with other detectors sharing the same trigger.
- R-A-12-4: Continue exploring the development of a fast-track trigger, emphasizing its potential to reduce background rates and ease the load on the HLT.
- >>A preliminary track trigger study is added in Section 12.4.2.1. The current results doesn't improvement the trigger selection, further study need be done in future.

Recommendations

- R-A-12-5: Demonstrate the necessity for RDMA technology in transferring data from the BEE to the HLT, including a justification based on system performance needs.

- >> Currently, CEPC's baseline design is to use the traditional TCP protocol for data transfer from the BEE to the HLT, while RDMA is primarily being considered as a research direction. This consideration is mainly based on the following points:

  - 1.RDMA supports direct memory access, significantly reducing CPU utilization during data transfer. This helps to overcome the performance bottlenecks of traditional protocols and meet the demands of future high-throughput data transmission (e.g., for high-luminosity Z mode).
  - 2.Validating RDMA on the existing readout electronics platform in advance can prevent large-scale hardware upgrades triggered by data volume growth, thereby lowering the cost and technical risks of future system upgrades.
  - 3.Applying RDMA in the high-level trigger system can reduce CPU load and interrupt overhead during data transmission, improve the efficiency of trigger algorithms, and lay the technical foundation for future one-to-many data distribution and real-time event assembly.

- In summary, although the current TCP-based solution can already meet present requirements, early research into RDMA is a forward-looking strategy that can meet the demands of future experiments for high-performance data transmission, aligning with the development trends of leading international particle physics projects.

Recommendations

- R-A-12-6: Describe the system's strategy for handling data flow in the event of full buffers to avoid data loss or system instability.
- >> This added in 12.2.4. BEE should generate full signal when buffer full and feedback to TCDS, TCDS will mask the L1 signal until full or error signals cleared to avoid data overwriting in data packing buffer in DAQ readout.
- R-A-12-7: Evaluate whether the L1 trigger hierarchy could be simplified, for example by collapsing it into a multiplexer layer feeding directly into boards handling full global trigger primitives.
- >> Fast trigger and Gobal trigger are combined as one layer according to the suggestion, see the Fig12.2. Trigger primitive generation is divided into local and global two layers one reason is that it is restricted by common trigger board IO number and FPGA resources we can purchase. Structure maybe optimized with the development of FPGA IO and resources we can buy in the future.
- R-A-12-8: Categorize the event rates into physics signals (e.g., ZH production, two- and four-fermion processes, Bhabha scattering), gamma-gamma interactions, beam-related backgrounds. The first category aims at full trigger efficiency, the second one is potentially of some interest but with lower priority and the last one must be reduced as much as possible.
- >>In table 12.1 and 12.2, the physical processes are categorized into two group "high priority" and "low priority". All the gamma-gamma interactions are under "low priority".

Recommendations

- R-A-12-9: Analyze the beam background distributions as functions of energy, multiplicity, and polar/azimuthal angle to optimize background suppression algorithms. In particular, investigate the origin of background peaks such as the one observed at ~7 GeV in the ECAL endcap.

- >>We studied the beam background energy distribution as function of polar/azimuthal angle and the background component(Beam-Gas Bremsstrahlung, Beam-Gas Coulomb, Pair Production...), and notice that the background peak is attributed to significant energy deposition in the supercells adjacent to the beam pipe in the endcap region from the Pair Production.

- The first figure presents the average energy deposition across ECal Endcap modules for 10,000 beam background events. The second plot illustrates the average energy deposition per Endcap supercell across distinct θ (polar angle). As shown in the first plot, about 6 GeV energy deposition is observed in the supercells around the center.

- To enhance background suppression, an angle-dependent energy thresholds will be explored in the R&D with better understanding of the beam background simulation.

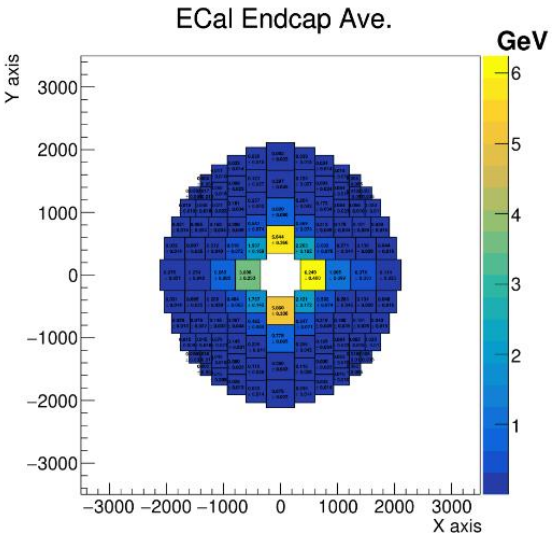

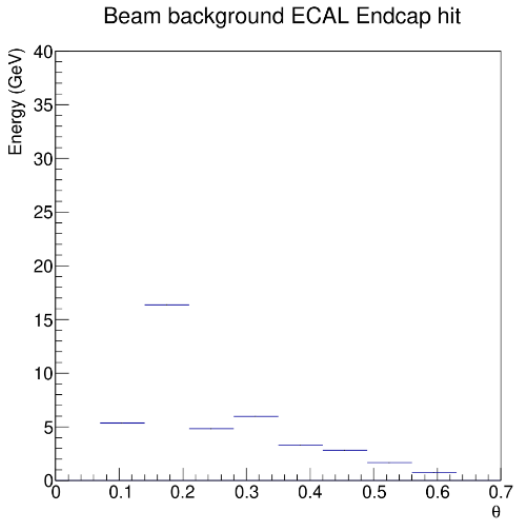

Comments from Bob on Draft v0.4

- C-B-12-1: It would help the reader to have stated early in the chapter the timelines associated with different decisions. For example, at lines 10835-10837 additional R&D is listed as being necessary. By when does this R&D need to be completed? Similar comment for lines 10875-10876. This arises again at lines 10944-10947. There is some discussion of timelines at the end of the chapter (lines 11836-11838); I suggest this timeline is referred to earlier.
  - This version of ref-TDR is aiming at Higgs and low lumi-Z modes. Current there is no technical bottleneck for CEPC Phase-I TDAQ. High lumi-Z mode is Phase-II of CEPC. The requirement of technical for High lumi-Z is not included in this version.
- C-B-12-2: In fact, it might be good to start the chapter with the summary and then give the details.
  - Add a summary section in overview

Comments from Bob on Draft v0.4

- C-B-12-3: Some minor things I noticed as I read:
- C-B-12-3 -1: 10849-10852: not sure what is being said here
- ->In the high luminosity Z mode, the data volume of the detector will be significantly increased. The \gls{TDAQ} system should have scalability to cope with such situations.
- C-B-12-3 -2: 10890-10893: not sure what is being said here

->Most of the \gls{L1} trigger algorithm will be running on \gls{FPGA} farm, which has the advantage of low latency and real time. As the principle of trigger is to keep all the good events and reduce the background events to acceptable level of \gls{DAQ} readout, it is challenging to maintain the data purity.

- C-B-12-3 -3: 10897-10900: repeated sentence.
- Deleted the repeat sentence
- C-B-12-3 -4: 10916-10917: trails = tracks?
- trails -> tracks
- C-B-12-3 -5: 10922-10924: not sure what is being said here
- ->The combination of these physical objects can be used to reconstruct the particle flow object and further suppress the background process.
- C-B-12-3 -6: 11090-11091: meaning unclear
- Global trigger resource allocations for each subsystem employ sector-based segmentation as the foundational calculation method. For global track trigger, Calorimeter track finding, and Global trigger, 60° will be defined as a sector. For the energy trigger of the calorimeter, 120° will be defined as a sector.
- C-B-12-3 -7: 11813-11814: text is garbled, not clear what is meant
- ->Following the recent update results of sub-detector design and simulation, significant progress in the technical development of the \gls{TDAQ} and online systems has been achieved.

SOFTWARE AND COMPUTING

Findings

- F-A-13-1: The review team acknowledges the very good progress made in software and computing since the last report. Almost all previous recommendations have been successfully addressed by the collaboration. The current status and advancements are thoroughly documented in the Ref-TDR and were presented and discussed during a dedicated session at this review. Overall, the Offline Software and Computing activities are in a strong position, the outlined approach appears highly feasible, and no significant challenges or showstoppers have been identified.
- F-A-13-2: The offline software, CEPCSW, is based on the international Key4hep project, which is used by all future collider projects. CEPC is making significant and well-aligned contributions to this effort within the global community. In terms of computing, CEPC leverages established tools and methodologies developed for the LHC. The current computing model follows the traditional Tier structure, though a transition to a more efficient model is envisaged, aligned with broader community developments.
- F-A-13-3: A detailed simulation model of the reference detector has been implemented. For track reconstruction, the collaboration is currently adapting tools and algorithms from the linear collider community while also developing more advanced techniques. A new particle flow algorithm, CyberPFA, has been developed, particularly to meet the challenges posed by the novel crystal ECAL design. This builds on prior work from the HCal side and has been successfully integrated into CyberPFA. The full simulation and reconstruction framework has been employed to produce a comprehensive set of technical performance plots, demonstrating that the detector concept, combined with sophisticated algorithms, can meet the required physics performance targets.
- F-A-13-4: The offline software has also been used to estimate the computing needs, based on reasonable— though not highly refined— assumptions regarding data rates, data volumes, processing schedules, and methodologies. However, the estimates also assume optimistic developments in CPU performance and cost trends over the next decade.

Comments

- C-A-13-1: The corresponding Ref-TDR chapter would benefit from some revisions: reducing the length of more general descriptive sections and expanding technical details where appropriate.

  The total number of pages has been reduced from 62 to 41, plus an additional 4 pages for citations.

- C-A-13-2: Some important aspects of the planned computing model remain insufficiently detailed, such as the structure for user analyses, data distribution strategies, open data policies, and long-term data preservation plans.

  Structure for user analyses, data distribution strategies:

Line 1064-1071: An efficient data distribution strategy within the data model is essential for optimizing data storage, access, and processing. Raw data will reside in central storage, while reconstructed data (RecData), simulation data (SimData), and analysis data (AnaData) will be distributed across Tier-1 storage. These datasets will be accessible on demand through a tiered storage and caching system, ensuring streamlined availability for various sites. A progressive reduction of the data format for user analysis, coupled with corresponding analysis facilities in \gls{Grid} and non-\gls{Grid} resources, creates a robust structure that enables fast and reliable user analyses.

Open data policies: A new section of 13.8 Open data was added.

Long-term data preservation plans: A new section of 13.9 Long term data preservation was added.

- C-A-13-3: The development of CyberPFA is a significant achievement and positions the collaboration as a leader in custom in-house algorithm development. However, the degree of reliance on existing tools like PandoraPFA and ArborPFA needs to be better explained and justified.

Line 533-536: The experience of clustering in high granularity calorimeter and integrating track and calorimeter information from \pandorapfa and Arbor are also adopted in \cyberpfa for the reconstruction in traditional high granularity \gls{HCAL} and optimal performance.

Comments

- C-A-13-4: While the event data model (EDM4hep) is well established, more detailed data formats for reduced, compact data levels (e.g., various stages of AODs) are not yet clearly defined.

Line 981-984:

\item AnaData (analysis data): which is a summary of the reconstructed event, and contains sufficient information for common analyses

\item TagData (event tag): summary of some general features of the event, allowing rapid access to the events and performing fast selection

Line 988-990:

AnaData and TagData are expected to be relatively smaller in scale compared to RecData. Given their importance for data analysis, they will be defined as soon as event-level reconstruction, following data reconstruction in sub-detectors, becomes available.

Comments

- C-A-13-5: The costs associated with the required computing infrastructure—such as whether a new data center will be necessary—are not discussed in the Ref-TDR.

Described in 13.10.4 Smart data center infrastructure

- C-A-13-6: While future technologies such as quantum computing, machine learning, and AI are mentioned, their potential roles and the motivation for pursuing them should be more clearly articulated, with better-defined staging scenarios

Line 723-736:

The trend in computing hardware is shifting toward increased CPU cores and more diverse architectures, including \gls{GPU}, FPGAs, and other accelerators. Machine learning plays a crucial role in high-energy physics experiments. Consequently, the development of software capable of efficiently handling simultaneous computations and leveraging machine learning techniques to enhance data processing and analysis has become an increasingly important topic.During Z-pole operation at CEPC, computing demands are expected to reach the exabyte scale, posing technical challenges comparable to those encountered at the High-Luminosity Large Hadron Collider. Advances in artificial intelligence, along with the integration of concurrent and heterogeneous computing, will form the operational backbone of future collider experiments. Meanwhile, quantum computing and its associated algorithmic frameworks present a potential paradigm shift in addressing these challenges, offering a promising—though ambitious—solution for the CEPC initiative.This section will present relevant research efforts exploring these advancements.

Recommendations

- R-A-13-1: Further develop and consolidate the detailed simulation model and reconstruction framework, with particular attention to:
  - R-A-13-1-1: Adding realistic estimates for detector imperfections, such as gaps or insensitive material from cables and services, to the simulation model.

    Line 163-167:

    \ddhep can also be used to represent more realistic geometry, rather than idealized models, by integrating alignment and calibration data. Misalignment corrections can be applied to reflect actual detector shifts, and calibration constants are included to ensure accurate detector responses. By incorporating these elements, DD4hep offers a comprehensive and precise detector description for the experiment.
  - R-A-13-1-2: Performing detailed studies of the CyberPFA performance, including jet energy resolution for light-quark dijet events, single particle responses, neutral hadrons, and neutrino energy measurements in b-decays.

    presented in Chapter 15
  - R-A-13-1-3: Studying the impact of misalignment on tracking performance.

    discussed in Chapter 15
- R-A-13-2: Develop a systematic performance monitoring framework, organized around a set of benchmark figures and analyses that qualify simulation and reconstruction quality. Each sub-detector should define its own "detector performance" plots, while a standard set of global physics performance plots should be maintained to validate software improvements.

  Line 217-219:

\item Release validation: Large-scale data production is manually triggered using predefined workflows, which are submitted to local or distributed computing systems. Key physical quantities are then compared against standard distributions, providing a clear reference for evaluating detector performance.

Recommendations

- R-A-13-3: Once consolidated, establish a clear reference for detector performance within the RefTDR, ensuring that future detector and physics performance studies use consistent versions and conditions (e.g., ensuring that jet resolution and b-tagging results are presented with the same software version and setup).

  Performance studies will be conducted using a fixed software release, as agreed upon with the physics group.

- R-A-13-4: Develop a more detailed and phased estimate of computing needs during the R&D and preparation phases, for example by organizing a sequence of increasingly challenging "data challenges." These would also serve as benchmarks for assessing the maturity of the offline software and computing infrastructure.

  Line 1023-1027: The allocation of computational and storage resources is divided into three distinct phases: 2\% during the TDR phase, 10\% during the construction phase, and 100\% during the data-taking phase. The detailed estimate of computing resources will be obtained through a series of increasingly complex data challenges, tailored specifically for the experiment.

Comments on Draft v0.4.1

- C-B-13-1: The Offline Software and Computing section of the TDR has been significantly improved wrt. version from the April review meeting at IHEP. Manyn of the comments have been well addressed, e.g. the overall length is reduced with replacing more general sections with technical descriptions, open data policies and long term data preservation plans have been added, the relation of CyberPFA to PandoraPFA is clarified.
- C-B-13-2: The CEPC Software and Computing group has also started to address the recommendations made in the previous review, e.g. by developing a more detailed and phased computing resource needs and the planing of dedicated computing challenges to monitor the progeress.
- A detailed data challenge plan has been incorporated into Section 13.6.2:

  “Detailed estimates of computing resource requirements will be obtained through a series of Data Challenges—large-scale Monte Carlo productions designed to validate computational needs before building the final system. These challenges will be conducted in multiple rounds, each increasing in complexity and data volume to more accurately simulate future CEPC operational conditions. Early stages will focus on prototype tests of offline software, profiling CPU, memory and storage demands for core algorithms, followed by full-chain processing from simulation to reconstruction, with particular emphasis on bottleneck and performance of key workflows. As the Data Challenges progress, later rounds will emphasize the generation of approximately 1 million Higgs events, complemented by inclusive Monte Carlo datasets that simulate one month of low-luminosity Z data collection. Those rounds will incorporate Grid computing integration, significantly enhancing the realism of both data processing workflows and analysis pipelines.

  The final phase of the program will feature collaborative efforts with the CEPC international sites, coordinated through a Common Computing Readiness Test. This structured approach ensures comprehensive validation of the computing model, overall operational readiness, paving the way for the full-scale deployment of the CEPC. ”

Comments on Draft v0.4.1

- C-B-13-3: At the same time a number of recommendations have not yet been addressed, e.g. performing detailed studies of the CyberPFA performance, including jet energy resolution for light-quark dijet events etc. We encourage the group to continue to pursue these recommendations, well aware that not all will be possible before handing in the TDR.

- we have already completed the jet energy resolution study of light-quark jet events from e+e-->ZH process, the dependence of JER on energy, costheta and phi are provided. Now we are working on the processes of e+e--> di-quark jets, and other single particles are IDRC recommended.

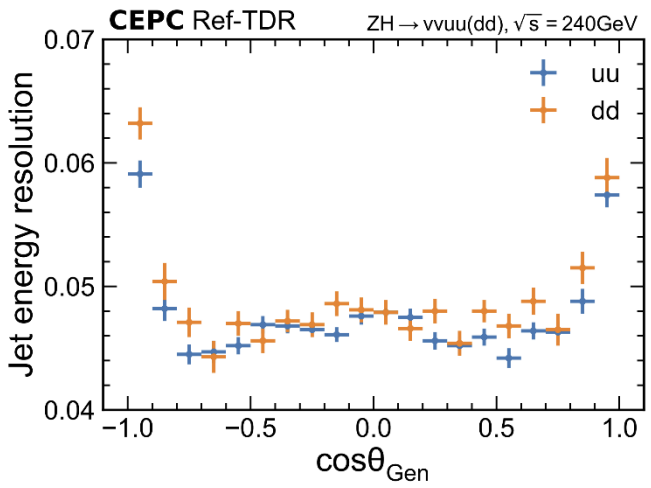

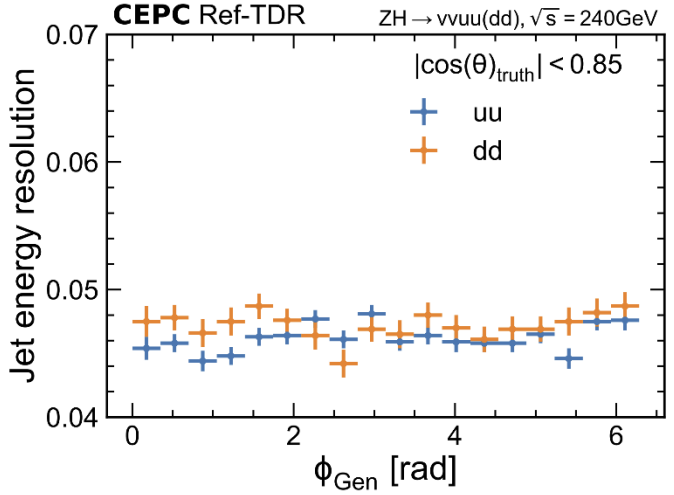

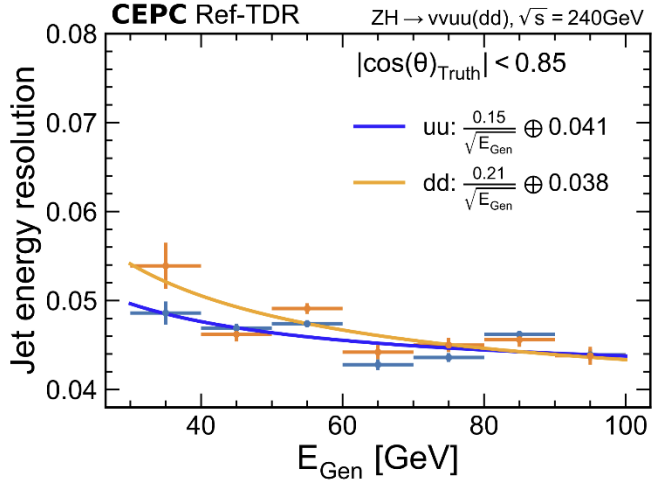

MECHANICAL INTEGRATION

Findings

- F-A-14-1: Significant progress has been made since the last review in the mechanical design of the CEPC reference detector. The weight and boundary dimensions of each sub-detector are now well defined in the Ref-TDR. Clearances between sub-detectors are typically around 10 mm, which appears adequate to ensure a seamless installation sequence. However, in the critical interface between the integrated beam-pipe/vertex detector assembly and the ITK, the clearance is reduced to just 2 mm.
- F-A-14-2: The issue of sagging of the magnet yoke under its own weight has been effectively addressed. The introduction of end-flanges satisfactorily mitigates the problem, reducing the sagging from about 13 mm to within the required limit of less than 1 mm.
- F-A-14-3: The installation sequence has been carefully developed. The core shaft designed for the installation of the barrel HCAL and ECAL detectors appears adequate, as does the cantilever system proposed for installing the TPC, ITK, and beam-pipe assembly (including the Vertex and LumiCal detectors). The animations presented clearly illustrated the feasibility and logic of the installation process.

Comments

- C-A-14-1: The mechanical connection structures between sub-detectors are well designed, considering the specific requirements of each system. However, the methods by which these structures will achieve the precise alignment of the sub-detectors are only briefly described in the current Ref- TDR. Reference is made to an alignment control network that would provide positional benchmarks, but further details would strengthen the documentation.

We have further optimized the connection structures between sub-detectors to ensure reliable mechanical connections while minimizing deformation that could affect installation accuracy. The relevant details and FEA have been added in the updated TDR documentation. Additionally, Section 14.4.1 Configuration of the experimental hall introduces the plan of the survey network in the experimental hall. During detector installation, in addition to relying on survey devices for positioning, we will also implement measures in the installation tooling and connection structures to enhance positioning accuracy and assembly efficiency. The installation coordinate system for the detector will be set before the yoke installation begins. All sub-detectors are equipped with alignment holes, and they are aligned during installation according to a unified coordinate system. These aspects will be further refined and elaborated in next work.

- C-A-14-2: Significant progress has also been made in designing the auxiliary facilities, which include the air- conditioning system for the experimental hall, gas and cooling systems for the various sub- detectors, power distribution and electronics systems, the cryogenic system for the superconducting magnet, and the hydraulic pump station used to move the detector to the collision point.

Next we will proceed with optimizing the spatial layout of the main hall and auxiliary halls, as well as the routing of pipeline systems, to ensure clear coordination with the accelerator in terms of space and facility usage. The layout and utilization of the ground hall will also be taken into consideration in next-stage planning.

Recommendations

- R-A-14-1: Further refine the routing plans for cables and services, especially in the critical interface areas between sub-detectors and through the barrel-to-endcap transitions to the outside of the detector and the auxiliary facilities.

We have supplemented the service section 14.3.2, describes the external service routing of sub-detectors. These services are still being finalized and optimized. The routing scheme has been studied, and we have checked and verified that the allocated space is sufficient. Preliminary interconnection schemes have been studied for cable routing from the yoke to the electronics room.

- R-A-14-2: Pay particular attention to the air-cooling and service routing for the vertex detector, where space within the beam-pipe assembly is extremely limited. It is essential to verify that sufficient space is available to ensure the proper functionality of the air-cooling system, without compromising reliability or maintenance access.

The space for the entire VTX inside the beam pipe is very compact, which has been validated with a full-size 3D printed mockup and flexible cable prototype. The trial results demonstrated that the routing scheme is fundamentally feasible. The mockup model with cable service is documented in Sec. 4.3.3.

Air-cooling performance for inner four curved MAPS layers and for outer planar layer are simulated. Thermal simulation results are documented in Sec. 4.3.2. In longer timescale, we will plan to built a mockup with curved dummy wafer and heaters to validate the thermal simulation.

- C-A-14-3: Regarding refrigerant choice for the other sub-detectors:
  - C-A-14-3-1: Supercritical CO_2 (sCO_2) could be considered as an alternative to water. As a single-phase refrigerant, it is user-friendly for complex, multi-branch systems. Like water, it is non-toxic, non-flammable, and readily available; unlike water, it is dielectric and harmless to electronics in case of leaks. While sCO_2 brings operational advantages, these must be weighed against some disadvantages (see appendix for details).
  - C-A-14-3-2: Boiling CO_2 (subcritical, operating around 20–25 ° C) is also simpler than twophase CO_2 systems, which require more complex design, maintenance, and expert operation. Thus, unless two-phase cooling is clearly necessary, a simple and efficient single-phase refrigerant (such as water or supercritical CO_2) is preferable

We are fully aware of the technical complexity of this option. Preliminary research has been initiated for some sub-detectors, while further in-depth studies and tests will be planed to demonstrate both the feasibility and safety of it.

Comments in backup

Detailed Considerations on the Advantages and Disadvantages of a Refrigeration System Based on Supercritical CO_2 (sCO_2) Compared to Water.

Advantages of sCO_2 Refrigeration:

- sCO_2 is fully dielectric, making it inherently safer for use near sensitive electronics.
- sCO_2 requires much smaller piping for the same flow rates due to its lower viscosity and higher operating pressure.
- It has a higher heat transfer coefficient, provided that operational conditions (temperature and pressure) are well optimized.
- The high fluid pressure allows for larger acceptable pressure drops in the heat exchanger (e.g., in the detector stave's tubes). With optimized heat exchanger design, it is theoretically possible to induce the necessary pressure drops to maintain nearly isothermal conditions—achieving single-phase flow with the same inlet and outlet temperatures while efficiently removing heat.
- Experience shows that low-pressure circuits tend to develop leaks over time due to lower quality construction standards, while high-pressure systems, requiring stricter quality controls, are more robust. This leads to lower long-term maintenance costs (both financial and operational).

Disadvantages of sCO_2 Refrigeration:

- High-pressure systems are generally estimated to be 15–20% more expensive than equivalent low-pressure systems.
- Operation at 30–35 °C might impact surrounding systems and needs to be considered during integration.
- A dedicated pressure control component ("bladder" or similar device) is required to maintain stable system pressure.
- Depending on the system volume, there are potential safety issues (especially personnel safety) associated with storing large quantities of CO_2 in confined underground spaces.
- The combined effects of all parameters (temperature, pressure, flow rates) on the thermal fluidic behaviour of supercritical CO_2 are not yet fully understood. However, significant research and development work in this area is currently ongoing

Comments on Draft v0.4.1

- C-B-14-1: However, unless I have overlooked something, the two main recommendations we made in April the 2nd review in April have been addressed yet:
  - C-B-14-1-1: Refine the routing plans for cables and services, especially in the critical interface areas between sub-detectors and through the barrel-to-endcap transitions to the outside of the detector and the auxiliary facilities.
  - C-B-14-1-2: Pay particular attention to the air-cooling and service routing for the vertex detector, where space within the beam-pipe assembly is extremely limited. It is essential to verify that sufficient space is available to ensure the proper functionality of the air-cooling system, without compromising reliability or maintenance access.
- C-B-14-2: They might not have had the time to do so yet, but I regret that in the to-do list at the beginning of the document it only says:
  - C-B-14-2-1: Mechanics and integration is mostly done, but requires improvements to the text, and cross references, and minor changes to increase plot sizes. No new studies are planned to be added.
- C-B-14-3: It would be important that they take at least note of the comment and indicate how they intend to address the topic in the future. If they could make at least an estimation that routing and cables and services works on paper, it would already be good.
- I have no line comments to provide yet and would prefer to do so only at a later stage, when the document has undergone further editing.

The routing and service had been studied and the internal cabling and piping of sub-detectors are presented in their dedicated chapters, the external service routing of sub-detectors are described in the section 14.3.2 of the new TDR version. The basic routing scheme has been proposed, and we have checked and verified that the allocated space is sufficient. These services are still being finalized and optimized.

DETECTOR PEREORMANCE

Findings

F-A-15-1: Although further improvements are possible and recommended, the collaboration’s response to the previous evaluation has been excellent and deserves recognition. The detector software, particularly the simulation component, now enables comprehensive studies of detector performance and physics benchmarks. Several design decisions have been made based on both detector and physics performance criteria. This progress has allowed the definition of a baseline detector concept. While still perfectible and requiring further detailed investigation, this is a significant and commendable step forward. The scope of physics performance studies has broadened considerably since the last assessment. The range of channels explored and the methodologies employed respond well to previous recommendations and collectively address key detector areas and primary physics topics.

Comments

- C-A-15-1: The Ref-TDR text could be improved and shortened by presenting certain aspects (e.g., particle identification, jet studies) more concisely, while still ensuring that the algorithms are described clearly and transparently.
- *Shortened and restructured: PID inputs and algorithms mainly described in Sec. 15.1.2, with properly reference to TPC chapter; Jets studies rewritten in Sec. 15.1.7 and 15.1.8, the JOI flavor tagging now chosen as default, and text on the BDT method reduced.*
- C-A-15-2: Many additional physics analyses are planned. Their presentation and motivation should be aligned with the main purpose of this document: demonstrating the feasibility and physics potential of the reference detector.
- *10 analyses conducted and documented in Sec. 15.2*
- C-A-15-3: Algorithms for particle identification, jet tagging, etc., are mentioned in multiple places and are still evolving. A systematic approach should be adopted to define and refer to these algorithms consistently across the document.
- *Restructured: XGBoost BDT approach is adopted for all PIDs, JOI chosen as default jet tagging method.*

Recommendations

- R-A-15-1: The studies encompass both physics benchmarks and detector performance metrics. A clearer distinction between these two aspects would be beneficial. The editorial team is encouraged to organize the content into:
  - R-A-15-1-1: Sub-detector technical performance — technical performance figures (used for sub-detector configuration decisions) should be placed in the relevant sub-detector chapters.
    - *Single photon reconstruction efficiency and resolutions now only shown in* Section 7.3.4 *(ECAL chapter)*
    - *Track impact parameters now appear only in Section 4.7 (Vertex chapter)*
    - *Plots for separation power of tof and dn/dx moved to Section 4.5 (Silicon Tracker chapter) and Section 6.4 (TPC chapter)*
  - R-A-15-1-2: Physics-related performance — to demonstrate baseline detector capabilities for physics analyses (e.g., particle identification, global variables like ETmiss), and to present the physics analyses themselves. This should be the main focus of the performance chapter.
    - *Sec 15.1 restructured to focus on physics-related performance*
    - *Now Tau leptons (15.1.5) and Missing E/p/m (15.1.9) also included.*

Recommendations

- R-A-15-2: The physics benchmarks listed in Table 15.3 are intended to demonstrate the performance of the reference detector. Each listed study should be discussed explicitly, explaining the role of the detector performance in achieving the result. Currently, only a subset (e.g., Higgs recoil mass, Higgs branching ratios, weak mixing angle from Z→μμ) are covered. Other channels (exotic Higgs decays, LLPs, CVP in D-meson decays) should also be summarized, possibly in a summary table.
- *Sections 15.2.2 – 15.2.11 discuss and cover 10 analyses listed in the Table 15.3, and Table 15.20 summarizes the achieved sensitivities for all those channels.*

Table 15.20: Physics benchmarks, relevant detector performances and expected precision.

Physics Benchmarks	Relevant Det. Performance	Expected Precision
Recoil H mass	Tracking	Δm_H=±4.1 MeV
$H \to$ hadronic decays	PID, Vertexing, PFA	relative unc. of BR = 0.3% $(b\bar{b})$ – 8.9% (ZZ^*)
$H \to \gamma\gamma$	photon ID, EM resolution	$\Delta(\sigma \times \mathrm{BR})/(\sigma \times \mathrm{BR})_{\mathrm{SM}}$=3.2%
$H \to$ invisible	PFA, MET, BMR	4.4σ to SM, BR<0.049% to BSM at 95% CL
$H \to$ LLP	Tracker, TOF, muon detectors	$\mathrm{BR}(H \to \chi\chi) < 4 \times 10^{-5}$ for m_χ=10 GeVand lifetime=0.1 ns
Smuon pair	Tracking	Discovery reach up to $m(\tilde{\mu})$=119 GeV
A_{FB}^{μ}	Tracking, muon ID	±0.000031 (stat.) ± 0.000028 (syst.)
R_b	PFA, jet flavor tagging	2.5×10^{-6} (stat. unc. only)
CPV in $D^0 \to h^+h^-\pi^0$	PID, vertex, π^0, EM resolution	Sensitivity to 0.05° (0.05%) asymmetry in phase (magnitude)
Top mass & width	Beam energy	Δm_{top}=21 MeV (optimistic syst.), 54 MeV (conservative syst.)

Recommendations

- R-A-15-3: The technical improvements planned for more detailed simulation (noise, event overlap, misalignments, calibration effects) should be pursued, and their impact on physics performance carefully demonstrated.
  - *Electronics noise in TPC/ECAL/HCAL is included as default; those in silicon detector has been studied and shown negligible impact, so not included in simulation to avoid CPU issue.*
  - *Preliminary studies on beam induced background through event overlap, including incoherent pairs creation (dominant)*
    - *No significant impact on tracking efficiency*
    - *5% worse resolution – negligible impact*
    - *Significant impact on missing energy/mass documented in 15.1.9, which can be mitigated by a requirement of $|\cos\theta|<0.98$ for neutral objects*

New BIBs studies still ongoing

13610 The missing energy and mass is sensitive to BIBs. The BIBs induce additional neutral
13611 objects in calorimeters, and lead to an increase of around 7 GeV to the visible energy. With
13612 $Z \to q\bar{q}$, $H \to 4\nu$, the mean value of the missing mass distribution decreases to around
13613 118 GeV, whereas the resolution rises to 7.2 GeV. Most neutral objects from BIBs lie in
13614 very forward and backward regions. By discarding neutral objects with $|\cos\theta| > 0.98$, the
13615 effect can be cleared, with the missing mass mean value back to around 125 GeV, and the
13616 resolution restored to 6.4 GeV.

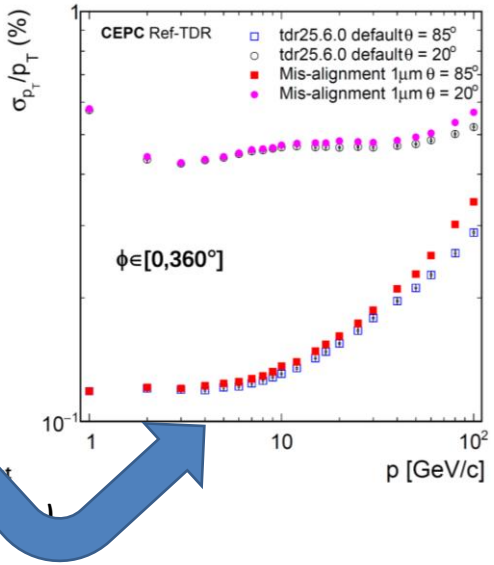

- *With alignment precision expected (1 μm), no significant misalignment effects expected on tracking*
  - *the effect can be further reduced by correcting the bias according to angle (post-TDR developme*
- *Calibration: PFA reconstruction includes preliminary simple calibration on ECAL/HCAL clusters*
  - *Figure 7.18 shows the ECAL energy resolution for 5 different calibration precision ranging from 1 % to 10 %, indicates that the calibration precision of 1 % yields around a 0.3 % degradation on the constant term*

Recommendations

Several specific technical issues should be clarified and potentially improved:

- R-A-15-4: The photon efficiency behaviour around E = 1 GeV appears unusual and should be either justified or corrected, as it could impact EM/hadronic separation in PFA and influence missing energy and mass resolution.
  corrected and shown in ECAL chapter, Figure 7.21(a).

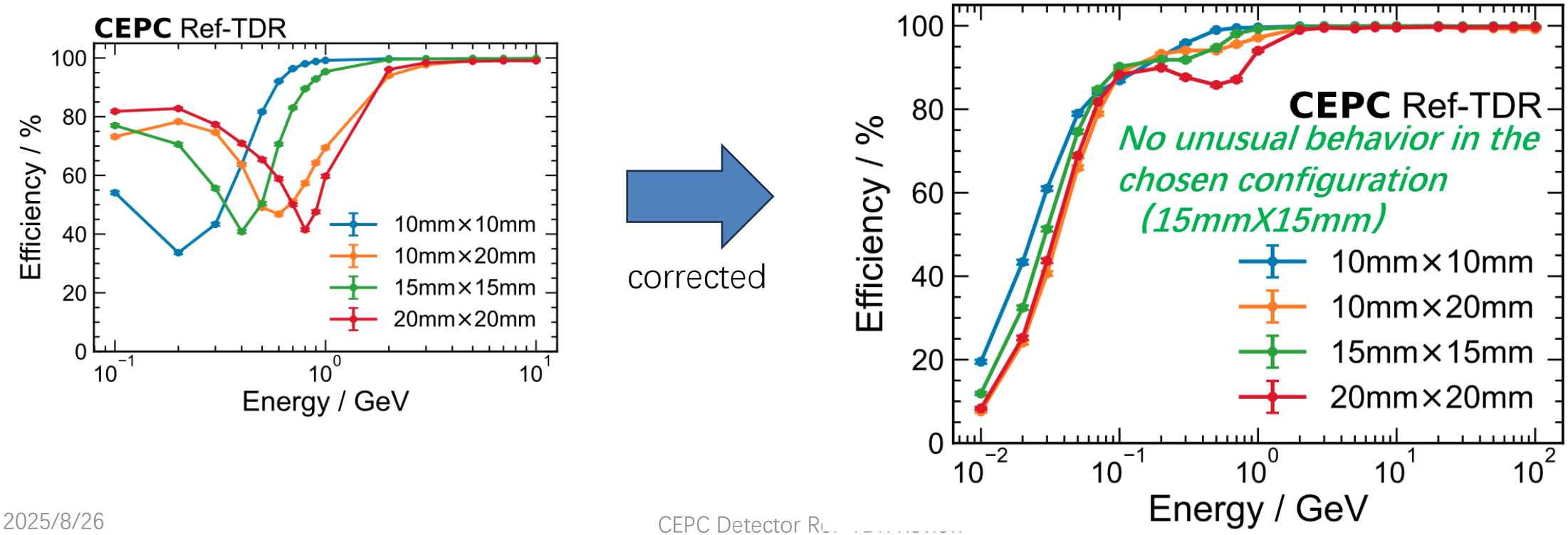

Recommendations

- R-A-15-5: Jet energy resolution for light quarks should be studied more systematically and used as a benchmark metric.

JER now made with u/d light quarks, similar performance seen as previous with b quarks

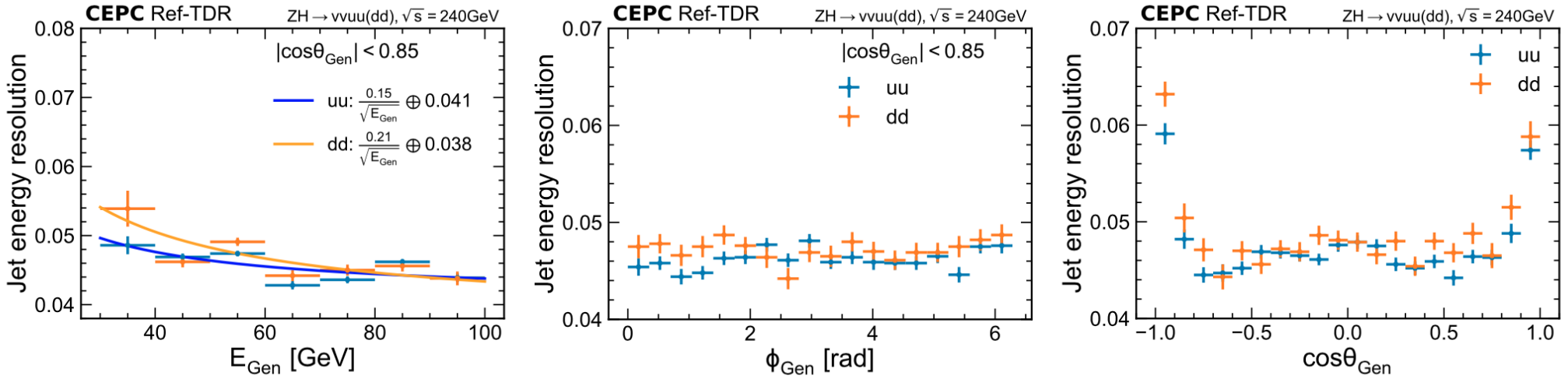

Figure 15.12: Jet energy resolution as a function of the (a) GenJet energy, (b) azimuth angle, and (c) $\cos\theta_{\mathrm{Gen}}$ for the $ZH \rightarrow \nu\nu uu$ and $ZH \rightarrow \nu\nu dd$ processes. Only the statistical uncertainty is presented.

Recommendations

- R-A-15-6: Missing energy reconstruction should be further investigated, particularly in b- and c-jet events with tagged leptons and in BSM channels with large ETmiss.
  New section 15.1.9 shows performance on " Missing energy, momentum, mass", see Figure 15.18
  Section 15.2.5 documents studies of the H->invisible channel

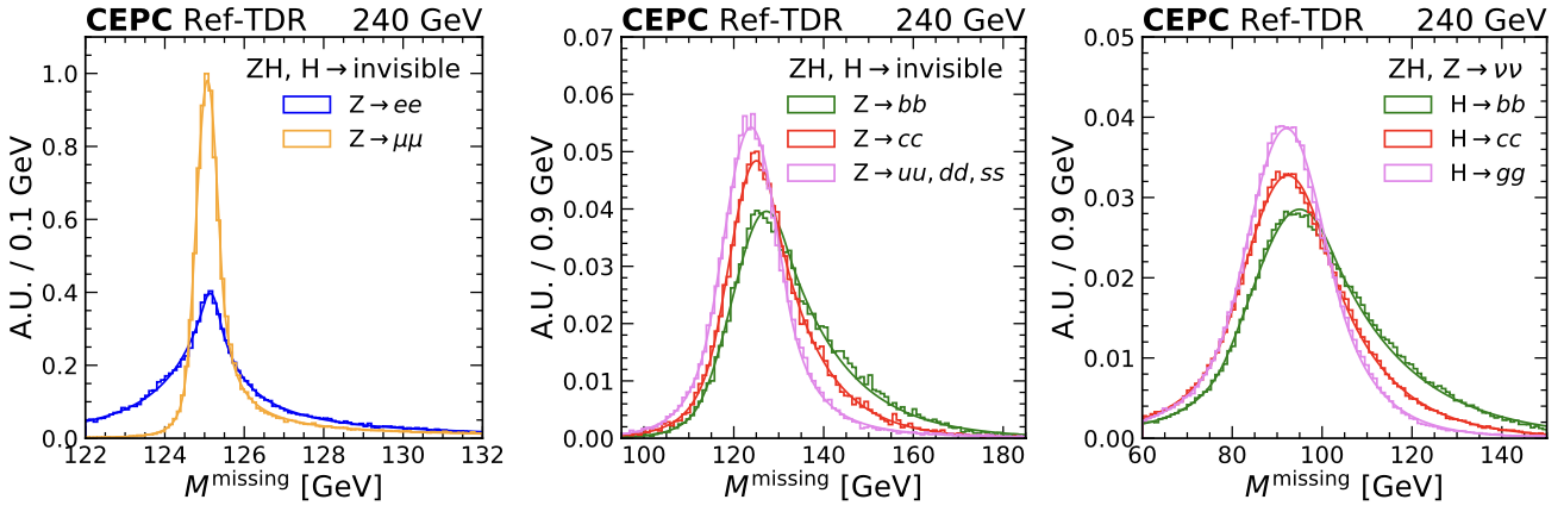

(a) (b) (c)

Figure 15.18: The distributions of reconstructed missing mass in the ZH production, with (a) $Z \to e^+e^-/\mu^+\mu^-, H \to 4\nu$, (b) $Z \to q\bar{q}, H \to 4\nu$ or (c) $Z \to \nu\bar{\nu}, H \to q\bar{q}$. The solid lines show the fitted DSCB functions. In the (b) and (c) plots, different quark flavors are drawn and fitted separately.

Recommendations

- R-A-15-7:(Longer term) Tracking performance should be tested in exotic scenarios, such as long-lived particles.
  Currently Section 15.2.6 shows studies on long-lived particles, but more detailed evaluation of tracking performance for such scenarios are left for future studies.
- R-A-15-8:(If possible) Include photon conversions in tracking studies as a material probe and describe their treatment in PFA.
  Figure 15.5 shows material budget and conversion rate vs. cos(theta).
  Currently converted photon treated as two charged tracks in PFA, further improvement planned in post-TDR development.
- R-A-15-9: Particle identification needs further organization and development:
  - R-A-15-9-1: Currently, simple cuts are applied; more sophisticated algorithms (including ML-based methods) should be considered, balancing the ambition against available time and resources. A simpler multivariate approach could serve as an intermediate step.
    XGBoost is default now
  - R-A-15-9-2: Different working points ("tight" for high purity, "loose" for high efficiency) should be defined and used consistently across analyses (e.g., Figure 15.7, where a 90% WP for muon/electron ID is mentioned). Coherence with PFA must be ensured (avoiding double-counting residual energy, etc.)
    Different working points are defined and BEST WP is now used consistently across analyses.

Recommendations

- R-A-15-10: The description of jet flavor identification needs to be streamlined. Currently, information is dispersed across sections (vertexing, tracking, PFA). A concise but complete description should be provided in one place *Now it's all in Section 15.1.8*
  - R-A-15-10-1: A brief overview of standard Jet Flavour Tagging (JFT) is given in Section15.2.6, while Jet Origin Identification (JOI) is discussed in 15.2.7. However, it is unclear what performance gains are achieved by moving from JFT to JOI.

    Figure 15.17 shows the improvement from standard JFT to JOI: 1-2 orders of magnitude lower mis-ID rate

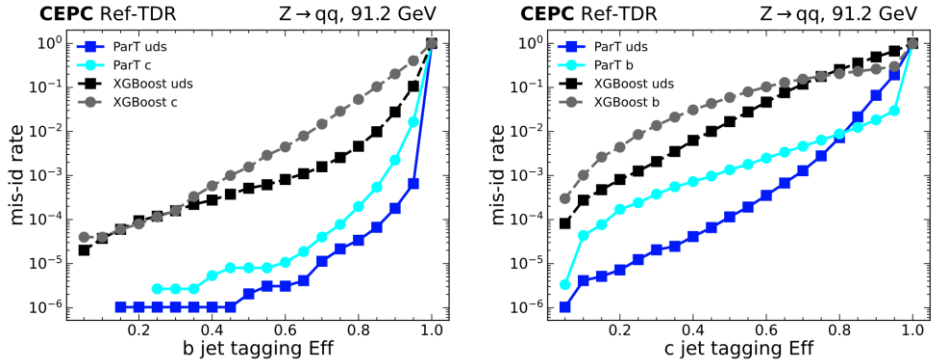

13571 Figure 15.17 compares the JOI performance with XGBoost method. Generally, JOI
13572 performance has lower mis-identification rates than the BDT method by one to two orders
13573 of magnitude for the fixed efficiencies. Remarkably, current JOI achieves a b-jet tagging
13574 efficiency of 94% with a mis-identification rate of only 0.2% for light-quark jets.

- R-A-15-10-2: Benchmark comparisons (b/c-tagging efficiency versus misidentification rates at Z-pole and ZH 240 GeV) should be provided to evaluate performance systematically.

  When JOI model trained with Higgs sample, and performance evaluated at ZH and Z-pole, no significant difference seen.

13575 This JOI model, optimized within a Higgs-boson production environment, demon-
13576 strates sufficient universality and capability across diverse kinematic energy scales. Its
13577 application to $Z \to q\bar{q}$ final states reveals no significant performance degradation when
13578 compared against JOI models tailored explicitly for $Z \to q\bar{q}$ data. Furthermore, consistent
13579 performance of JOI is validated for $e^+e^- \to q\bar{q}$ jet samples at $\sqrt{s}$ = 240 and 360 GeV,
13580 highlighting its energy-independent robustness beyond the training environment.

Recommendations

- R-A-15-11: The offline software environment is evolving rapidly. Performance studies should be conducted with synchronized and version-controlled frameworks, especially as CyberPFA depends critically on tracking, particle ID, calibration, and alignment inputs.

  yes, all performance shown have been obtained with CEPCSW-25.3.7

- R-A-15-12: A centralized database tracking the produced samples and their statistics should be maintained and updated (extending Table 15.4). Technical samples (e.g., single electrons, muons, decaying kaons for PFA studies) should be included and documented similarly for use in detector performance validation.

  a centralized database created and maintained with IHEP gitlab service (in CEPCSW code repository)

Recommendations

- R-A-15-13: Longer-Term Considerations (for post-TDR development)
  - R-A-15-13-1: Consider a dedicated chapter for jet flavour tagging, especially given the comprehensive nature of JOI (which involves many sub-detectors). Comparative studies between "ideal" and "compromised" performance would also help derive systematic uncertainties in the AI-based approach.
    - *Section 15.1.8 now focuses on JOI, and also show the comparative studies in Figure 15.16*
  - R-A-15-13-2: The confusion matrix (Fig. 15.22) suggests JOI could distinguish quarks from antiquarks. If validated, this could significantly improve flavour-specific AFB measurements. Physics benchmarks involving b/c-quark AFB (or even strange quarks) should be added if feasible.
    - *Study already ongoing, but not mature yet, no plan to include it in TDR*
  - R-A-15-13-3: Organizing "data challenges," as mentioned in the "Offline Software and Computing" section, could be valuable. These would serve both as benchmarks for detector performance and stress tests for computing models (through massive production, analysis, and quality checks)
    - *From the experience of March exercise, it will take ~2 months for full sample production and another 1-2 months for updating all results. We will organize such data challenges post-TDR*

Comments on Draft v0.4.1

- C-B-15-1: The particle ID section 15.1 are now readable and well structured It would be nice if the section 15.1 ends up with a conclusion summarizing the salient performance features observed in these studies. I suggest a table of this type.

Section 15.1.10 is added to summarize the performance with a table with objects ordered consistently with the subsection structure.

Table 15.2: Performance of physics object reconstruction and identification

Physics Object	Processes considered	$E_{\text{c.m.}}$(GeV)	Performance
Track efficiency	$ZH \to q\bar{q}jj$	240	99.7% for track p >1 GeV
Track p resolution	Single muon gun	–	$\sigma_{1/p_T} = 2.9 \times 10^{-5} \oplus 1.2 \times 10^{-3}/(p \cdot \sin^{3/2}\theta)$
Electron ID	ZH inclusive	240	eff.>90% for p_T> 2 GeV, misID <1% (BEST WP)
Muon ID	ZH inclusive	240	eff.>90% for p_T> 2 GeV, misID <0.1% (BEST WP)
Photon ID	Single photon gun	–	eff.~100% for E > 3 GeV, misID $\lesssim$2% (BEST WP)
Charged hadron ID	$Z \to q\bar{q}$	91.2	overall kaon eff.=92% and purity=90.7%
Tau ID	$ZH \to q\bar{q}\tau^+\tau^-$	240	eff.~80% and purity$\gtrsim$90 GeV (visible E=30–90 GeV)
Vertex reconstruction	b^+b^-	91.2	eff.>90% for number of tracks ≥ 4
Primary vertices	$ZH \to \ell^+\ell^- b\bar{b}$	240	resolution < 3μm
Secondary vertices	b^+b^-	91.2	longitudinal (transverse) resolution $\lesssim$ 25(5)μm
JER	$ZH \to \nu\bar{\nu}b\bar{b}$	240	$0.22\sqrt{E_{\text{Gen}}} \oplus 0.043$ GeV ($\lvert\cos(\theta)_{\text{truth}}\rvert < 0.85$)
JAR	$ZH \to \nu\bar{\nu}b\bar{b}$	240	0.01 radian (θ) and 0.012 radian (ϕ)
BMR	$ZH \to \nu\bar{\nu}gg$	240	3.87% (barrel), approximately 6% (endcap)
Jet flavor tagging	$ZH \to \nu\bar{\nu}jj$, $Z \to q\bar{q}$	240, 91.2	b-tag eff.=95% with mis-ID rate=0.1% for uds
Missing mass resolution	ZH	240	0.288 GeV ($e^+e^-4\nu$), 0.40 GeV ($\mu^+\mu^-4\nu$) 6.4 GeV ($q\bar{q}4\nu$), 9.2 GeV ($\nu\bar{\nu}q\bar{q}$)

Comments on Draft v0.4.1

- C-B-15-2: The physics benchmarks in section 15.2 should be listed by physics domain and in the same order as introduced in table 15.3
  - We have updated the table based on the physics domain and center-of-mass energies. The subsections are ordered consistently now.
- C-B-15-3: in table 15.3 W fusion appears out of order (the domain is “Higgs”). Maybe move it up together with “Higgs”.
  - We have decided to remove the W fusion, as the analysis did not converge on time & is unlikely to do so in a short time scale.

Table 15.3: Physics benchmarks and relevant detector performances

Physics Benchmarks	Process	$E_{c.m.}$ (GeV)	Domain	Relevant Det. Performance
Recoil H mass	$\mu\mu H$	240	Higgs	Tracking
$H \to$ hadronic decays	ZH	240	Higgs	PID, Vertexing, PFA
$H \to \gamma\gamma$	ZH	240	Higgs	photon ID, EM resolution
$H \to$ invisible	ZH	240	Higgs/BSM	PFA, MET, BMR
$H \to$ LLP	ZH	240	BSM	Tracker, TOF, muon detectors
Smuon pair	$\tilde{\mu}^+\tilde{\mu}^-$	240	BSM	Tracking
A_{FB}^{μ}	$\mu^+\mu^-$	91.2	EW	Tracking, muon ID
R_b	$Z \to q\bar{q}$	91.2	EW	PFA, jet flavor tagging
CPV in $D^0 \to h^+h^-\pi^0$	$Z \to q\bar{q}$	91.2	Flavor	PID, vertex, π^0, EM resolution
Top mass & width	$t\bar{t}$	Threshold scan ~ 345	Top	Beam energy

Comments on Draft v0.4.1

- C-B-15-4: 15.2 please make sure that each analysis presented have 1-2 phrases at the end to compare with a reference analysis (for instance present state of the art, limits from LHC or previous LEP results etc) This exists in some places but not everywhere.
  - Sentences are added at the end of each analysis subsections.

In summary, the uncertainty of A_{FB}^{μ} measurement is ±0.000031 (stat.) ±0.000028 (syst.), based on the dataset from the one-month low-luminosity Z-pole data taking during the first year of ZH operation. The CEPC result improves the precision of the LEP result (±0.0013) [34] by two orders of magnitude.

- C-B-15-5: This is not necessarily for this document, but on a few benchmarks items (MHiggs, MTop etc.) it would be good to have a direct comparison with FCCee studies. (and good answers if significant differences are observed) → We don't include in the document, but a direct comparison to FCCee are provided in the final review talk

Mhiggs

These systematic uncertainties contribute to an additional 2.5 MeV to Δm_H, resulting in a final precision $\Delta m_H = \pm$ 4.1 MeV, which is a significant improvement from the current

Assuming the same integrated luminosity, the statistical uncertainty obtained in this analysis is comparable with the latest Future Circular Collider (FCC) result [16]. The slight difference between the two results can be attributed to the FCC analysis employing a different fitting strategy, where the signal modelling is performed separately for event categories defined by the polar angle of the leptons. In both analyses, the dominant sources of systematic uncertainty arise from the center-of-mass energy and the lepton momentum scale, with comparable impacts reported.

MTop

In summary, the top quark mass precision is expected to be 7 MeV, considering only the statistical uncertainty. Taking into account the systematic uncertainties, the top quark mass can be measured at the precision of 21 MeV optimistically and 54 MeV conservatively at CEPC. The statistical uncertainty is equivalent to the latest FCC-ee result (quoted as experimental in Table 3 from Ref. [66]) after scaling to the same luminosity. FCC-ee scans over 10 energy points with a step of 0.5 GeV and applies a total integrated luminosity of 410 fb^{-1}. Both the CEPC and FCC-ee studies adequately discussed the impact of systematic uncertainties. Differences mainly originate from the input uncertainty of α_S. CEPC takes 7×10^{-4} based on the world summary of α_S in 2015 [74], while FCC-ee adopts 1×10^{-4} that is evaluated from a projection using the FCC-ee measurements [75]. The two studies show a comparable level of precision on the top quark mass measurement.

Comments on Draft v0.4.1

- C-B-15-6: Table 15.18: maybe having the cell limits would help readability?
  - Added a vertical line and made a few minor cosmetic changes (e.g. avoided merging cells)

V0.4.1

SR-ΔM^h	SR-ΔM^m	SR-ΔM^l
$E_{\mu 1,2} > 40$ GeV	$9 < E_{\mu 1,2} < 48$ GeV	–
$E_{\mu 1,2} \in (40-50, >50)$ GeV	$E_{\mu 1,2} \in (9-25, 25-48)$ GeV	
$\Delta R(\mu, \text{recoil}) < 2.9$	$1.5 < \Delta R(\mu, \text{recoil}) < 2.8$	
$M_{\mu\mu} < 60$ GeV	$M_{\mu\mu} < 80$ GeV	–
$M_{\text{recoil}} > 40$ GeV	–	$M_{\text{recoil}} > 220$ GeV

Table 15.18: Summary of selection requirements for the direct smuon production signal region. ΔM means difference of mass between $\tilde{\mu}$ and $\tilde{\chi}_1^0$.

New

Table 15.14: Summary of selection requirements for the signal regions to search for the direct smuon production.

SR-ΔM^h	SR-ΔM^m	SR-ΔM^l
$E_{\mu 1,2} > 40$ GeV	$9 < E_{\mu 1,2} < 48$ GeV	–
$E_{\mu 1,2} \in (40-50, >50)$ GeV	$E_{\mu 1,2} \in (9-25, 25-48)$ GeV	–
$\Delta R(\mu, \text{recoil}) < 2.9$	$1.5 < \Delta R(\mu, \text{recoil}) < 2.8$	$1.5 < \Delta R(\mu, \text{recoil}) < 2.8$
$M_{\mu\mu} < 60$ GeV	$M_{\mu\mu} < 80$ GeV	–
$M_{\text{recoil}} > 40$ GeV	–	$M_{\text{recoil}} > 220$ GeV

- C-B-15-7: Figure 15.33 : are the contours right? They seem to be confined at the right of the figure and are not readable.
  - The contours are correct, but indeed were not readable. We zoomed in the figure. The left side of the contours are fully excluded.

V0.4.1

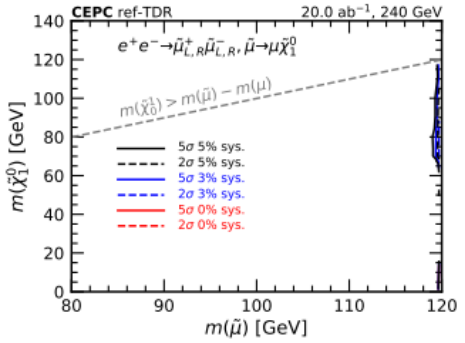

New

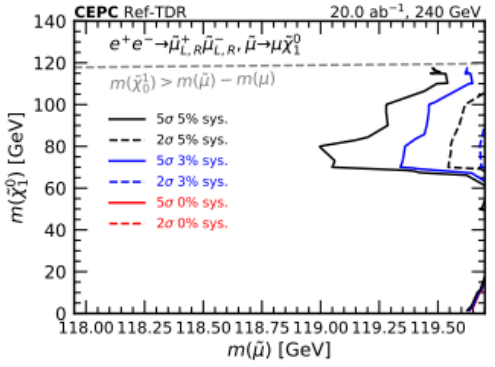

Comments on Draft v0.4.1

- C-B-15-8: The section 15.3 : I suggest to move the subsection 15.3.4 as a part of the final section, to be renamed as “Summary and future plans”.
- C-B-15-9: I suggest to rename the section 15.3 as: “Further performance aspects”
  - The new structure is as below.

V0.4.1

New

- C-B-15-10: I suggest a proof reading, there are a few editorial minute errors left in the text. (make the references uniform etc.) But in general the text is OK.
  - We went through the chapter again and made detailed updates to improve readability.

OVERALL CONSTRUCTION COST AND TIMELINE

Findings

- F-A-16-1: The cost estimation is provided as an ancillary table outside the Ref-TDR, following a standard Work Breakdown Structure (WBS). Only summary tables for the baseline detector option are included within the TDR text itself. Costs are primarily based on raw material prices (by volume, weight, or area), projected over the next 5 to 10 years, and multiplied by a fabrication factor.
- F-A-16-2: Currently, only a very rough timeline for detector construction is presented in Chapter 16 of the TDR.

Comments (1)

- C-A-16-1: For future, more informed cost reviews, it would be beneficial to provide the full WBS information, with a breakdown of:
  - Raw material costs
  - Production costs (including fabrication losses)
  - Labour costs
  - Integration costs
- C-A-16-2: Additionally, for each item, the following should be clearly specified:
  - Unit description (clearly linked to the detector design)
  - Unit cost (in original currency)
  - Basis of the estimate (e.g., vendor quote, internal prototype, previous projects, catalogue pricing)
  - Quantity required for the detector
  - Quantity including yield loss
  - Total quantity and total cost
- C-A-16-3: It should be explicitly stated whether the current costs include allowances for yield loss.
- C-A-16-4: A structured, consistent table format for each major cost item would greatly improve clarity and traceability.
- C-A-16-5: Regarding the detector construction timeline, the information currently provided is too limited to allow for a meaningful assessment.

- We plan for an internal cost review for each system after the TDR is released, with all recommendations taking into account. An international cost review is under consideration.
- A detailed timeline will be worked out in the detector EDR stage.

Comments (2)

- C-A-16-6: Concerning computing costs: while the extrapolations appear reasonable, the model could be further refined by considering data size, number of re-processing, number of data copies, and data accumulation schedules. Even a small additional effort to refine or document these factors would be valuable.
- The resource modeling and extrapolations account for the following parameters:
- Raw data size: 306 KB (DAQ system estimate)
- MC data size: 1 MB (offline software estimate)
- Reprocessing: Both MC simulation and reconstruction data are generated in 2 versions
- The resources are allocated for a 5-year period: four years of Higgs data collection and one year of low-energy Z data collection. The low-energy Z data is acquired in 2-month intervals annually, distributed across the 5-year Higgs data-taking period.
- Currently, we have only accounted for baseline requirements and assumed a single copy for all data types.

Comments (3)

- C-A-16-7: The projections for hardware performance and price evolution over 10 years seem somewhat optimistic, as they combine assumptions of improved CPU performance per core with reductions in cost per core.
- **The projection of a 50% reduction in average cost per CPU core over the next ten years is based on two key estimations:**
- Advances in semiconductor manufacturing: The transition from 7nm to 3nm and even 2nm process nodes enables significantly more transistors per core, enhancing both speed and energy efficiency. AMD's upcoming Zen 6 "Medusa" architecture, expected around 2026–2027, may deliver up to 30% higher single-core performance compared to Zen 3, driven by improved core design and interconnect technology.
- Industry cost trends: According to Future Market Insights, the average cost per core in data center CPUs is projected to decline by 30–50% over the next decade, particularly in mid-range and high-volume deployments. (www.futuremarketinsights.com)
- **HDD storage costs are projected to decline by 40%-50% over the next decade:**
- HDDs are evolving from traditional Perpendicular Magnetic Recording (PMR) to advanced methods like Heat-Assisted Magnetic Recording (HAMR) and Microwave-Assisted Magnetic Recording (MAMR). These technologies dramatically increase areal density, allowing more data to be stored per platter and reducing cost per terabyte.

ECAL BGO Crystals (1)

- R-A-16-1: The cost of BGO crystals significantly impacts the overall budget. The table presented dates back to 2019. We recommend engaging with multiple vendors to ensure the required quality, production rate (given the enormous volume), and lowest possible price.
- We visited three suppliers of BGO, and received new quotes
- 50% higher price compared to 2019, mainly due to increased GeO_2 price (next page)

Supplier	SIC	Boya	Xiamen Tungsten
Production method	Bridgman	Czochralski	Kyropoulos
Available BGO samples	40 cm	20 cm	40 cm
Quote ($/cc)	7 (2019)→10.6 (2025)	10.6	Production costs could be lower
Raw material cost fraction	~60%	51%	N/A
Production ability	1/3-1/2 of the total BGO volume in 5 years	Working on 40 cm BGO	Working on mass production plan

Thank Prof. Renyuan Zhu to help get new quotes

ECAL BGO Crystals (2)

- We also visited the research institute of the Aluminum Corporation of China (Chinalco) and its subsidiary, Yunnan Chihong Germanium International Co., Ltd.
  - Production capacity fully meets CEPC's requirement (~50 ton GeO_2)
  - **GeO_2 price increased by a factor of 2-3 since 2020, hard to predict the future trend**
  - **Action: potential collaboration with Chinalco through a high-level channel.**

- **Alternative option: BSO**
  - SIC is able to produce 40 cm BSO bars, quality to be studied

- Keep BGO and current cost estimation ($5/cc) as the target price. Looking for reduction of GeO_2 cost and developing BSO.

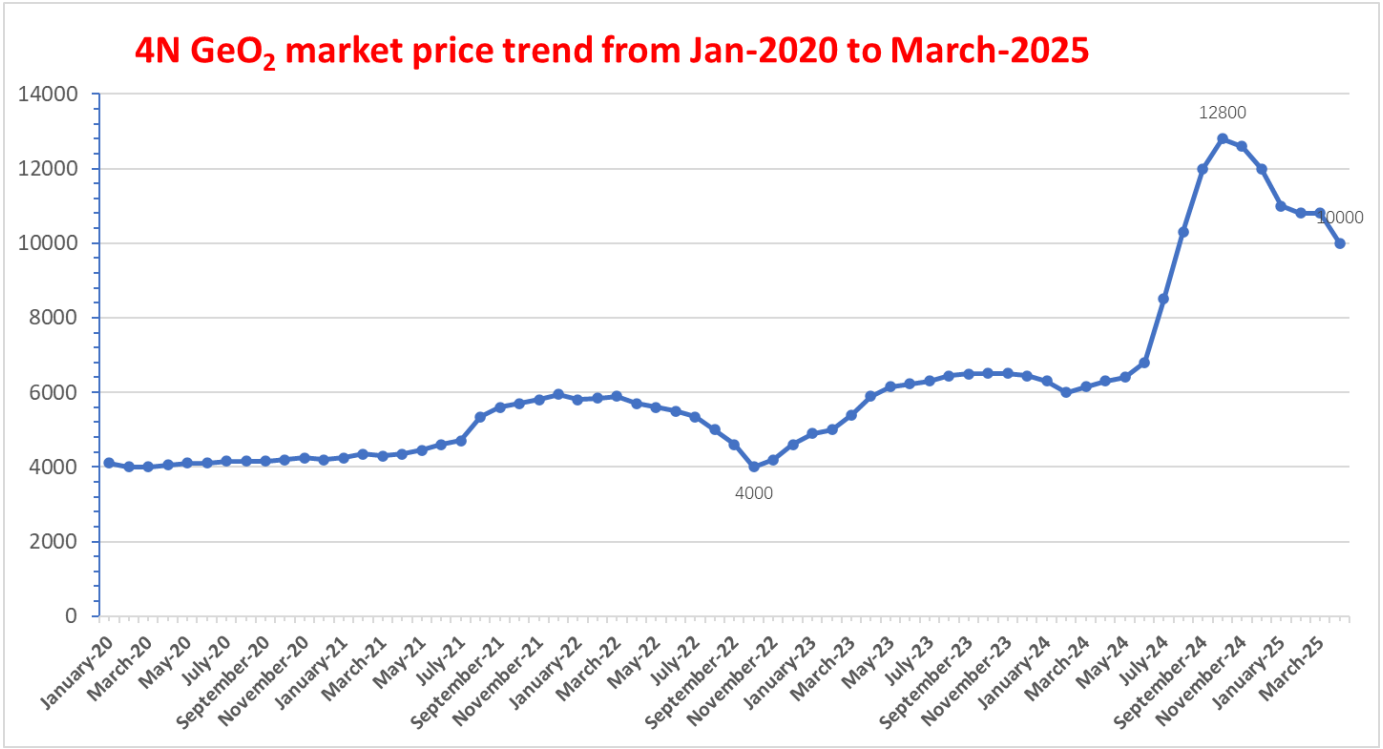

SiPM Packaging Costs

- R-A-16-2: The cost of packaging could be as high as 50% or more. It should be clarified whether packaging costs are included in the quoted SiPM price, and this should be explicitly reflected in the WBS. The current estimate of 1.25 CHF (10 RMB) per channel may be optimistic.
  - TAO uses SiPM 6×12 mm^2, 8 times larger than CEPC SiPM 3×3 mm^2
  - Assuming the cost packaging for CEPC is 50%, and for TAO is 25%, the new estimation is 20 RMB/piece, twice of our expectation.
  - Obtained new quotes from three suppliers (including Hamamatsu), two of them below 20 RMB/piece including packaging. Further reduction expected in the next 5-10 years.

	TAO	Extrapolated to CEPC
Material	10 RMB	10 RMB
Packaging	3 RMB	10 RMB

Price of SiPM per 3×3 mm^2 based on TAO's experience

Extrapolation from TAO is consistent with new quotes: ~20 RMB/piece

HCAL Cost Estimates

- R-A-16-3-1: Currently, the lowest informal offer is used for the cost of glass plates. Until it is confirmed that the lowest bidder meets the required specifications, it would be more prudent to use the average of the three quotes.
- The average price is 0.8 CHF/cc, 40% higher than our expectation (~0.5 CHF/cc). After careful comparison, we found vendor 2 has very high labor cost, power and depreciation; vendor 3 has very high cost for manufacturing and management. For now, we choose the lowest as our target and will work with all vendors to further understand their differences.
- R-A-16-3-2: Some cost uncertainty reflecting the outcome of ongoing R&D should be included.
- Considering the “unreasonable” items introduced before, the difference between each vendor is largely reduced, which should be cover by 20%-30% uncertainty assumed for each system.
- R-A-16-3-3: Additionally, the cost estimate assumes one SiPM per glass plate, whereas the detector design currently requires four SiPMs per plate for viability.
- In the new version of the TDR, the baseline design has been changed to one SiPM per glass plate.

Muon Detector Electronics

- R-A-16-4-1: The cost book reports 43,000 ASICs, 43,000 FEE units, and 43,000 Readout FEE units. However, the readout architecture has recently been updated to a three-stage system, and the number of FEE boards (uFEBs) should be significantly lower than the number of SiPM channels. The cost estimate should be updated to reflect this new architecture.
- In the WBS, 43,000 is the number of channels, instead of ASICs or units. The cost estimation has already converted the total cost of ASICs, FEE boards into the cost per single channel.
- R-A-16-4-2: Additionally, the TDR mentions the need for 72 Management Boards for slow control and DAQ interfacing—these boards are currently missing from the cost book and should be added.
- Management boards are part of the on-detector FEE. They are also converted into the cost per single channel and are already included in the cost estimation.

Magnet Cost Comparison

- R-A-16-5: The TDR quotes a magnet cost of about 22 MCHF, compared to around 130 MCHF for the more complex ILD system (which includes the yoke). A cross-check should be performed to understand and justify the difference between these two estimates.
- Excluding Yoke, the cost of ILD magnet is 38103 kILCU ~ 30711 kCHF, 40% higher than CEPC

Table III-7.6
Cost table of the coil and the iron yoke.

Item	Cost [kILCU]	Item	Cost [kILCU]
Coil		**Yoke**	
Conductor and winding	12900	Steel, including machining	80400
Internal Cryogenics	1000	Support	1700
Suspension system	560	Moving System	3500
tooling, assembly	10000	Assembly	6700
Qualification, testing	1100	Survey	500
Ancillaries			
Cryogenics, vacuum	6800	Integration	933
Electrical installation	1700	Field Mapping	560
Control and Safety system	350	Engineering	2200
Sum	131000		

arXiv:1306.6329

Magnet parameters comparison

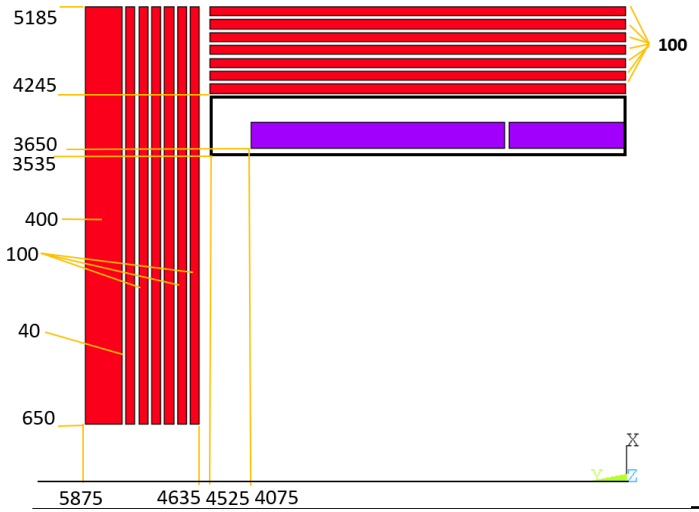

- ILD: 20%-30% higher magnetic field and 4 times larger yoke

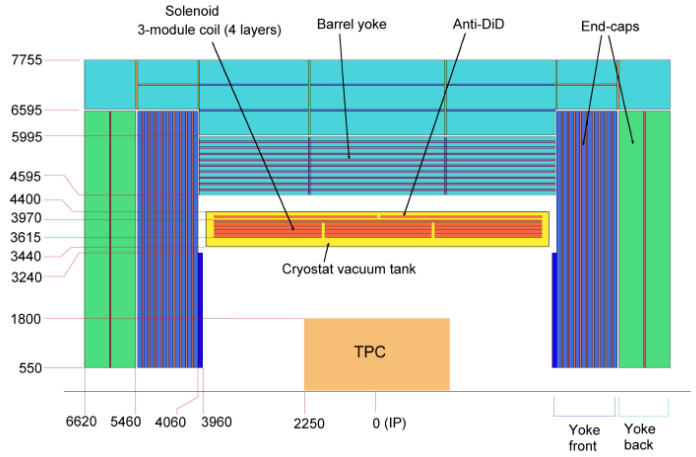

	CEPC	ILD
Magnetic field (T)	3	3.5~4
Cryostat inner radius (mm)	3535	3440
Cryostat outer radius (mm)	4235	4400
Cryostat length (mm)	9050	7810
Cold mass weight (t)	185	168
Total yoke weight (t)	3010	13400

	CEPC	ILD
Design maximum solenoid central field (T)	3	4
Nominal current (kA)	17	22.5
Inductance (H)	11	9.26
Stored Energy (GJ)	1.54	2.27
Cable length (km)	33	31.2
Total ampere-turns solenoid (MAt)	23.8	27.65

Magnet cost comparison

- Not completely apple-to-apple comparison due to lack of detailed information
- Much higher labor cost in ILD (6-7 MCHF VS 0.6-0.7 MCHF)
- Remain difference 10%-20%, reasonable considering higher magnetic field in ILD

Item	CEPC (kCHF)	ILD (kCHF)	
Conductor and winding	10,128	10397	Cable length (km) 33 vs 31.2
Internal Cryogenics	1008	806	Cryostat
Suspension system	242	451	Coil and Shield Suspension System
Tooling, assembly	1024	8060	Assembly Jigs and Tools
Qualification, testing	1103	887	Liquid helium, testing Dewar, machine
Cryogenics, vacuum	4144	5481	Refrigeration System 1000W@4.5K
Electrical installation	2589	1370	Power source, dump resistor, Circuit breaker
Control and Safety system	131	282	Interlock and control
Integration	640	752	Installation
Field Mapping	269	451	
Engineering	688	1773	
Total	**21,966**	**30,711**	

Yoke	CEPC	ILD	Ratio
Weight (t)	3010	13400	4.5
Cost (MCHF)	13.7	76.9	5.6

TPC Cost Comparison

- R-A-16-6: Similarly, the TPC cost is estimated at 5 MCHF, whereas the ILD TPC estimate was 36 MCHF. This discrepancy should be investigated and explained.
- A total cost 35.9 MILCU = 24.7 MCHF in ILD TDR, no details.
- Obtained a cost table from an ILD member, with a total cost of 15416 + 4689 (labor cost) = 20.1 MCHF

7.3.3 Time Projection Chamber

The estimate of the TPC price comes largely from the prices found in the construction of the STAR and ALICE TPCs. It has been updated for inflation but does not contain any added contingency. The cost of the field cage includes the experience from the construction of the large prototype, which was built in industry, using technology similar to the one to be used for a full scale field cage. A significant part of the TPC cost will be in the readout electronics, estimated to be around 30% of the total cost. The field cage - the iner cylinder, the outer cylinder, and the endplates, will account for around 20% of the cost, the rest being in tooling, anciliary systems and control systems. The total cost of the detector is estimated to be 35.9 MILCU.

arXiv:1306.6329

TPC Cost update

- After the April review, the cost estimation was updated from 5223 to 6179 kCHF, with additional 1094 kCHF backend electronics, sum to 7273 kCHF

	April	August	Difference	
Common Mechanics and calibration	1998	2640	+642	Fieldcage: Hanging, damping and shipping 230 mesh and DLC 350, Laser system 325 Optimized design of carbon fiber barrel -260
Readout	518	518	0	
Electronics (FEE)	2149	2435	+286	Optimized design of electronics cooling
HV/Gas system/Calibration	407	407	0	
Installation (3%)	152	180	+28	
Sum	5223	6179	+956	

Comparison with ILD

- Significant discrepancy in electronics and labor cost.
- Proceed with the updated cost and continue detailed comparison, preparing for a dedicated cost review

Item	CEPC (kCHF)	ILD (kCHF)	Comments
Endplate Mechanics	806	1038	Aluminum-alloy machining costs domestically are more than 50 % lower than international rates
Field cage	931	1814	Domestic PCB prices are roughly half those overseas
Readout	518	1325	Domestic PCB prices are roughly half those overseas
Electronics (FEE)	2010	7196	The high-granularity readout employs a common ASIC-based solution rather than discrete-component electronics.
HV/Gas system	406	450	
Calibration system	385	508	Radiation source and the laser calibration
Water cooling	435	\	Water cooling system cost
CO_2 cooling	\	963	CO_2 cooling system cost
Shipping and management	\	686	International shipping cost (Europe to Japan)
Back end electronics	1094	1436	
Installation (3%)	180	\	
Labor cost	\	4689	Personnel costs for R&D and installation
Total	**7273**	**15416 + 4689**	